

6-23-2008

Peroxynitrite Chemistry: Formation, Decomposition and Possible Deactivation Mechanisms by Thiols

Olufunke Modupe Olagunju
Portland State University

Follow this and additional works at: https://pdxscholar.library.pdx.edu/open_access_etds

 Part of the [Environmental Sciences Commons](#)

Let us know how access to this document benefits you.

Recommended Citation

Olagunju, Olufunke Modupe, "Peroxynitrite Chemistry: Formation, Decomposition and Possible Deactivation Mechanisms by Thiols" (2008). *Dissertations and Theses*. Paper 6147.
<https://doi.org/10.15760/etd.8007>

This Dissertation is brought to you for free and open access. It has been accepted for inclusion in Dissertations and Theses by an authorized administrator of PDXScholar. Please contact us if we can make this document more accessible: pdxscholar@pdx.edu.

PEROXYNITRITE CHEMISTRY: FORMATION, DECOMPOSITION AND
POSSIBLE DEACTIVATION MECHANISMS BY THIOLS

by

OLUFUNKE OLAGUNJU

A dissertation submitted in partial fulfillment of the
requirements for the degree of

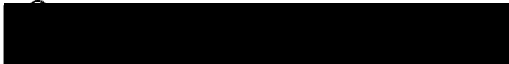
DOCTOR OF PHILOSOPHY
IN
ENVIROMENTAL SCIENCES AND RESOURCES: CHEMISTRY

Portland State University
2008

DISSERTATION APPROVAL

The abstract and dissertation of Olufunke Olagunju for the Doctor of Philosophy in Environmental Sciences and Resources: Chemistry were presented June 23, 2008, and accepted by the dissertation committee and the doctoral program.

COMMITTEE APPROVALS:


Reuben H. Simoyi, Chair


Albert S. Benight


Scott Reed


Jonathan J. Abramson


John Rueter
Representative of the Office of Graduate Studies

DOCTORAL PROGRAM APPROVAL:


M. A. K. Khalil, Director
Environmental Sciences and Resources
Ph.D. Program

ASBTRACT

An abstract of the dissertation of Olufunke Olagunju for the Doctor of Philosophy in Environmental Sciences and Resources: Chemistry presented June 23, 2008.

Title: Peroxynitrite Chemistry: Formation, Decomposition and possible Deactivation Mechanisms by Thiols

Kinetics of formation and decomposition of peroxynitrite was studied in acidic and buffer solutions. Peroxynitrous acid was formed in acidic media by the reaction of H_2O_2 with HNO_2 and NO^+ . Bimolecular rate constant for reaction of H_2O_2 with HNO_2 at 25°C was determined to be $3.7 \times 10^3 \text{ M}^{-1} \text{ s}^{-1}$. Peroxynitrous acid formed is highly unstable with half life of approximately 1 second. Decomposition of peroxynitrite is highly pH-dependent. In acidic media, peroxynitrous acid decomposes to nitrate while at neutral to slightly basic media, products of decomposition is nitrite, oxygen and acidic protons. In strongly basic pH, the products of peroxynitrite decomposition were nitrite and oxygen in a 2:1 ratio.

Decomposition dynamics showed first order dependence with respect to pH. Rate constant of decomposition of peroxynitrite in absence of a substrate at pH 3.0 was determined to be 0.98 s^{-1} and 0.10 s^{-1} at pH 8.0. Data generated from EPR studies indicates generation of $\cdot\text{OH}$ radical as a decomposition product of peroxynitrite.

Kinetics and mechanism of oxidation of cysteine (CYSH) and glutathione (GSH) by peroxynitrite, as radical deactivation agents were also studied.

Peroxynitrite reacts with CYSH/GSH at acidic pH to produce corresponding S-nitrosothiol and disulfide. The reaction is first order in peroxynitrite, acid and thiol. Mass spectrometer technique confirms formation of nitrosothiol as product of oxidation. Mechanism of formation can be rationalized as occurring through acid catalyzed decomposition of PN through intermediacy of $\text{HNO}_2/\text{N}=\text{O}$, which is capable of nitrosating thiol function.

In basic pH, peroxynitrite oxidizes CYSH/GSH through a two electron oxidation mechanism via sulfinic acid to corresponding disulfide. Mass spectrometer technique suggests that stable product of CYSH/GSH oxidation by peroxynitrite at pH 7.4 is disulfide of corresponding initial thiol. EPR studies on oxidation of CYSH/GSH by peroxynitrite at pH 7.4 suggest pathway of oxidation goes via formation of thiyl radicals. Bimolecular rate constants for oxidation of GSH by peroxynitrite at 25 °C (pH 7.0) was determined to be $587 \text{ M}^{-1} \text{ s}^{-1}$, while the bimolecular rate constants for oxidation of CYSH by peroxynitrite at 25 °C (pH 7.4) was determined to be $2.0 \times 10^3 \text{ M}^{-1} \text{ s}^{-1}$.

DEDICATION

I dedicate this thesis
To my husband-
Knowing you'll be in all my tomorrows
makes my today so wonderful...

And

To my daughter-
I could not have asked for
a more special gift than you
for all the pleasant footprints
you leave on my
soul everyday.

ACKNOWLEDGEMENTS

I would like to thank Dr. Reuben. H. Simoyi for being my research supervisor over the years. I am very grateful for his trust in me, guidance and encouragement to go another step further and for supporting this work. You have impacted in me the ability to write scientifically, independence in research work, up until the completion of this project.

My thanks go to all members of my dissertation committee. Dr. Albert S. Benight, who always have open door policy when ever I needed his help one way or the other, Dr. Scott Reed, for being critical and constructive in going over my thesis, both at the Masters and PhD levels, Dr. Jonathan J. Abramson for his fatherly and constructive help towards the successful completion of my project and lastly, but not the least, Dr. John Rueter, who was always approachable when ever I needed to schedule time for my many oral examinations.

I express my thanks to all past and present members of my research group. I have gone through academic as well as personal lessons that will last me a life time.

I would also like to sincerely thank Portland State University (PSU) BioAnalytical Mass Spectrometry Facility, in the person of Dr. Andrea DeBarber, for running all samples using the mass spectrometer.

I am indebted to the chemistry department; they are a big family, for smiles on the hallway and assurance of being a part of one big happy academic family. Special

thanks go to Sinnamon Tierney (Department Manager and Research Administrator) for all the administrative efforts put towards the successful defense of my dissertation.

This research was funded by the National Science Foundation (NSF), thanks to tax payers for making funding available to enable scientific research progress.

On a personal note, I want to say thank you to my parents for their patience, love, support, both morally and spiritually, believing in me and guiding me to independence. Most importantly, I thank my husband Tayo, for his moral and financial support, invaluable advice, standing by me through tough times as a graduate student, your love has seen me through. I cannot forget my daughter, Adeola, you have been a source of inspiration and encouragement to me.

TABLE OF CONTENTS

ACKNOWLEDGEMENTS	ii
LIST OF TABLES	x
LIST OF FIGURES	xi
LIST OF SCHEMES	xvi

CHAPTER 1: NITRIC OXIDE CHEMISTRY: FORMATION, REACTIVITY AND PHYSIOLOGICAL IMPORTANCE

1. 1.1 INTRODUCTION	1
1.2 MOLECULAR NO AND ITS OXIDES	2
1.3 BIOLOGICAL CHEMISTRY OF NO	5
1.3.1 Biosynthesis of NO: Historical perspective	5
1.3.2 NO formation	6
1.3.3 Isoforms of Nitric oxide synthase (NOS)	7
1.4 BIOLOGICALLY IMPORTANT REACTIONS OF NO	9
1.4.1 Reactions of NO with metals and metalloproteins	10
1.4.2 Reactions of NO with oxygen	15
1.4.3 Reactions of NO with radical species	19
1.5 CHEMISTRY OF S-NITROSOTHIOLS	22
1.5.1 Physical properties	26
1.5.2 Synthesis of S-nitrosothiols	26
1.5.2.1 Reaction between thiols and nitrogen oxides	26

1.5.2.2 Reaction of thiols with alkyl nitrites	28
1.5.2.3 Reaction of thiols with nitrites	29
1.5.3 Decomposition of S-nitrosothiols	30
1.5.3.1 Metal ion catalyzed decompositions	31
1.5.3.2 Thermal decomposition	32
1.5.3.3 Transnitrosation	33
1.5.3.4 Photochemical decomposition	34
1.5.3.5 Enzymatic decomposition	35
1.5.3.6 Potential therapeutic applications of S-nitrosothiols	36
1.6 CHEMISTRY OF PEROXYNITRITE	38
1.6.1 Relationship between NO and peroxynitrite	38
1.6.2 Properties of peroxynitrite	38
1.6.2.1 Spectral properties	38
1.6.2.2 Conformation properties	39
1.6.2.3 Thermodynamic properties	40
1.6.3 Synthesis of peroxynitrite	40
1.6.4 Decomposition of peroxynitrite in aqueous solution	46
1.7 SOME BIOLOGICALLY IMPORTANT PEROXYNITRITE REACTIONS	
1.7.1 Peroxynitrite-CO ₂ reaction	48
1.7.2 Nitration reactions	49
1.7.3 Peroxynitrite-thiol reaction	50
1.8 SUMMARY OF NO REACTIVITIES IN BIOLOGICAL SYSTEMS	52

CHAPTER 2: INSTRUMENTATION, MATERIALS AND METHODS

2.1 INTRODUCTION	53
2.2 INSTRUMENTATION	54
2.2.1 Conventional UV/Vis Spectrophotometry	54
2.2.2 Stopped-Flow Spectrophotometry	54
2.2.3 Electron Paramagnetic Resonance (EPR) Studies	60
2.2.4 Mass Spectrometry	64
2.2.5 High Performance Liquid Chromatography (HPLC)	68
2.2.6 Computer Simulations	70
2.2.6.1 Role of the computer in modeling	71
2.3 MATERIALS	73
2.3.1 Analytical chemicals	73
2.3.2 Tests for adventitious metal ion catalysis	73
2.3.3 Oxidant	73
2.3.4 Peroxynitrite synthesis	74
2.3.5 Thiols	74
2.3.6 Ionic Strength	75
2.4 EXPERIMENTAL METHODS	75
2.4.1 Stoichiometric determination	75
2.4.2 Reaction kinetics	76
2.4.3 Electron Paramagnetic Resonance (EPR)	77
2.4.3.1 Peroxynitrite decomposition	77

2.4.3.2 Cysteine/glutathione oxidation by peroxynitrite	77
2.4.4 High Performance Liquid Chromatography (HPLC)	77
2.4.5 Mass Spectrometry (MS)	78

**CHAPTER 3: KINETICS OF PEROXYNITRITE FORMATION AND
DECOMPOSITION IN PERCHLORIC ACID AND SODIUM PHOSPHATE
BUFFER SOLUTIONS**

3.1 INTRODUCTION	79
3.2 PRODUCT DETERMINATION FOR PN FORMATION AND DECOMPOSITION	80
3.2.1 Formation reaction	80
3.2.2 Decomposition reaction	82
3.3 REACTION DYNAMICS	84
3.3.1 Formation of PN	84
3.3.1.1 Effect of acid	84
3.3.1.2 Effect of nitrite	85
3.3.1.3 Effect of hydrogen peroxide	88
3.3.2 Decomposition of PN	91
3.3.2.1 Effect PH	91
3.3.2.2 Effect HCO_3^-	94
3.4 EPR STUDIES	96

3.4.1 Radical formation in decomposition of PN	96
3.5 MECHANISM OF FORMATION OF PN	99
3.6 CONCLUSION	102
CHAPTER 4: MECHANISTIC BASIS OF PEROXYNITRITE (PN)	
DEACTIVATION BY GLUTATHIONE	
4.1 INTRODUCTION	105
4.2 STOICHIOMETRY AND PRODUCT DETERMINATION	107
4.3 REACTION DYNAMICS	108
4.3.1 S-nitrosation reactions	108
4.3.1.1 Acid dependence	111
4.3.1.2 GSH dependence	113
4.3.1.3 PN dependence	114
4.3.2 Direct GSSG formation at 302 nm	116
4.3.2.1 GSH dependence	117
4.3.2.2 PN dependence	119
4.3.2.3 Effect of pH on glutathione oxidation by PN	121
4.3.2.4 Effect of sodium bicarbonate on glutathione oxidation by PN	124
4.4 EPR STUDIES	127
4.4.1 Oxidation of glutathione by PN	127
4.4.2 Effect of sodium bicarbonate on oxidation of glutathione by PN	128
124 4.5 CONCLUSION	134

CHAPTER 5: KINETICS AND MECHANISM OF THE OXIDATION OF CYSTEINE BY PEROXYNITRITE

5.1 INTRODUCTION	137
5.2 STOICHIOMETRY AND PRODUCT DETERMINATION	139
5.3 REACTION DYNAMICS	141
5.3.1 S-nitrosation reactions	141
5.3.1.1 Acid dependence	141
5.3.1.2 CYSH dependence	143
5.3.1.3 PN dependence	145
5.3.2 Cystine (CYS) ₂ formation at 302 nm	147
5.3.2.1 CYSH dependence	148
5.3.2.2 PN dependence	149
5.3.2.3 Effect of pH on oxidation CYSH by PN	151
5.3.2.4 Effect of HCO ₃ ⁻ on CYSH oxidation by PN	153
5.4 EPR STUDIES	156
5.5 CONCLUSION	158
REFERENCES	160

LIST OF TABLES

Table 1.1 Various oxides of nitrogen and their oxidation states	4
Table 1.2: Properties of the three isoforms of nitric oxide synthase (NOS)	8
Table 1.3: Various methods for synthesis of peroxynitrite	41

LIST OF FIGURES

Figure 1.1: Lewis dot structure of nitric oxide	2
Figure 1.2: Molecular orbital diagram for NO in its ground state	3
Figure 1.3: Biosynthesis of NO	7
Figure 1.4: Mechanism by which NOS isoforms produce NO	9
Figure 1.5: Structure of heme	12
Figure 1.6: Signal transduction pathway for NO-cGMP system in mammalian cells	14
Figure 1.7: Mechanism of NO-mediated inhibition of cytochrome P-450	15
Figure 1.8: Some synthetic and naturally occurring S-nitrosothiols	25
Figure 1.9: (a) Path way is the reduction of Cu^{2+} to Cu^+ by extrinsic reducers such as ascorbic acid	31
Figure 1.9: (b) Reduction of Cu^{2+} by added RS^-	31
Figure 1.10: Resonance structure of S-nitrosothiol	33
Figure 1.11: Enzymatic decomposition of S-nitroso-L-glutathione	37
Figure 1.12: Cis, trans conformation of peroxynitrite	39
Figure 1.13: Pathways of thiol oxidation by peroxynitrite	
Figure 1.13: (a) two electron pathway	51
Figure 1.13: (b) one electron pathway and	51
Figure 1.13: (c) pathway leading to formation of nitrosothiols	51
Figure 1.14: NO reactivity in the biological system	52
Figure 2-1: Schematic diagram showing the SF-61-DX2 stopped-flow fluorimeter	58
Figure 2-2: Sample Handling Unit (SHU) flow circuit diagram for the double mixing	

SF-61-DX2 stopped-flow system	59
Figure 2.3: General outline of an EPR spectrometer	62
Figure 2.4: Block diagram of the microwave bridge	63
Figure 2.5: The main feature of a mass spectrometer	64
Figure 2.6: Schematic diagram of a Micro TOF Q spectrometer	65
Figure 2.7: (a) Generation of ions by Electrospray Ionization (ESI)	66
Figure 2.7: (b) Matrix Assisted Laser Desorption Ionization (MALDI)	66
Figure 2.8: Diminishing of the size of the charged droplets with solvent evaporation	67
Figure 2.9: The basic liquid chromatography	69
Figure 3.1: Formation and decomposition of peroxyxynitrite	81
Figure 3.2: UV –vis spectral of peroxyxynitrite at pH 12	82
Figure 3.3: Product of decomposition of peroxyxynitrite in buffer pH 1.0, 7.0, 8.0, 9.0	83
Figure 3.4: Acid variation in the formation of PN	85
Figure 3.5: Initial rate plot formation of PN	86
Figure 3.6: Nitrite variation in formation of PN	87
Figure 3.7: Initial rate plot for nitrite variation in formation of PN	88
Figure 3.8: Hydrogen peroxide variation in formation of PN	89
Figure 3.9: Initial rate plot for hydrogen peroxide variation in formation of PN	90
Figure 3.10: Effect of pH on PN decomposition	92
Figure 3.11: Initial rate plot for decomposition of PN in phosphate buffer pH 3-9	93
Figure 3.12: Rate constants for effect of pH on PN decomposition	94
Figure 3.13: Effect bicarbonate on PN decomposition at pH 6.5	95

Figure 3.14: Effect bicarbonate on PN decomposition at pH 7.4	95
Figure 3.15: EPR spectral DMPO radical adduct PN decomposition	98
Figure 3.16: Products of decomposition of PN as a function of pH	104
Figure 4.1: Pathways of thiol oxidation as a function of pH	106
Figure 4.2: Product determination of the nitrosation reaction of GSH by PN	109
Figure 4.3: Spectral GSH, PN and reaction of H ⁺ , GSH and PN	110
Figure 4.4: Acid variation in the formation of GSH nitrosothiol	111
Figure 4.5: Initial rate plot for acid variation in the formation of GSH by PN	112
Figure 4.6: GSH variation in the formation of GSNO	113
Figure 4.7: Initial rate plot for variation of GSH in formation of GSNO	114
Figure 4.8: PN variation in formation of GSNO	115
Figure 4.9: Initial rate plot for variation of PN	116
Figure 4.10: Variation of GSH at 302 nm	118
Figure 4.11: Initial rate plot variation of GSH at 302 nm	119
Figure 4.12: Variation of PN at 302 nm	120
Figure 4.13: Initial rate plot variation of PN at 302 nm	121
Figure 4.14: Effect pH on GSH oxidation by PN	122
Figure 4.15: Initial rate plot for effect pH on GSH oxidation by PN	123
Figure 4.16: Rate constants for effect pH on GSH oxidation by PN	123
Figure 4.17: Effect bicarbonate on GSH oxidation	125
Figure 4.18: Initial rate plot for the effect bicarbonate on GSH oxidation	126

Figure 4.19: EPR radical adducts of DMPO with the oxidation products of GSH obtained at room temperature	131
Figure 4.20: EPR radical adducts of PBN with oxidation products GSH, spectra obtained at room temperature.	132
Figure 4.21: EPR radical adducts of DMPO with HCO_3^- , PN and GSH, spectra obtained at room temperature	133
Figure 4.22: Pathways of GSH oxidation by peroxynitrite	136
Figure 4.22: (a) two electron pathway	136
Figure 4.22: (b) one electron pathway and	136
Figure 4.22: (c) pathway leading to formation of nitrosothiols	136
Figure 5.1: Product determination of the nitrosation reaction of CYSH by PN	140
Figure 5.1: (a) 300 mM CYSH + 100 mM PN + 12.5 mM H^+	140
Figure 5.1: (b) 8.0 mM CYSH + 0.8 mM PN in buffer pH 7.4	140
Figure 5.2: Spectral CYSH, NO_2^- and PN	142
Figure 5.3: Acid variation in the formation of CYSH nitrosothiol	142
Figure 5.4: Initial rate plot for acid variation in the formation of CYSH by PN	143
Figure 5.5: CYSH variation in the formation of CYSNO	144
Figure 5.6: Initial rate plot for variation of CYSH in formation of CYSNO	145
Figure 5.7: PN variation in formation of CYSNO	146
Figure 5.8: Initial rate plot for variation of PN	147
Figure 5.9: Variation of CYSH at 302 nm	148
Figure 5.10: Initial rate plot variation of CYSH at 302 nm	149

Figure 5.11: Variation of PN at 302 nm in buffer pH 5.0	150
Figure 5.12: Initial rate plot variation of PN at 302 nm	151
Figure 5.13: Effect pH on CYSH oxidation by PN	152
Figure 5.14: Initial rate plot for effect pH on CYSH oxidation by PN	152
Figure 5.15: Rate constants for effect pH on CYSH oxidation by PN	153
Figure 5.16: Effect bicarbonate on CYSH oxidation	154
Figure 5.17: Initial rate plot for the effect bicarbonate on GSH oxidation	155
Figure 5.18: EPR radical adducts of DMPO with the oxidation products of CYSH obtained at room temperature	157
Figure 5.19: Pathways of CYSH oxidation by peroxynitrite	159
Figure 5.19: (a) two electron pathway	159
Figure 5.19: (b) one electron pathway and	159
Figure 5.19: (c) pathway leading to formation of nitrosothiols	159

LIST OF SCHEMES

Scheme 1.1: Valence bond description of metal nitrosyls (a) resonance structures for linear metal nitrosyl (b) resonance structure for bent metal nitrosyls.	10
Scheme 1.2: Possible mechanism for anaerobic oxidation of thiols by NO	22
Scheme 1.3: Mechanism of reaction of CO ₂ with ONOO ⁻	48

CHAPTER 1

NITRIC OXIDE CHEMISTRY: FORMATION, REACTIVITY AND PHYSIOLOGICAL IMPORTANCE

1.1 INTRODUCTION

Early scientists, like J.B van Helmont (1648), Robert Boyle (1671) and G.E Stahl (1703) had written about nitric oxide (NO), but the chemical properties of NO were first characterized by Joseph Priestley in 1772. He prepared NO by the reaction of nitric acid on metallic copper.



NO is thermodynamically unstable with a large positive Gibbs energy of formation of $+86.32 \text{ KJ mol}^{-1}$ ¹. Consequently, synthesis of NO from N₂ and O₂ occurs at high temperatures. Lightning is known as one of the major anthropogenic sources of NO^{2,3}. Nitric oxide is an environmentally important gas produced by car engines and industrial power plants⁴. It is also known to play a major role in the formation of photochemical smog⁵. The Environmental Protection Agency (EPA) includes NO among the various oxides of nitrogen (NO_x) which are responsible for environmental pollution and degradation⁶. Examples of NO's deleterious effects on the environment include ozone depletion⁶, production of acid rain and toxic chemicals, atmospheric particulates, eutrophication, and global warming. NO is produced industrially and

primarily used for preparation of nitric acid for the *Ostwald process*⁷

1.2 MOLECULAR NO AND ITS OXIDES

NO is a two-atom molecule with a unique and physiologically important chemistry.

The NO molecule is a colorless gas at room temperature and pressure. It consists of nitrogen and oxygen atoms chemically bonded together with one unpaired electron.

Lewis dot structure of NO (**Figure 1.1**) shows the lone electron which makes NO a free radical species.



Figure 1.1: Lewis dot structure of nitric oxide.

Lewis dot structure in **Figure 1.1** shows that nitrogen has five valence electrons while oxygen has six valence electrons. Combination of nitrogen and oxygen atomic orbitals with their valence electrons gives eight sets of molecular orbitals in which four are bonding and remaining four are antibonding. In order of increasing energy the molecular orbitals comprise of one σ bonding orbital (σ_{2s}^b) and its corresponding antibonding orbital (σ_{2s}^*), two degenerate π bonding orbitals (π_{xy}^b), one σ bonding orbital (σ_{2z}^b), two degenerate antibonding π (π_{xy}^*) orbitals and finally a σ antibonding orbital (σ_z^*). The arrangements of 11 electrons in the ground state orbitals are shown in **Figure 1.2**.

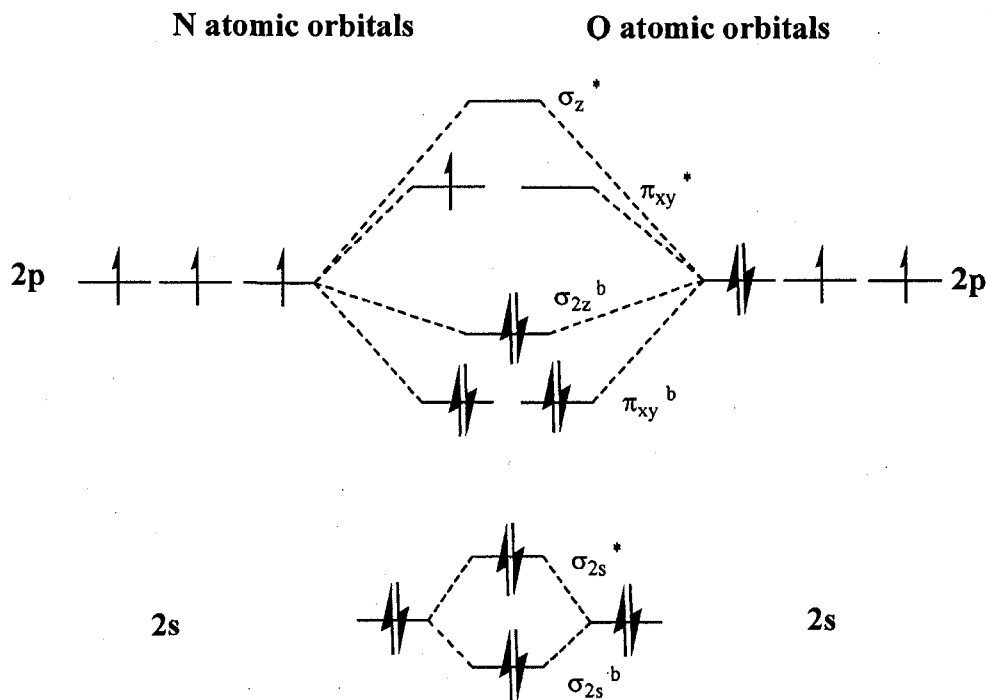


Figure 1.2: Molecular orbital diagram for NO in its ground state⁸.

According to distribution of electrons into orbitals shown in **Figure 1.2**, NO possesses eight bonding and three antibonding electrons. Calculating the bond order gives a bond order of 2.5. Consequence of a bond order of 2.5 is that the nitrogen oxygen bond length in free NO (1.154 Å) is intermediate between known triple (1.06 Å) and double bond (1.18 Å) lengths. When the unpaired electron in the π^* antibonding orbital is removed, NO is oxidized to NO^+ (nitrosyl ion), this specie has a bond order of 3. Similarly, reduction of NO by gain of one electron forms NO^- (nitroxyl ion), resulting in a bond order of 2. NO molecule has nitrogen in a +2 oxidation state and can undergo redox reaction in the biological system to form a range of oxides of nitrogen with oxidation states of nitrogen ranging from -1 to +5. These oxides are highlighted in

Table 1.1

Formula	Name	Oxidation state of Nitrogen
NH_2OH	Hydroxylamine	-1
N_2	Nitrogen	0
N_2O	Nitrous oxide	+1
HNO/NO^-	Hyponitrous acid/nitroxyl anion	+1
NO	Nitrogen monoxide	+2
N_2O_2	Dinitrogen dioxide	+2
NO^+	Nitrosonium ion	+3
N_2O_3	Dinitrogen trioxide	+3
$\text{ONOOH}/\text{ONOO}^-$	Peroxynitrous acid/peryoxynitrite	+3
$\text{HNO}_2/\text{NO}_2^-$	Nitrous acid/nitrite	+3
NO_2	Nitrogen dioxide	+5
N_2O_4	Dinitrogen tetroxide	+4
N_2O_5	Dinitrogen pentoxide	+5
$\text{O}_2\text{NOOH}/\text{O}_2\text{NOO}^-$	Peroxynitric acid/peryoxynitrate	+5
$\text{HNO}_3/\text{NO}_3^-$	Nitric acid/nitrate	+5

Table 1.1: Various oxides of nitrogen and their oxidation states.

1.3 BIOLOGICAL CHEMISTRY OF NO

1.3.1 Biosynthesis of NO: Historical perspective

The biological community used to assume that acetylcholine acted directly on vascular smooth muscle cells to cause vasodilation. But in 1980, Robert Furchgott in his publication in *Nature*, illustrated that acetylcholine acts on receptors on endothelial cells to produce a diffusible molecule that causes vasodilation⁹. Other researchers such as T. M. Griffith, and T. M. Cocks, attempted to isolate the endothelium derived relaxing factor (EDRF) but were not successful because of its high reactivity^{10,11}.

Independently of Furchgott; Murad and Ignarro, in their research work on nitroglycerin and nitrates, showed that nitroglycerin and organic nitrates are by themselves inactive, but elicit blood vessel relaxation after they have been converted to nitrates^{12,13}.

In 1987, Ignarro observed that both EDRF and NO produced comparable increases in cyclic guanosine monophosphate (cGMP) accumulation in artery and vein and concluded that, EDRF released from arteries and veins have identical biological and chemical properties as NO¹⁴. The definite proof that EDRF is NO was provided by Moncada and his group¹⁵. They found that NO was synthesized from L-arginine and was responsible for relaxation of muscles, inhibition of blood clotting by prevention of aggregation of blood platelets¹⁴⁻¹⁹. In 1998, Furchgott, Ignarro and Murad received the 1998 Nobel prize for medicine and physiology for their pioneering work and discovery of NO as the elusive 'Endothelium Derived Relaxing Factor' (EDRF) and its role in vasodilation²⁰. Moncada was also recognized by "Science watch" a subscription newsletter that performs compilations of statistical information

like publications, citations, and cites-per-paper counts for scientists, institutions, countries, and journal publication houses. In 1999, Science watch, named Salvador Moncada as the most-cited United Kingdom researcher of the 1990s for his work on NO²¹. After the award of the noble prize a lot of research effort has been directed to the study of NO chemistry, reactivity and physiological importance.

1.3.2 NO formation

Biosynthetically, NO is produced in mammals by the enzymatic oxidation of amino acid L-arginine in the presence of oxygen²². The reaction is a two stage process: first step is a two-electron oxidation of L-arginine to N-hydroxy-L-arginine. This step is analogous to a P-450-type monooxygenase reaction consuming one equivalence of NADPH and one equivalence of oxygen as cosubstrates^{22,23}. In addition, the N-hydroxyarginine oxidation step requires tetrahydrobiopterin (BH₄), calcium and calmodulin as catalysts^{24,25}. The second oxidation uses half a mole of NADPH, requires oxygen, additional three electrons, calmodulin/calcium and accelerated by BH₄²². The final organic product is L-citrulline with the formation of NO^{26,27}.

The full biosynthesis route of NO is shown in **Figure 1.3**.

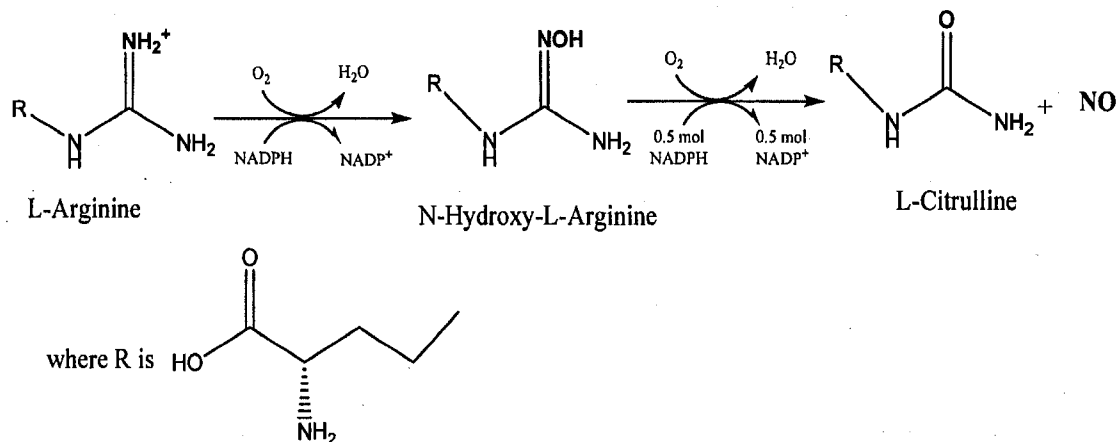


Figure 1.3: Biosynthesis of NO.

1.3.3 Isoforms of Nitric oxide synthase (NOS)

NOS isoforms are enzymes responsible for catalysis of the sequential oxidation of substrates L-arginine, NADPH and oxygen to L-citrulline and NO²⁸. There are three isoforms of NOS: isoforms I, II and III. They are encoded by three different genes but can be classified into two families, constitutive and inducible^{29,30}. NOS I and III are classified as constitutive while NOS II is inducible³¹⁻³⁴ (**Table 1.2**). Constitutive NOS I and III have been characterized in cell tissue types such as neurons and endothelia respectively. These two have similarity of being both regulated by and dependent on Ca²⁺/calmodulin. Catalytic action of NOS I and NOS III produces short lived and small amounts of NO, which activate soluble guanylyl cyclase to produce regulatory roles in neurotransmission and cardiovascular systems³⁵. NOS II has been isolated from murine macrophages and has a high affinity for calmodulin, NOS II is calcium independent and produces NO with a long half life³⁶ which produces deleterious effects such as mitochondrial complex

damage, DNA damage and even cell death. This is shown schematically in **Figure 1.4**.

Isoforms And types	Molecular Weight (kD)	Intracellular Location	Human Cellular Sources	Ca ²⁺ /calmodulin dependence	Activation
NOS I (nNOS) constitutive	155	cytosol	Neurons, adrenal medullary (brain)	Yes	Ca ²⁺ increase only, leads to calmodulin binding
NOS II (iNOS) inducible	125-135	Cytosol	Macrophages, monocytes, leukocytes,	no	Transcriptional Induction, Ca ²⁺ independent, calmodulin always bound
NOS III (eNOS) constitutive	135	Membrane and Cytosol	Endothelia cells of blood vessels, smooth muscles	Yes	Ca ²⁺ increase only, leads to calmodulin binding

Table 1.2: Properties of the three isoforms of nitric oxide synthase (NOS)

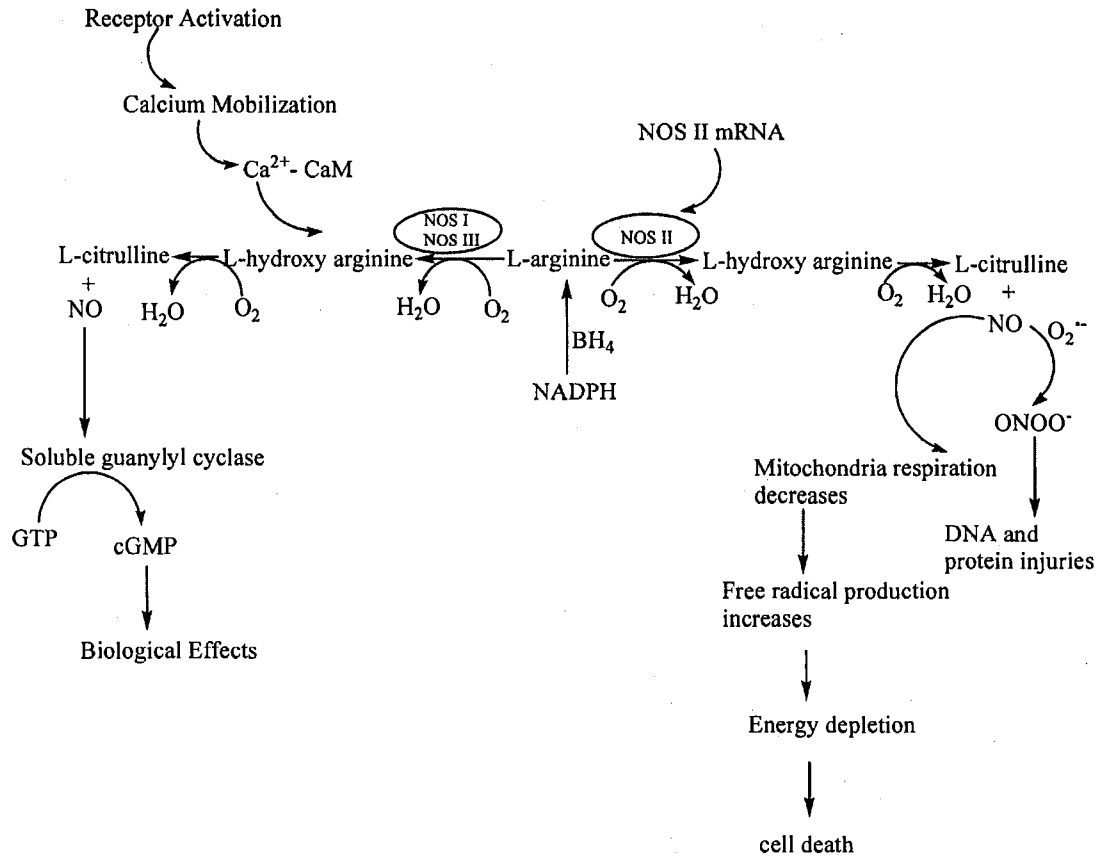


Figure 1.4: Mechanism by which NOS isoforms produce NO and subsequent biological effect.

1.4 BIOLOGICALLY IMPORTANT REACTIONS OF NO

The propensity for NO to readily undergo redox reactions and to form a range of reactive nitrogen species has great implications in biological systems. NO reacts in biological systems with compounds such as transition metals and metalloproteins, molecular oxygen (O_2), and radicals. Each of these reactions and their biological implications will be briefly examined.

1.4.1 Reactions of NO with metals and metalloproteins

NO is capable of forming nitrosyl complexes (M-NO) with a variety of transition metals such as iron, cobalt, nickel, vanadium, molybdenum, tungsten and copper³⁷.

Formation of NO complexes can be generally represented by the R1.2-type reaction:

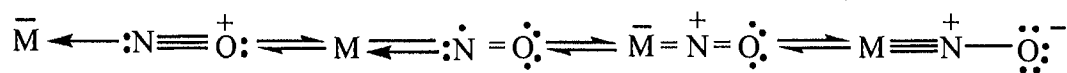


Where,

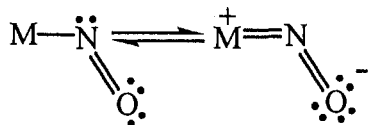
M = metal, L = ligand, X = leaving group

The formation of NO complexes with metal centers may have the character of NO range from nitrosyl cation (NO⁺) which binds to the metal in linear geometry, to that of nitroxyl anion (NO⁻) which binds in a bent geometry. In the linear geometry, the net bond interaction between the metal and NO consist of σ donation from NO to the metal and back π bonding from metal d-orbital to π^* antibonding orbital on NO. In the bent geometry, however, the metal donates an electron to NO to form NO⁻ which then binds to the metal using a σ bond (**Scheme 1.1**).

a) Linear NO (NO⁺, 3 electron donor)

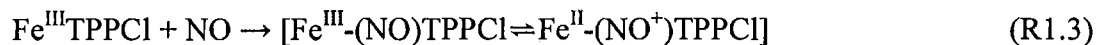


b) Bent NO (NO^- , 1 electron donor)



Scheme 1.1: Valence bond description of metal nitrosyls (a) resonance structures for linear metal nitrosyl (b) resonance structure for bent metal nitrosyls.

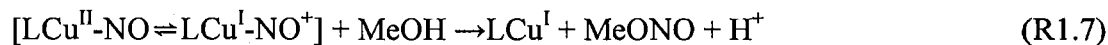
Coordination of NO to a metal as NO^+ or NO^- predicts that metal bound nitrosyl can either be electrophilic or nucleophilic, but mostly they undergo nucleophilic attack. For example, reaction of NO with synthetic tetraphenylporphyriniron (III) chloride ($\text{Fe}^{\text{III}}\text{TPPCl}$) in a protic solvent (methanol) results in the formation of ferrous nitrosyl adduct which is susceptible to nucleophilic attack. The mechanism of the reaction was determined as³⁸:



Another example is the formation of cuprous complex (LCuI) from the reduction of synthetic cupric complex by bound NO through an inner sphere charge transfer mechanism. Nucleophilic attack by methanol on the bound hydroxyl ligand resulted in the generation of the cuprous complex³⁹:



Where L = ligand system



Vast majority of nitrosyl complexes formed *in vivo* are a result of binding of NO with metalloproteins containing iron. Many notable heme complexes (hemoglobin, guanylate cyclase, cytochrome P-450 and nitric oxide synthase), can be nitrosylated by NO.

The most studied NO-heme complex is the NO-hemoglobin complex. Hemoglobin consists of four protein chains and four heme groups. Each heme group consists of a non-protein group with an iron atom at the center of an organic ring called porphyrin (**Figure 1.5**).

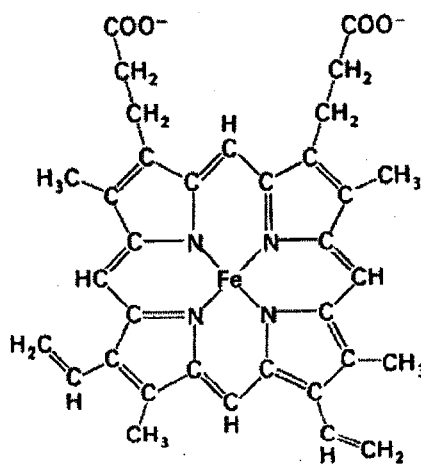


Figure 1.5: Structure of heme.

NO is able to bind strongly to the four iron atoms in hemoglobin forming four nitrosyl complexes. NO binds even more strongly with ferrous heme than CO⁴⁰⁻⁴². The greater affinity of NO for heme compared to affinity of CO for heme is explained by the different dissociation rates. The dissociation rate constant for loss of NO from deoxyhemoglobin is 10⁻⁵ s⁻¹, while dissociation rate constant for loss of CO is 20 s⁻¹^{42,43}. NO binds to both Fe(II) and Fe(III) hemes⁴⁰ by first reducing Fe(III) hemes to Fe(II) and then forming a stable Fe(II)-NO complex⁴⁴. Vandegriff and co-workers proposed that the binding of NO to ferrous deoxyhemoglobin (Hb) is the main mechanism for NO depletion⁴⁵.



The most notable NO-protein complex in the physiological environment is Fe-NO adduct in soluble guanylate cyclase⁴⁶. Binding of NO to soluble guanylate cyclase causes the position of iron in the porphyrin ring to shift such that the distal histidine is uncoupled in favor of a newly formed five co-ordinate nitrosyl complex^{47,48}. The change in the protein configuration at low NO concentrations (100 nM)⁴⁹ leads to conversion of guanosine triphosphate (GTP) to cyclic guanosine monophosphate (cGMP). Implications of conversion of GTP to cGMP, is prevention of some apoptotic processes⁵⁰, ability of NO to mediate vascular smooth muscle vasodilation, inhibition of platelet aggregation and

neurotransmission⁴⁶. This pathway is represented by the sketch shown in

Figure 1.6.

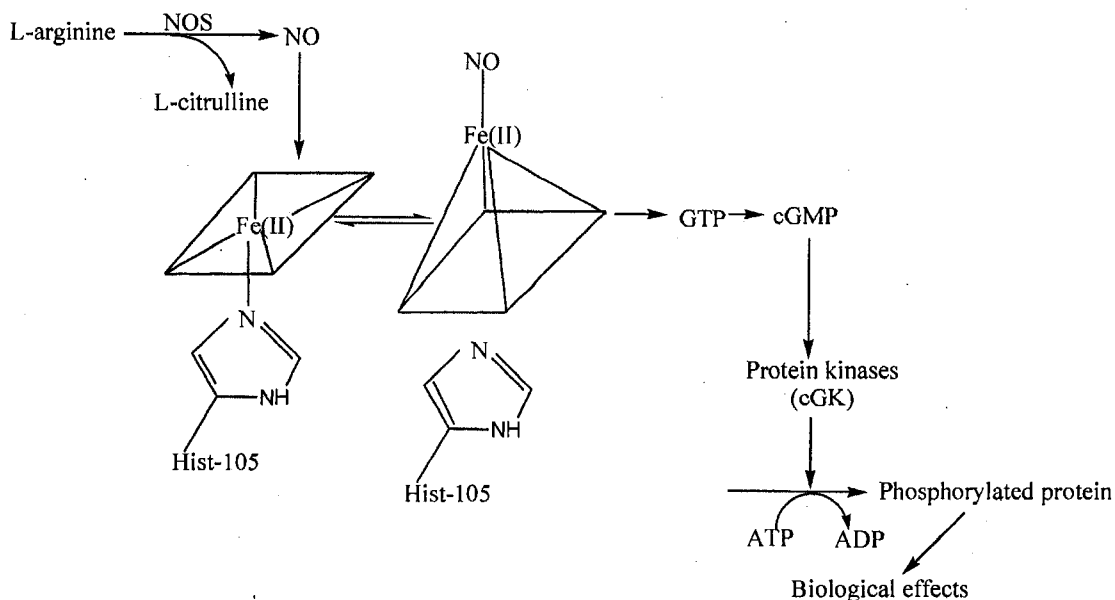


Figure 1.6: Schematic representation of signal transduction pathway for NO-cGMP system in mammalian cells.

Cytochrome P-450 enzymes are a very large and diverse super family of hemoproteins which require oxygen to facilitate oxidative chemistry. Binding of NO to cytochrome P-450's results in competition between NO and oxygen for the heme binding site (see **Figure 1.7**). This inhibition of P-450 activity by NO is known to regulate hormone production such as testosterone synthesis⁵¹. Another important regulatory/pathological role of NO binding to cytochrome P-450 occurs in high concentrations of NO formed during chronic infections which can lead to inhibition of liver cytochrome P-450's and subsequently depress metabolic break down of synthetic drugs⁵².

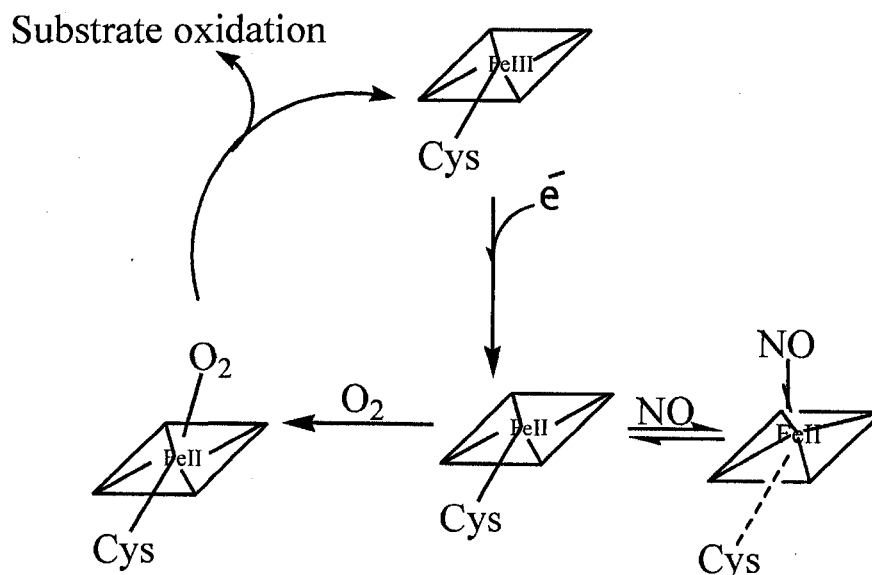


Figure 1.7: Mechanism of NO-mediated inhibition of cytochrome P-450.

NO complexes with the iron center of heme protein L-arginine, thereby forming a nitrosyl complex. It is known that L-arginine is enzymatically oxidized by oxygen at the heme domain to L-citrulline and NO⁵³. The Fe-NO complex formation with the heme protein L-arginine prevents oxygen binding at the active sites⁵⁴⁻⁵⁶. Inhibition of oxygen binding at the active sites prevents formation of L-citrulline and NO. Biological implication is that NO can regulate its own synthesis through nitrosylation of L-arginine (**Figure 1.7**).

1.4.2 Reactions of NO with oxygen

NO is a stable radical which does not exhibit a strong tendency to dimerize⁵⁷

but upon exposure to molecular oxygen generates reactive nitrogen oxide species (RNOS). Formation of gas phase nitrogen dioxide in nitrogen's autooxidation has long been of interest to environmentalists as the brown haze in smog⁵⁸. And so, extensive research work has been done in this area. The gas phase reaction of NO with O₂ to form NO₂ has been determined to be second order in NO and first order in O₂ with $k = 3.4 \times 10^5 \text{ atm}^{-2} \text{ s}^{-1}$ at 20 °C⁵⁹:



Radical combination of NO and NO₂ would produce dinitrogen trioxide (N₂O₃) or NO₂ would dimerize to dinitrogen tetraoxide (N₂O₄)⁵⁸:



Hydrolysis of N₂O₄ from the gas phase dimerization of NO₂ results in the disproportionation of N₂O₄ to give nitric acid:



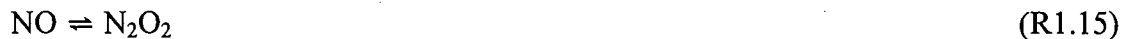
Formation of HNO₂ and HNO₃ contributes to acid rain in the atmosphere.

Different mechanisms have been proposed for the formation of NO₂ in the

intermediate from autooxidation of NO followed by reaction of peroxy nitrite with NO to form NO₂⁶⁰:



Other proposed mechanism by Olbregts suggest the dimerization of NO followed by reaction with oxygen:



Nevertheless, the above equilibria both displayed negative enthalpies of activation with overall third order rate law in NO and O₂. Since third order rate laws are rare, this may be an indication of a non plausible mechanistic pathway.

However, it was found that autooxidation reactions of NO in aerobic aqueous solutions quantitatively generate nitrite ions⁶¹. The mechanism of the reaction was determined to be reaction R1.9 + 2(R1.10) which generated 2N₂O₃, followed by hydrolysis of N₂O₃:



Overall reaction R1.18 is the stepwise addition of reaction R1.9, R1.10 and R1.17:



Awad and Stanbury, using stopped flow spectrophotometric and conductometric measurements determined the rate law of reaction of NO with O₂ in aqueous solution to be equation (1):

$$\frac{-d[\text{O}_2]}{dt} = k[\text{NO}]^2[\text{O}_2] \quad (1)$$

with rate constant $k = 2.1 \times 10^6 \text{ M}^{-2} \text{ s}^{-1}$ at 25 °C⁶².

Major differences in the gas phase and aqueous phase autooxidations include; (a) the final product of autooxidation in the gas phase N₂O₄ can be hydrolyzed to form HNO₂ and HNO₃, while final product of autooxidation in aqueous phase is NO₂⁻ (b) rate constant in aqueous phase autooxidation is an order of magnitude faster than in gas phase.

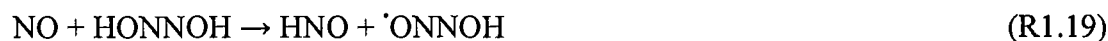
Autooxidation of NO at limiting NO concentrations is inversely concentration dependent with respect to half-life (equation 2):

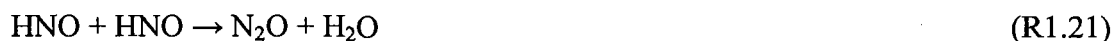
$$t_{1/2} = \frac{1}{k} [\text{NO}][\text{O}_2] \quad (2)$$

In other words, the lower the concentration of NO the higher the half-life. This is explained from the second-order dependence of autooxidation rates on NO concentrations. Implications of this to the physiological environment is that at low concentrations (0.1-0.5 μM) at which NO participates in regulatory processes such as vascular relaxation, neurotransmission and inhibition of platelet aggregation⁶³ NO depletion due to autooxidation will be slow. This allows NO to reach many biological targets without appreciable depletion. NO is produced at much higher concentrations ($> 10 \mu\text{M}$) in activated macrophages and neutrophils⁶⁴. At this condition, half-life of NO due to autooxidation decreases while the production of reactive nitrogen species increases⁶⁵. RNOS's are much more potent oxidative species than NO and O_2 and have been implicated in nitrosation reactions, tissue damage and in a wide range of potential toxicities for the physiological environment⁶⁶.

1.4.3 Reactions of NO with radical species

Since NO has one unpaired electron, it rapidly reacts with other carbon, nitrogen and oxygen centered radical species. However, unlike other radical species such as $\cdot\text{NO}_2$, $\text{OH}\cdot$; NO is unable to readily abstract hydrogen atoms. This is due to its low reduction potential⁶⁷. Surprisingly, reactions in which abstraction of hydrogen by NO occurred have been reported in the reaction of NO with hyponitrous acid ($\text{H}_2\text{N}_2\text{O}_2$) at high acidity⁶⁸:

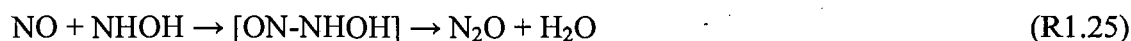




Another example of hydrogen abstraction by NO is the reaction of NO with hydroxylamine (NH_2OH)⁶⁹:



The proposed mechanism for the reaction of NO with hydroxylamine was confirmed using doubly labeled nitrogen and oxygen ($^{15}\text{N}^{18}\text{O}$)⁶⁹:

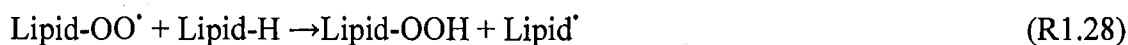


NO is able to “quench” the radical intermediates of radical species by terminating the radical chain reaction step. A good example is in the process of lipid peroxidation, where oxidative damage to cell membranes occurs due to the removal of an allylic hydrogen atom of unsaturated fatty acid. This abstraction of hydrogen generates a lipid radical (Lipid \cdot). The lipid radical then reacts with oxygen to generate alkylperoxy radical (Lipid-OO \cdot), which undergoes chain propagation by reacting further with

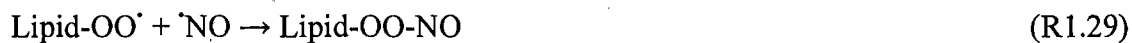
another molecule of lipid to form another lipid radical that can also react with oxygen and continue the chain propagation.



(X[·] = Chain initiating species)



Continuation of this series of reactions results in what is known as lipid peroxidation. Physiological implications of this process are the destruction or modification of many lipid molecules which can result in loss of membrane strength or integrity. NO is known to limit lipid peroxidation by acting as a chain terminating species⁷⁰.



It has been suggested that the termination of alkylperoxy radical reactions makes NO a protective agent under oxidative stress⁷¹.

One of the most studied physiologically important indirect reactions of NO in the

scientific community is its reaction with superoxide radical anion ($O_2^{\cdot -}$) to form peroxyntirite ($ONOO^-$)⁷².



The pK_a of peroxyntirous acid ($ONOOH$) has been reported to be 6.8 which is close to the physiological pH, in other words, a significant amount exists at the physiological pH of 7.4⁷². Peroxyntirous acid is a much more potent oxidizing agent than NO and $O_2^{\cdot -}$ and has been implicated in a variety of oxidation reactions in the physiological system^{73,74}. Peroxyntirous acid is very unstable and readily decomposes into various species as a function of pH of reaction medium^{75,76}. $ONOO^-$, the conjugate base of peroxyntirous acid is relatively stable in high pH medium and known to be a very potent nucleophile which can react with electrophiles such as carbon dioxide⁷⁷. The chemistry of $ONOOH/ONOO^-$ is diverse and relevant in the physiological system and will be treated comprehensively in this thesis.

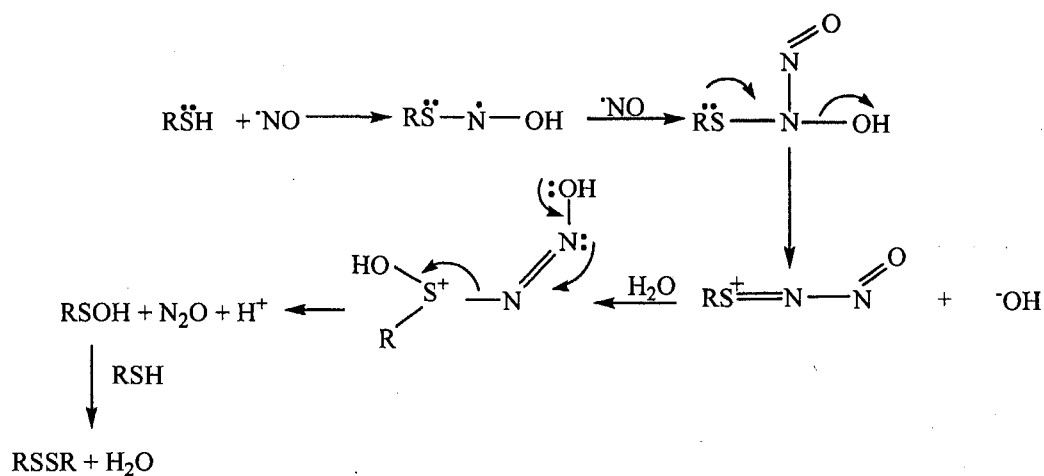
1.5 CHEMISTRY OF S-NITROSOTHIOLS

Thiols are compounds which have sulfur atom and hydrogen atoms chemically bounded together ($-SH$) as the distinguishing functional group. Physiologically relevant thiols include cysteine, glutathione and homocysteine. NO can react directly with thiols in the absence of oxygen through the formation of an adduct ($RS-N-OH$) that

then reacts with another molecule of NO to form an intermediate which decomposes into N₂O and water with the formation of disulphide corresponding to the starting thiol⁷⁸. In other words, NO does not react with thiols to form nitrosothiols, but disulfides.



The possible mechanism for the above reaction was postulated by DeMaster⁷⁹ and shown below in **scheme 1.2**:



Scheme 1.2: Possible mechanism for anaerobic oxidation of thiols by NO⁷⁹.

NO can indirectly oxidize thiols, in the presence of oxygen via electrophilic attack by nitrosating agents on the nucleophilic sulfur center of thiols, producing S-nitrosothiols. For example, reaction of N₂O₃ (a nitrosating agent) with thiols generates S-nitrosothiols (RS-N=O), also known as thionitrites:



There are various types of nitrosation reactions. But for the purpose of this thesis attention will be paid only to the chemistry of S-nitrosothiols.

S-nitrosothiols (RSNO's) are biological metabolites of NO, that may prolong and spatially extend the *in vivo* actions of locally produced NO⁸⁰. RSNO's are thio-esters of nitrite and analogues of the nitrite esters of alcohols. RSNO's are biologically important, and have been implicated in properties peculiar to NO, such as smooth muscle relaxation and anti-platelet aggregation properties⁸¹. Examples of endogenously produced RSNO's are S-nitrosoalbumin, S-nitrosoglutathione (GSNO) and S-nitrosocysteine (CYSNO) which have been shown to be present in low concentrations *in vivo*⁸²⁻⁸⁴ (**Figure 1.8**). Due to the ability of RSNO's to release NO, RSNO's determinations in biological fluids appear to provide a direct measure of NO synthase (NOS) activity⁸⁵⁻⁸⁷. Concentrations of RSNO's have been found to increase with local administration NOS and fall with administration of NOS inhibitors⁸⁶. Changes in levels of RSNO's have been seen to be associated with pathological conditions such as septic shock⁸⁸, pneumonia, and neonatal respiratory distress⁸⁶.

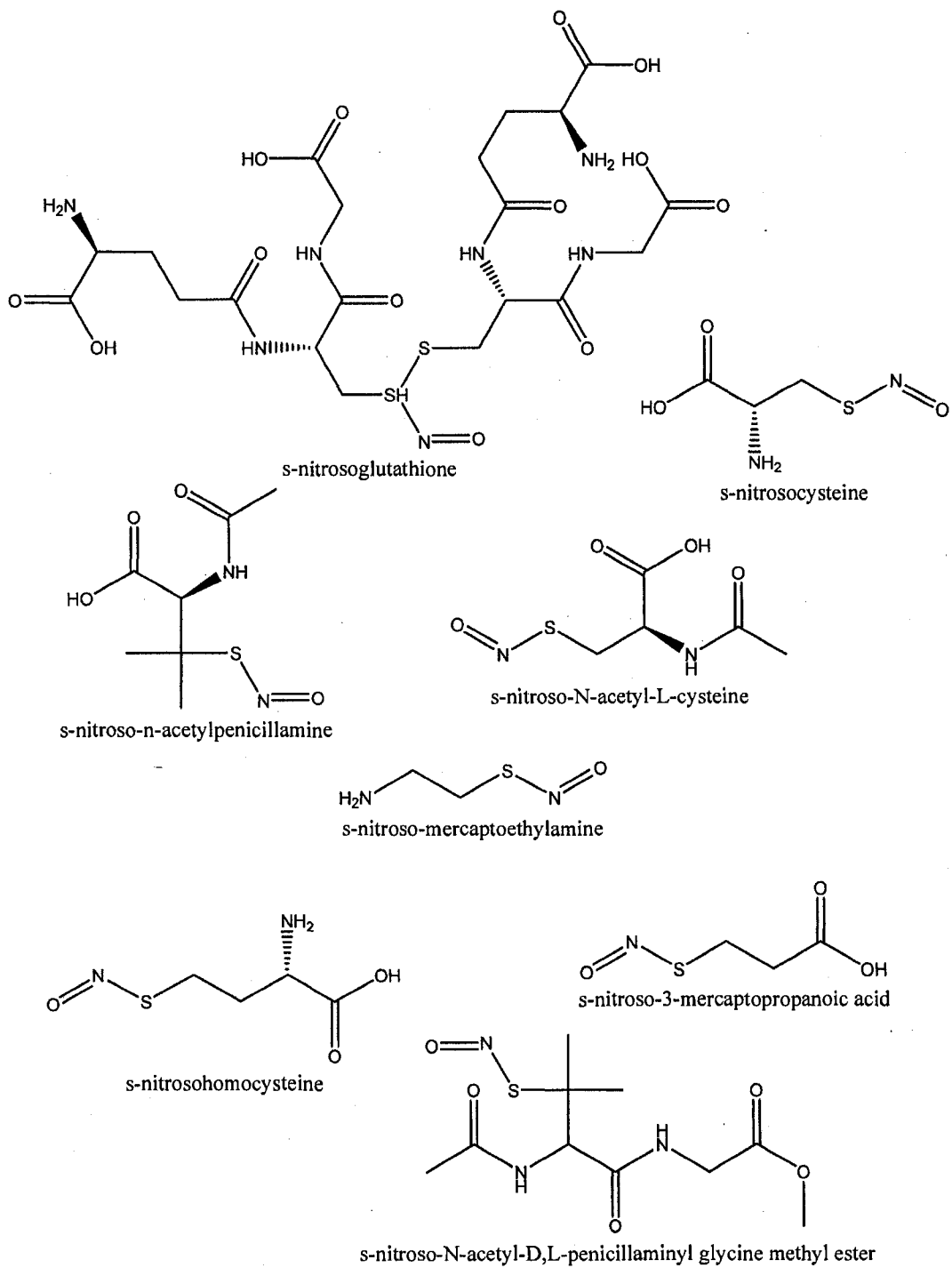


Figure 1.8: Some synthetic and naturally occurring S-nitrosothiols.

1.5.1 Physical properties

Stable nitrosothiols in their pure form are colored, with colors ranging from green in S-nitroso-N-acetylpenicillamine (SNAP), to pink in S-nitroso-glutathione (GSNO) and red in S-nitroso-3-mercaptopropanediol.

RSNO's have two major wavelengths by which they absorb in the UV-vis. These are 330-350 nm region with molar extinction coefficients of around $500 \text{ M}^{-1} \text{ cm}^{-1}$ and 550-600 nm with a much smaller molar extinction coefficient of about $20 \text{ M}^{-1} \text{ cm}^{-1}$ ⁸⁹. These wavelengths can be used to monitor the progress of reaction of RSNO in solution.

Aliphatic RSNO's exhibit two characteristic IR peaks at range of 1450-1530 cm^{-1} , 1152 cm^{-1} and 1167-1171 cm^{-1} ⁹⁰. These IR bands have been attributed to N-O and N-S stretching vibrations respectively. Both ^1H and ^{13}C NMR chemical shifts were analyzed for RSNO's. S-nitrosation results in ^1H and ^{13}C NMR chemical shifts changes with respect to α and β hydrogen atoms and carbon atoms of the pure thiol.

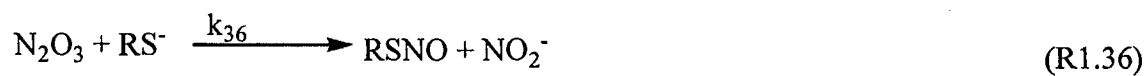
1.5.2 Synthesis of S-nitrosothiols

There are many pathways by which S-nitrosothiol can be synthesized, namely a) reaction between thiols and NO derivatives such as (NO_2 and N_2O_3), b) reaction of thiols with alkyl nitrites, and c) reaction of thiols with nitrites (NO_2^-).

1.5.2.1 Reaction between thiols and nitrogen oxides

Aromatic and straight chain thiols react with NO in the presence of oxygen to produce

the corresponding S-nitrosothiols:



The rate for the above reaction was derived to be⁹¹⁻⁹³:

$$\frac{d[\text{RSNO}]}{dt} = k_{33}[\text{NO}] \frac{k_{35}[\text{RSH}]}{2(k_{34}[\text{H}_2\text{O}] + k_{35}[\text{RSH}])} [\text{NO}]^2 [\text{O}_2] \quad (3)$$

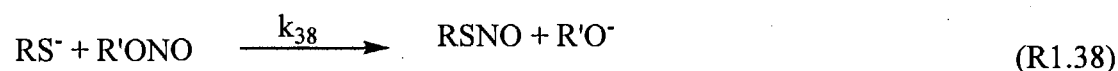
The rate law equation at high RSH concentrations becomes:

$$\frac{d[\text{RSNO}]}{dt} = k_{\text{NO}}[\text{NO}]^2[\text{O}_2] \quad (4)$$

This implies that in the synthesis of RSNO, NO is the rate determining step⁹¹.

1.5.2.2 Reaction of thiols with alkyl nitrites

Reaction of thiols with alkyl nitrites is facile with almost complete conversion of initial thiol concentration to nitrosothiols. The rate of formation of nitrosothiol is acid dependent, with a direct relationship which increases until about pH 10, where the rate levels off⁹⁴. This suggests a thiolate anion nitrosation pathway.



The rate law for the above reaction was proposed as⁹⁵:

$$\frac{d[\text{RSNO}]}{dt} = \frac{k_{38}k_{37}}{k_{37} + [\text{H}^+]} [\text{RS}^-][\text{R}'\text{ONO}] \quad (5)$$

This at high pH can be simplified to:

$$\frac{d[\text{RSNO}]}{dt} = k_{38} [\text{RS}^-][\text{R}'\text{ONO}] \quad (6)$$

1.5.2.3 Reaction of thiols with nitrites

The most widely used synthetic method in the synthesis of S-nitrosothiols is the reaction of acidified nitrites with thiols. This reaction is acid catalyzed and quantitatively generates nitrosothiols.



Reaction R1.39 has a derived rate law⁹⁶⁻⁹⁸:

$$\frac{d[\text{RSNO}]}{dt} = k[\text{HNO}_2][\text{RSH}][\text{H}^+] \quad (7)$$

The above rate law suggests that in strongly acidic solution the nitrosating species is HNO_2 . The first order dependence in $[\text{HNO}_2]$ in the above rate law proves that there is no contribution of N_2O_3 . If the nitrosating species were N_2O_3 , there would have been a second order dependence on $[\text{HNO}_2]$, according to reaction⁹⁸ (R1.40):

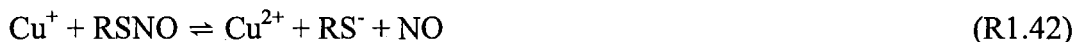


1.5.3 Decomposition of S-nitrosothiols

RSNO are susceptible to decomposition by various mechanisms. The rate of decomposition can be influenced by a number of factors, such as metal catalyzed decomposition, thermal decomposition, transnitrosation, photochemical decomposition, and enzymatic decomposition.

1.5.3.1 Metal ion catalyzed decompositions

The decomposition of RSNO's is catalyzed by the reduction of Cu^{2+} to Cu^+ in the presence of thiolate anion (RS^-)⁹⁹. Reaction then occurs between Cu^+ and RSNO regenerating Cu^{2+} , RS^- and releasing NO^{100} , with the organic final product being disulphide.



The kinetics of decomposition of RSNO by Cu^+ in solution was confirmed by the effect of added thiol¹⁰¹. It was proposed that if Cu^+ decomposition pathway is correct, then decomposition rate should be very dependent on $[\text{RS}^-]$. When RSNO is generated in situ;



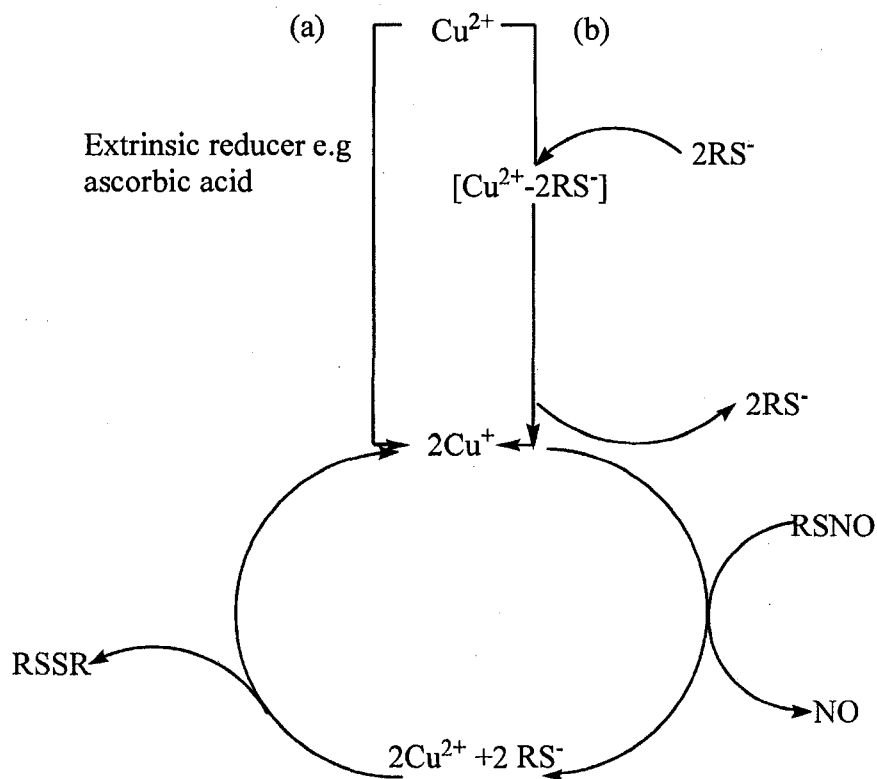


Figure 1.9: Catalytic cycle for copper catalyzed decomposition of S-nitrosothiols. Path way (a) is the reduction of Cu^{2+} to Cu^+ by extrinsic reducers such as ascorbic acid, while pathway (b) is through reduction of Cu^{2+} by added RS^- .

with the addition of Cu^{2+} and excess HNO_2 to push the reaction equilibrium to products side and ensure consumption of most of initial $[\text{RS}^-]$, decomposition of RSNO was found to be inhibited¹⁰¹. In effect, it is possible to stabilize RSNO in solutions by depletion of $[\text{RS}^-]$. On the other hand, thiol addition, ascorbate or other extrinsic reducers that are able to reduce Cu^{2+} to Cu^+ accelerate the decomposition of RSNO ¹⁰² (**Figure 1.9**). Further increase in added thiol results in retardation of decomposition rate. Dicks and his group attributed this effect to the formation of

thiolate complexation of Cu^{2+} , which make the copper ion less available for reduction to Cu^{+100} . No thiyl radicals were detected by EPR in the copper mediated decomposition of RSNO^{103} .

1.5.3.2 Thermal decomposition

S-nitrosothiols are very reactive intermediates formed during electrophilic attack of NO^+ on the thiolate anions. Since Cu^{2+} has been implicated in decomposition of RSNO 's, only at very low concentrations of Cu^{2+} (10^{-8} M), does thermal decomposition of S-nitrosothiol become dominant. Products of decomposition are thiyl radical, NO and disulfide of the parent thiol¹⁰⁴. EPR studies proved that thiyl radicals are formed; thus implying that the formation of disulfide is a two-step process¹⁰⁵:



The first step reaction (R1.44) relies on the homolytic cleavage of the S-N bond.

The second step generated thiyl radicals which are unstable, and so two thiyl radicals combine together to form disulfide (R1.45).

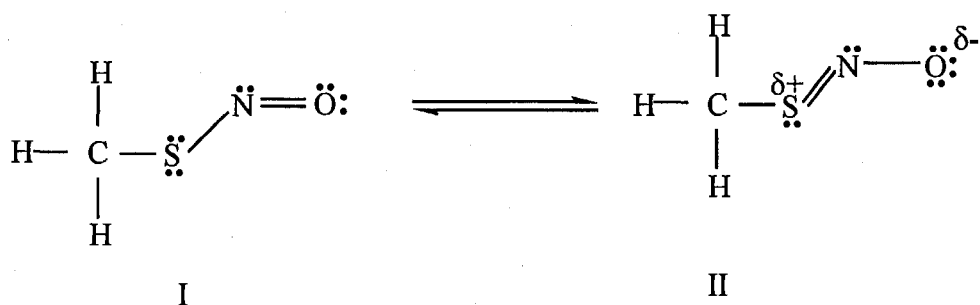


Figure 1.10: Resonance structure of S-nitrosothiol

The thermal stability of RSNO is controlled by the strength of the S-N bond.

The strength of the S-N bond is a function of the electron releasing substituents near the SNO group. The R group in S-nitrosothiols are electron releasing, they induce electron shift from the lone pairs located on the sulfur atom towards the oxygen (resonance structure II, in **Figure 1.10**). This effect generates a local positive charge on the sulfur atom and therefore strengthens the S-N bond.

This explains why tertiary or secondary S-nitrosothiols are more thermally stable than primary S-nitrosothiols, for example, S-nitroso-N-acetyl D, L-penicillamine (SNAP) and S-nitrosoglutathione (GSNO) have been isolated in the crystalline form while, S-nitrosocysteine (CYSNO) has not yet been isolated¹⁰⁵.

1.5.3.3 Transnitrosation

Transnitrosation is the transfer of the NO functional group from S-nitrosothiols to other thiols through a nucleophilic attack on the nitrogen atom of the S-nitrosothiol¹⁰⁶.



The rates and equilibrium of transnitrosation reactions between different thiols have been determined by Hogg and Meyer^{107,108}. Equilibrium constants and rates of reactions have been obtained for the transfer of the NO group from S-nitroso bovine serum albumin to other thiols¹⁰⁹. If transnitrosation occurs between a relatively stable S-nitrosothiol such as S-nitrosoglutathione (GSNO) or S-nitroso-N-acetyl-D,L-penicillamine (SNAP), to a lower molecular weight thiol such as cysteine, a relatively unstable S-nitrosothiol, such as S-nitrosocysteine (CYSNO) is formed. In the presence of Cu⁺ ion, CYSNO can decompose due to its relative instability to release NO. In the same analogy as above, S-transnitrosation has been implicated as the predominant mechanism through which thiol containing proteins are nitrosated in vivo¹¹⁰.

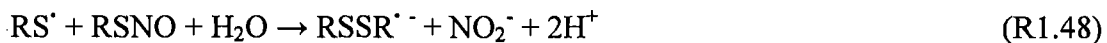
1.5.3.4 Photochemical decomposition

When S-nitrosothiols are irradiated with light at their absorption bands, homolytic cleavage of the S-N bond may occur generating NO and thiyl radicals¹¹¹⁻¹¹⁴:



The generation of the NO and thiyl radical was confirmed by EPR trapping experiments¹¹¹. The mechanism of the reaction was elucidated by flash and laser

photolysis and the following reaction sequence was proposed¹¹⁵:



Peroxynitrite (ONOO^-) was identified as the final product of photolysis of S-nitrosothiols¹¹⁵. Photochemical decomposition of S-nitrosothiols has found many uses in therapeutic applications. For example, photolysis of S-nitrosothiols is used for localized generation of NO and ONOO^- , laboratory experiments with HL-60 leukemia cells have shown that visible light irradiation of S-nitrosoglutathione resulted in an enhanced cytotoxic effect of S-nitrosoglutathione on HL-60 leukemia cells¹¹⁶ while NO radical generated has been implicated in proper eye functions due to its ability to relax smooth muscles¹¹⁷.

1.5.3.5 Enzymatic decomposition

Gamma glutamyl transpeptidase (GGT) is a liver enzyme which transfers amino acid across cell membranes¹¹⁸. It is known that metal ion catalysis greatly accelerates the decomposition of SNAP, but has little effect on GSNO¹¹⁹. Askew and his group discovered that the decomposition pathway of GSNO is through enzymatic cleavage

of the glutamyl-cystyl peptide bond, resulting in the generation of S-nitrosocystylglycine which is more susceptible to metal ion catalysis, with the release of NO¹¹⁹. This is schematically shown in **Figure 1.11**.

1.5.3.6 Potential therapeutic applications of S-nitrosothiols

S-nitrosothiols have some potential therapeutic applications in physiological systems due to properties such as transnitrosation, metal-catalyzed decomposition and enzymatic decomposition. These above mentioned properties of S-nitrosothiols have been discussed, along with their relevant physiological activities and in all; NO are released. The ability of RSNO's to release NO makes the future of RSNO's as drugs promising, particularly in cardiovascular therapeutics. Some RSNO's have made it into the commercial market, examples of which are, SNAP, N-acetyl-S-nitrosopenicillaminy-S-nitrosopenicillamine and GSNO, where therapeutic application is for elicitation of vascular relaxation particularly in areas of damaged endothelium¹²⁰. An important endogenous RSNO is S-nitrosoalbumin, the most abundant circulating S-nitrosothiol in vivo, which acts as a reservoir of NO⁸⁵. S-nitrosoalbumin has been used as a vascular support coating inside of blood vessels to reduce platelet adhesion¹²¹. Other common applications of RSNO's are in decreasing acute and chronic elevations of blood pressure^{122,123} and host defense by inhibiting HIV-1 protease, an enzyme involved in replication of HIV virus^{124,125}. GSNO has been shown to prevent T-cell mediated inflammation¹²⁶.

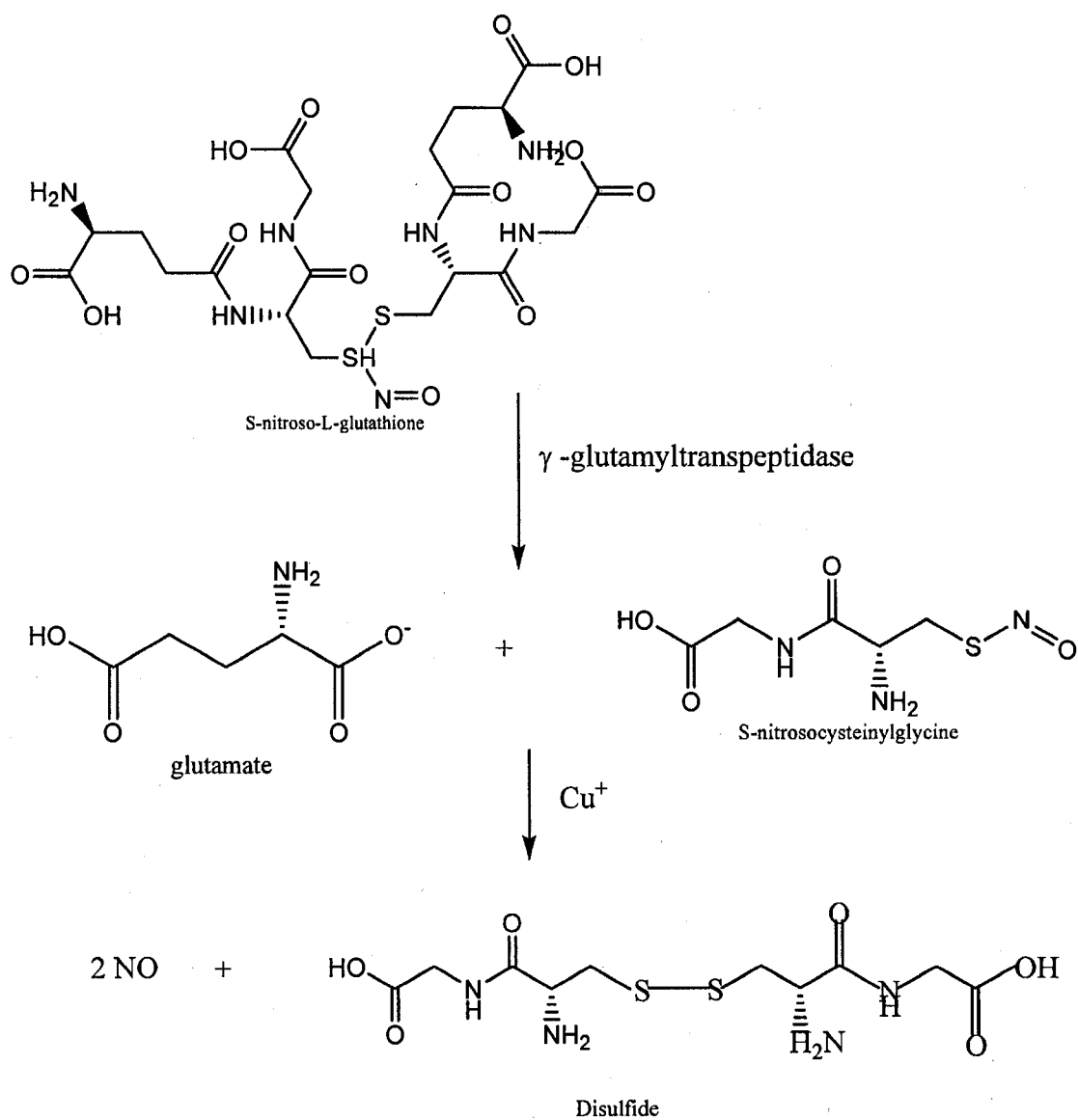


Figure 1.11: Enzymatic decomposition of S-nitroso-L-glutathione

1.6 CHEMISTRY OF PEROXYNITRITE

1.6.1 Relationship between NO and peroxynitrite

NO is a simple inorganic molecule that is produced in the endothelial cells of vessels, neurons, macrophages. It is a free radical capable of oxidative-reductive chemistry. Peroxynitrite [O=NOO⁻, oxoperoxonitrate (-1)] (PN) is a strong oxidant that can be generated from nitric oxide^{127,128}. It is produced by activated alveolar macrophages¹²⁹, neutrophils^{130,131} and endothelium¹³², from the reaction of NO with superoxides radical anions^{133,134}. The rate constant for this radical-radical combination reaction is $3.8-6.7 \times 10^9 \text{ M}^{-1} \text{ s}^{-1}$, as determined by flash photolysis¹³⁵⁻¹³⁸. This reaction constitutes an important sink for superoxide radical anion (O₂^{•-}) because it is about twice as fast as the maximum velocity of superoxide dismutase (SOD)¹³⁹. PN is not a free radical but an oxidant and nitrating agent. The unpaired electrons on nitric oxide and superoxide radical anion combined to form a new N-O bond. PN has a high rate of diffusion, as it has been reported to diffuse through cell membranes before its decomposition^{140,141}. Consequently, PN is known to oxidize cells which leads to pathologically relevant conditions, such as lipid peroxidation¹⁴², rapid oxidation of sulfhydryls¹⁴³ and methionine^{144,145}, ischemia and reperfusion¹⁴⁶ brain injury¹⁴⁷ and ultimately apoptosis¹⁴⁸.

1.6.2 Properties of peroxynitrite

1.6.2.1 Spectral properties: Peroxynitrous acid (ONOOH) and its conjugate base (ONOO⁻) have a yellow color with the color of the anion being more intense.

Peroxynitrite has a single, rather broad absorption band in the ultraviolet region centered at 302 nm in aqueous alkaline solution¹⁴⁹. Molar absorptivity coefficient of $1670 \pm 50 \text{ M}^{-1} \text{ cm}^{-1}$ was reported by Hughes and Nicklin¹⁴⁹. Solid state peroxynitrous acid IR absorption lines were determined by Cheng and co-workers as 3545.5, 1703.6, 1364.4, 952.0, and 772.8 cm^{-1} .

1.6.2.2 Conformation properties: According to quantum mechanical calculations, there is partial double bond character between nitrogen and the first peroxide oxygen. Around this bond, peroxynitrite can occur in two conformations; *cis* and *trans*¹⁵⁰. X-ray structure analysis shows that peroxynitrite crystallizes in the *cis* form (most stable conformation), relative to the N-O bond^{151,152}.

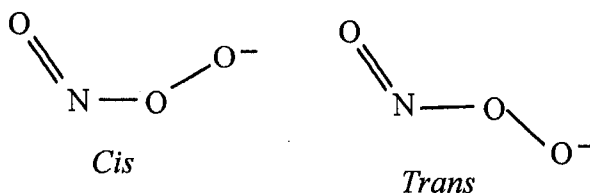


Figure 1.12: *Cis*, *trans* conformation of peroxynitrite.

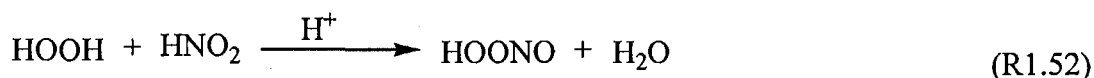
The *cis* conformation is stabilized by 3-4 kcal mol^{-1} relative to the *trans* conformation. This stability is achieved by delocalization of the negative charge over the entire molecule. Only the *trans* form, however, is able to rearrange or isomerize to

nitrate¹⁵³, thus explaining its instability.

1.6.2.3 Thermodynamic properties: The enthalpy of formation of peroxyxynitrite was determined to be $\Delta_f H = -42 \pm 4 \text{ kJ mol}^{-1}$ by calorimetric measurements while the enthalpy of isomerization of peroxyxynitrite to nitrate was measured by solution calorimetry and determined to be $-163 \pm 4 \text{ kJ mol}^{-1}$ at 24°C ¹⁵⁴. Based on the results of standard Gibbs energy of homolysis of (16 kcal mol^{-1}) and rate of homolysis of $1.0 \times 10^{-2} \text{ s}^{-1}$, enthalpy of peroxyxynitrous acid ionization was determined by Koppenol and his group as $4 \pm 2 \text{ kcal mol}^{-1}$ ¹⁵⁵. It is generally agreed that peroxyxynitrite ionizes near pH 6.0.

1.6.3 Synthesis of peroxyxynitrite

Peroxyxynitrite was synthesized as early as 1922 from a mixture of acidified hydrogen peroxide and nitrous acid:



Better results were achieved with the use of quench flow reactor, which was first described in 1974¹⁵⁶. Recently, there have erupted many different methods for the synthesis of peroxyxynitrite. Some of these methods are listed in **Table 1.3**, below:

Preparative synthesis (Methods)	References
Reaction of ozone with azide ions	157
Autooxidation of hydroxylamine	158
Reaction of hydrogen peroxide with nitrous acid	156,159,160
Reaction of hydrogen peroxide with alkyl nitrites (RONO)	161
Reaction of nitric oxide with hydrogen peroxide	162
Reaction of nitric oxide with potassium superoxide	160
Reaction of nitric oxide with tetra methyl ammonium super oxide ($\text{Me}_4\text{N}^+\text{O}_2^-$)	163-165
Photolysis of solid potassium superoxide	166
<i>In situ</i> syntheses	
Nitric oxide and superoxide anion radical generated independently and continuously	167
Nitric oxide and superoxide anion radical formed simultaneously from a single source	168

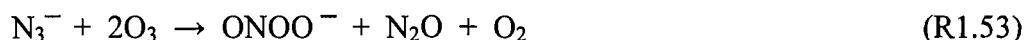
Table 1.3: Various methods for synthesis of peroxyxynitrite

The first eight methods are used in studies where concentrated solutions of peroxyxynitrite are needed, while the last two methods are for production of low concentrations of peroxyxynitrite over an extended period of time.

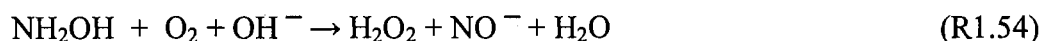
Synthesis of concentrated solutions:

The ozonation of azide ions in mildly alkaline solution (pH ~12) produces stable, concentrated solutions of peroxynitrite, that are low in alkaline and free from hydrogen peroxide. Contaminants are unreacted azide and nitrite ($\leq 5\mu\text{M}$).

Reaction stoichiometry is summarized as:



In autooxidation, hydroxylamine is reacted with oxygen in a moderately alkaline solution containing 0.1-0.5 M NaOH:



Yields of peroxynitrite are approximately 25 % of the starting concentration of hydroxylamine. This synthesis contains nitrite, hydrogen peroxide and some unreacted hydroxylamine as contaminants.

Acidified solutions of hydrogen peroxide rapidly react with sodium nitrite followed by stabilization of the product with sodium hydroxide:





This method of synthesis produces a significant amount of alkaline, nitrite and hydrogen peroxide as contaminants.

Alkaline hydrogen peroxides react with alkyl nitrites (RONO) to produce peroxyxynitrite:



where R = 2-ethoxyethyl, 2-methoxyethyl or isoamyl nitrite

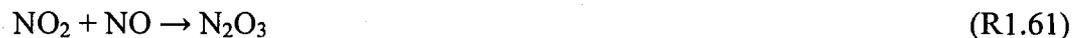
If hydrogen peroxide and alkyl nitrite are used in equimolar amounts, then the peroxyxynitrite solution produced has nitrite, hydrogen peroxide, alkaline and 2-ethoxyethanol (or 2-methoxyethanol) as contaminants in about the same concentration as peroxyxynitrite.

Nitric oxide reacts with hydrogen peroxide in basic media (pH 12.5 – 13.5) to also produce peroxyxynitrite:



Yield is about 2 % of the starting concentration of hydrogen peroxide. The mechanism of this reaction is not clear because nitric oxide is not a known

nitrosating agent. It is most probable that oxygen is involved in the conversion of NO to N₂O₃, to produce a good nitrosating agent:



The reaction of nitric oxide with solid potassium superoxide generates potassium superoxide.



The potassium peroxyxynitrite formed is extracted into a mildly alkaline solution. This synthesis may contain some peroxide formed from disproportionation of unreacted potassium superoxide.

Reaction of nitric oxide with tetramethylammonium superoxide in liquid ammonia produces analytically pure tetramethylammonium peroxyxynitrite. This method uses the same principle as the reaction of solid NO and KO₂ method above, but the use of liquid ammonia and tetramethylammonium superoxide as starting materials is very critical:



Solid state peroxyxynitrite is obtained by fractional crystallization from liquid ammonia.

This dry sample is stable over many months if stored under nitrogen.

Radiation of solid potassium nitrate with 254 nm UV light causes accumulation of peroxyxynitrite to a steady state level of about 30 $\mu\text{mol/g}$ of potassium nitrate.

Overall yield is $\sim 0.3\%$.



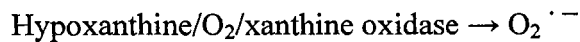
Contaminants in this method of preparing peroxyxynitrite are nitrite and nitrate.

Synthesis in situ

In the *in situ* synthesis of peroxyxynitrite (the last two methods in **Table 1II**), source of nitric oxide is spermine NONOate, a nitric oxide releasing system:



A good source of superoxide radical anion includes the hypoxanthine, oxygen and xanthine oxidase mixtures:



This superoxide radical can then be reacted with NO generated from biological

activity to yield peroxynitrite:

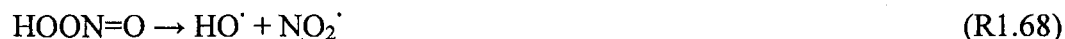


These methods allow the preparation of low steady state concentrations of peroxynitrite even under physiologically-relevant conditions.

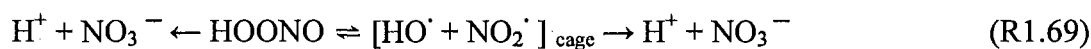
The method of choice for preparation of peroxynitrite in this study will be the synthesis from nitrite and acidic hydrogen peroxide. Residue nitrite and hydrogen peroxide, the two most troublesome contaminants, are less than 2 % of the peroxynitrite concentration. Nitrite contamination can be minimized by making nitrite the limiting reagent. Hydrogen peroxide contamination can then be removed by passing the peroxynitrite solution over manganese dioxide¹⁶⁹.

1.6.4 Decomposition of peroxynitrite in aqueous solution

The chemistry of decomposition of PN in aqueous solution is very complex^{170,171}. In general, two pathways of PN decomposition have been proposed. The first pathway suggests that the product of decomposition of PN at pH < 5 is nitrate. Some studies have argued that PN is cleaved homolytically to generate hydroxyl radical and NO₂ radical^{171,172}:



Beckman *et al*'s suggestion that PN could undergo O-O bond homolysis to generate hydroxyl radical (HO \cdot) and nitrogen dioxide radical (NO $_2\cdot$) has been skeptically received. Against this, Koppenol *et al*¹⁷³ concluded from molecular dynamic calculations that homolytic cleavage of PN is highly improbable. It was later suggested that isomerization/rearrangement of PN to NO $_3^-$ at low pH conditions might involve the formation of an activated ("in cage") intermediate (ONOOH*), which might account for the "hydroxyl radical-like" reactivity of peroxyxynitrite^{174,175}.



The second pathway indicates that PN decomposes at pH > 7 to nitrite and oxygen at the expense of nitrate¹⁴². Mayer and colleagues¹⁷⁶ reported that at pH > 7 nitrite and oxygen were produced in a pH dependent manner in a 2 : 1 stoichiometric ratio. The yield of nitrite was found to level out at pH 9-10 to a value of 50-55 percent relative to the initial amount of PN. This finding was confirmed by others¹⁷⁷⁻¹⁷⁹. The 2 : 1 stoichiometric ratio of nitrite/oxygen was explained by a bimolecular reaction of the peroxyxynitrite anion with peroxyxynitrite acid through the formation of an adduct:



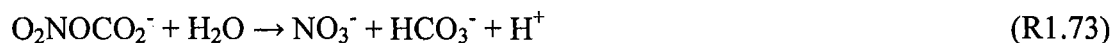
1.7 SOME BIOLOGICALLY IMPORTANT PEROXYNITRITE REACTIONS

1.7.1 Peroxynitrite-CO₂ reaction

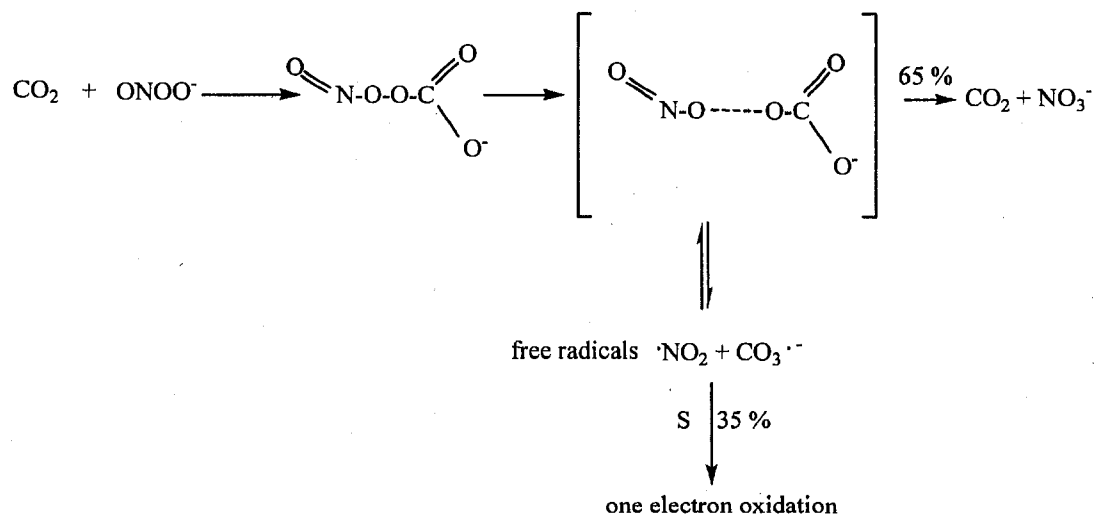
Peroxynitrite is a nucleophile which reacts with electrophilic CO₂ in physiological milieu to form nitrosoperoxycarbonate (ONOOCO₂⁻), reaction (R1.71):



This reaction is very fast, and said to determine the fate of peroxynitrite in the physiological system due to the high concentrations of CO₂ (>1 mM) in the human plasma. Once formed, ONOOCO₂⁻ is unstable and can either spontaneously rearrange to the nitrocarbonate anion which later hydrolyze to generate nitrate and bicarbonate (reaction R1.72):



O₂NOCO₂⁻ can also decompose through homolysis of the O-O bond to yield 35 % carbonate radical (CO₃^{-•}) and nitrogen dioxide radicals (NO₂) and 65 % carbon dioxide and nitrate anion¹⁸⁰⁻¹⁸² (Scheme 1.3). In this manner, CO₂ helps to decompose ONOO⁻ in the physiological systems.



Scheme 1.3: Mechanism of reaction of CO₂ with ONOO⁻

1.7.2 Nitration reactions

Peroxynitrite is a good nitrating agent for phenolic compounds such as phenol, tyrosine, and salicylate¹⁸³. Peroxynitrite mediated the nitration of tyrosine at pH 7.0 and 25 °C¹⁸⁴. Ramezani and his group found out that the nitration of tyrosine is independent of the rate of decomposition of peroxynitrite and so concluded that $\cdot\text{OH}$ and $\cdot\text{NO}_2$ are responsible for nitration¹⁸³. The formation of bityrosine during nitration was concluded as a clear evidence of radical mechanism¹⁷². The mechanism of tyrosine reaction with peroxynitrite was proposed to proceed as follows¹⁸⁵:





The overall nitration mechanism can be summarized as a one electron oxidation of the aromatic ring of tyrosine followed by the radical-radical reaction of tyr^\cdot and $\cdot\text{NO}_2$ to form nitrotyrosine (tyrNO_2)^{185,186}.

1.7.3 Peroxynitrite-thiol reaction

Thiolate ions, being nucleophilic may be oxidized in the presence of peroxynitrite.

The oxidation of thiols by peroxynitrite (ONOO^\cdot) can occur through multiple pathways whose mechanisms are, presently, poorly understood. It is known, however, that ONOO^\cdot may directly oxidize thiols, in the basic medium through a two-electron pathway, probably with the formation of sulfenic acid and formation of disulfide (**Figure 1.13, pathway a**). The apparent second-order rate constants for the reaction of thiols with ONOO^\cdot have been reported to range from 2.0×10^3 to $5.9 \times 10^3 \text{ M}^{-1} \text{ s}^{-1}$ ^{143,187} at pH 7.4 and 37 °C. These rate constants are three orders of magnitude greater than the corresponding rate constant for the reaction of hydrogen peroxide with sulfhydryls at similar pH^{143,188}. At lower thiol/ ONOOH ratio and acidic pH, a one electron oxidation process occurs through the formation of $\cdot\text{OH}$ and $\cdot\text{NO}_2$ yielding thiyl radicals^{189,190} (**Figure 1.13, pathway b**). It is also note-worthy that

ONOO⁻ reacts with thiols at acidic pH (pH = 0) to produce the corresponding thionitrites¹⁹¹ as an intermediate. Grossi *et al*, concluded that at very low pH conditions, peroxyxynitrous acid undergoes decomposition to form NO⁺, which is capable of nitrosating thiols¹⁹² (**Figure 1.13, pathway c**). Disulfides are also formed as the final products in a manner independent of the pH. They also claimed that, in basic media (pH 10.5 – 13), thiols catalyze the decomposition of peroxyxynitrite, which promotes oxidation of thiols through sulfanyl radicals and finally to the disulfides¹⁹³.

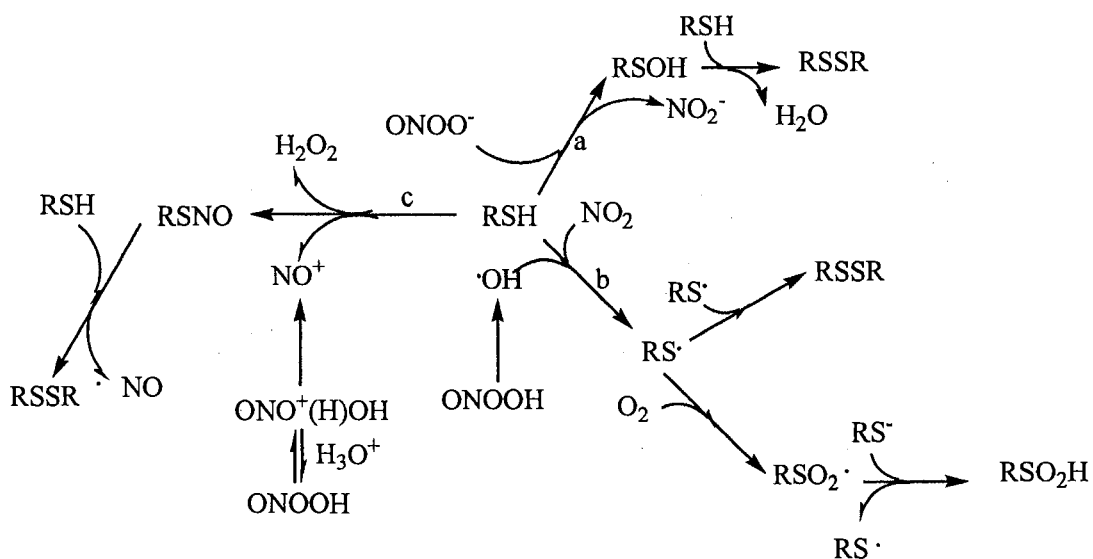


Figure 1.13: Pathways of thiol oxidation by peroxyxynitrite (a) two electron pathway (b) one electron pathway and (c) pathway leading to formation of nitrosothiols.

1.8 SUMMARY OF NO REACTIVITIES IN BIOLOGICAL SYSTEMS

Biosynthesis of NO is possible through the enzymatic oxidation of L-arginine to L-citrulline^{194,195}. Once NO is produced, it is facile to undergo vast reactions with products of distinct life times and biological activities. NO, being a free radical, can lose an electron and exists in the +3 oxidation state (NO^+), while it could gain an electron and exists with an overall negative (-) charge, in the +1 oxidation state (NO^-). NO^+ reacts with H_2O_2 to produce ONOO^- ¹⁹⁶, also NO^- reacts with O_2 to produce ONOO^- ¹⁹⁷. However, differences in rate constants for association and dissociation of NO have great biological significance. Some of the biologically significant reactions of NO have been discussed, and the array of possible reactions of NO and products are schematically summarized in **Figure 1.14**.

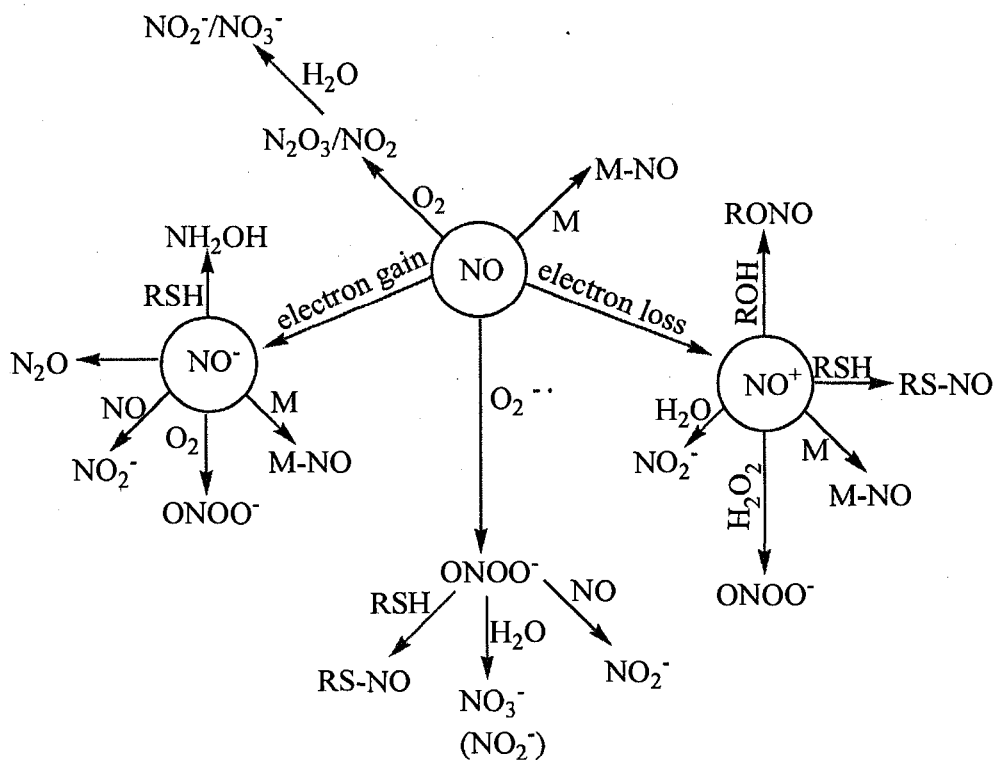


Figure 1.14: NO reactivity in the biological system

Chapter 2

2. INSTRUMENTATION, MATERIALS AND METHODS

2.1 INTRODUCTION

The study of chemical reaction dynamics requires as much information as possible about the progress of a reaction. This information includes all dynamical variables within the reaction mixture: reactant depletion, intermediate(s) formation, product formation, pH and temperature variations as well as change in ionic strength. First and foremost, the stoichiometry of the reaction under study must be established. Determination of reaction stoichiometry will identify and establish the optimum conditions under which all the species involved can be studied. Rate data from elementary steps are needed in elucidating complex reaction mechanisms. The rate is determined by monitoring the concentrations or specific property of the reagents as a function of time using an appropriate or adequate analytical technique. Analytical techniques used in kinetic studies to make rate measurements include nuclear magnetic resonance, electron paramagnetic resonance, ultraviolet and visible spectroscopy, chemical trapping, and mass spectroscopy. Many of these techniques however, are incapable of monitoring reactions that occur on fast time scales. A valuable procedure for rapid kinetics studies is the stopped-flow technique.

This chapter gives an overview of the instrumentation, materials, as well as the experimental methods and techniques that were used in quantifying the extent to which selected thiols deactivated peroxyxynitrites, rates of the deactivation processes and reaction products generated by peroxyxynitrite oxidation.

2.2 INSTRUMENTATION

2.2.1 Conventional UV/Vis Spectrophotometry

Slow reactions with half-lives of several minutes or more were followed on a Perkin Elmer Lambda 25S UV/Vis spectrophotometer with wavelength range from 190 nm to 1100 nm. The visible region uses a tungsten lamp and the UV wavelength region uses deuterium lamp. The Perkin Elmer spectrophotometer is interfaced to a Pentium IV computer and uses the UV WinLab Software for data collection and analyses. Path length of cuvette is 1 cm and a constant temperature of 25 °C was maintained during the duration of the measurements by using a thermostated water bath.

2.2.2 Stopped-Flow Spectrophotometry

Fast reactions with a half-life of few seconds or less; require use of a stopped-flow essemble for kinetics investigations. The use of stopped-flow techniques allows reactions with time scales as short as milliseconds to be followed. Fast kinetics studies in this work were carried out on a SF-61 DX2 double mixing spectrophotometer. The schematic diagram of this instrument, which is shown in **Figure 2.1** reveals all its essential components. The stopped-flow spectrophotometer is essentially a hybrid UV/Vis spectrophotometer, designed to follow fast signal changes, with a rapid mixing accessory: the sample handling unit. Two or more reagents are held in the drive syringes, these are rapidly driven into the mixing chamber causing them to mix rapidly,

initiating the reaction under study and displacing the aged solution as a new reaction mixture is driven into the observation cell (**Figure 2.2**). The SF-61 DX2 Sample Handling Unit (SHU), facilitates both the single mixing of two reagents, using only one of the drives, or double mixing of three reactants by a push-push mode of operation. The latter mode of operation enables transient species formed by mixing, to be subsequently mixed with a third reactant after a delay period¹⁹⁸. The resulting reaction is followed in the manner associated with classical stopped-flow techniques. A stop syringe, used to set a driven volume, stops the flow. The stop syringe plunger's travel is finally restrained by a rigid stop block which causes rapid deceleration of the solutions and subsequently triggers the data acquisition system. This instrument enables reactions on seconds timescales to be followed by optical changes using both absorbance and fluorescence detection. The process of mixing in a stopped-flow apparatus can be considered as occurring in two stages. The mixer takes in two liquids: solution A and solution B, and partitions each into small volume elements, so that a region of A is next to a region of B. Mixing is completed by the diffusion of the solute in A into the region of B, and vice versa. Part of this diffusion occurs in the liquid as it flows from mixer to observation point, in the dead volume. The more efficient the mixer, the finer is the subdivision into small volumes, and the more rapid the subsequent diffusion. Diffusion is slower in more viscous solvents, and mixing is slower. Chemical reaction can only occur after the second stage, when the reagents of A and B are in contact at the molecular level¹⁹⁸. This is why reaction traces for very fast reactions, at the limit of measurability, have a characteristic sigmoid shape.

This is due to the fact that the reaction goes slowly over the millisecond time period because the reagent concentrations have not reached the value for complete mixing. A short dead time, as measured above, is not necessarily a good thing. The solution at the observation point may be young, not because it was transported rapidly from the mixer, but because it is still being mixed in the observation cell. Mixing sets an upper limit for rate constant obtainable from this instrument. The apparatus is designed such that the mixing time is less than the dead time, but not much less. When observed rate constants in excess of 1000 s^{-1} are measured, experimental values are significantly less than what linear extrapolation predicts because mixing is incomplete on the time scale at which reaction occurs. The extent of the effect depends on the nature of the reaction and on solvent viscosity, and has to be studied for each particular system.

The SF-61AF spectrophotometer sample handling unit facilitates only single mixing of two reagents. It uses proprietary software for data acquisition and analysis. Any good data-collection program, such as the Hi-Tech IS 1.0, filters out the noise by digital processing of the data. The virtue of such a procedure lies in "digitization error". The voltage from the photometric circuitry is converted into a digital form suitable for computer processing by a 12-bit analog-to-digital converter. A logarithmic time base is incorporated into the Hi-Tech Scientific IS-1 program; this is particularly powerful in recording complex multiple exponentials, especially where there is a limited quantity of reagent available, since one can span milliseconds to minutes in only one or two runs. With a logarithmic distribution of data points with respect to time, it is possible to achieve good definition of fast phases, while also achieving good definition of

endpoints for slower phases in a single run. The radiation source is a 12 V, 50 W quartz tungsten halogen lamp. The instrument can also be operated with a 75 W super quiet Xenon arc lamp or 100W short arc mercury lamp as the radiation sources. The monochromator used is a Czerny-Turner type mounted on a rail. There are two photomultipliers, a PM-60e (an end-on ½ inch Hamamatsu R1463) and a PM-60s (a side-on 1-1/8 inch Hamamatsu R928 HA). The passage of light from the monochromator to the photomultiplier is through a 600-micron pure silica optic fiber. The optical cell is made from fused UV silica. It measures 10 mm x 1.5 mm x 1.5 mm. The path length is 10 mm or 1.5 mm depending on the position of the optic fiber. The diode array attachment is a compact multi-channel detector incorporating a linear image sensor. The linear image sensor is a self-scanning photo diode array with scanning circuit using N-channel transistors turned on by a positive gate voltage. In conjunction with the "IBM-PC KINETASYST" software, the Rapid Scan diode array provides a facility to collect and display a sequence of spectrally resolved data which can be manipulated, analyzed and stored; furthermore cross-sections can be cut through multiple traces to generate time-resolved kinetic traces.

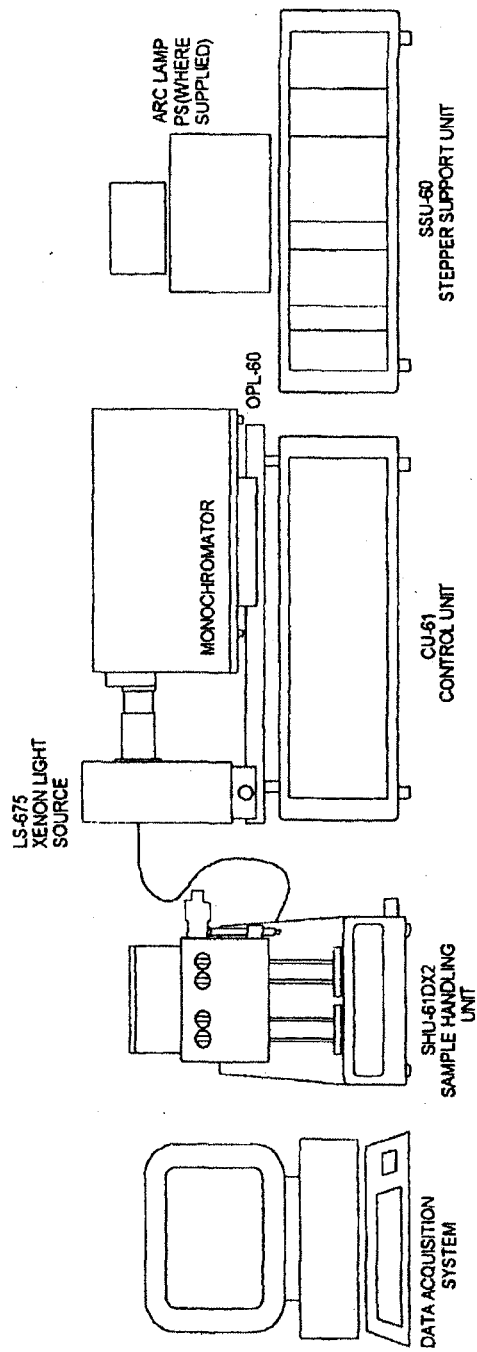
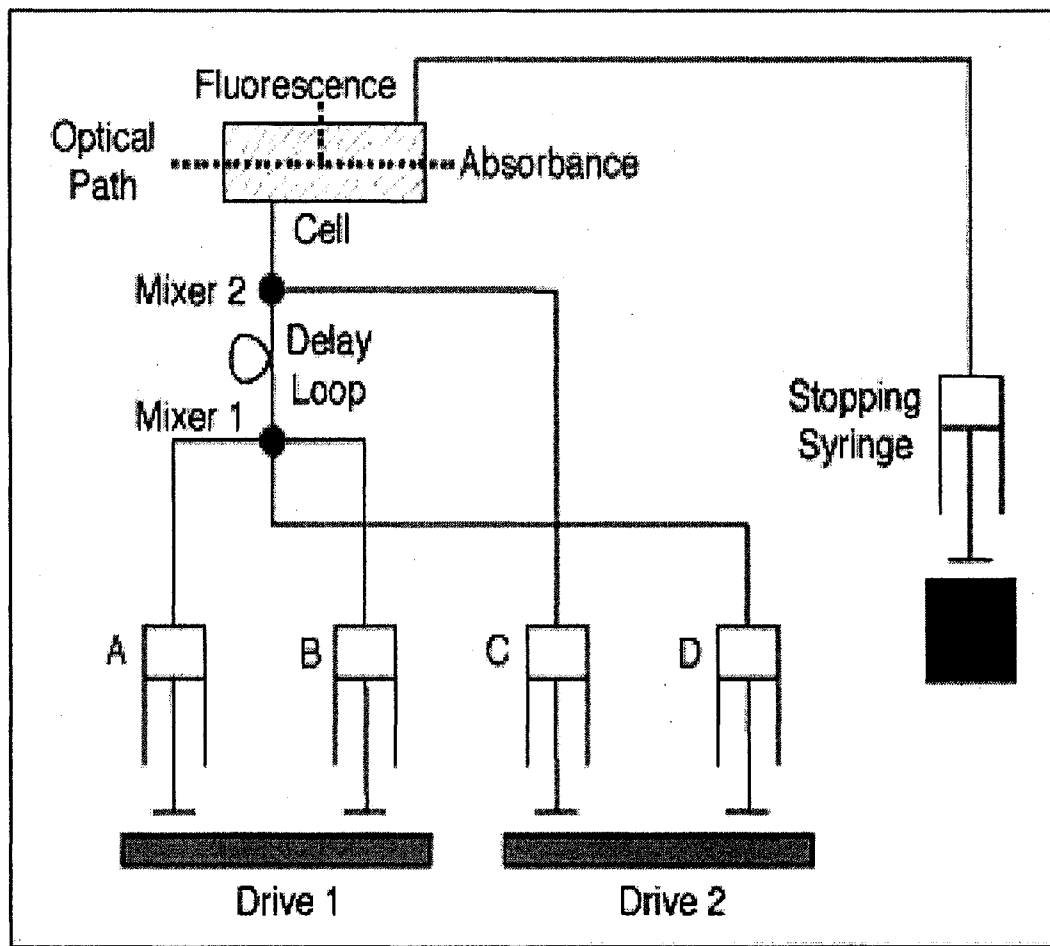


Figure 2-1: Schematic diagram showing all components of the SF61-AF stopped-flow fluorimeter.

[Courtesy of Hi-Tech Scientific Operator's Manual].¹⁹⁸



Double Mixing Stopped-Flow

Figure 2-2: Sample Handling Unit (SHU) flow circuit diagram for the double mixing SF-61-DX2 stopped-flow system.
 [Courtesy of Hi-Tech Scientific Operator's Manual]¹⁹⁸

2.2.3 Electron Paramagnetic Resonance (EPR) Studies

EPR has matured into a powerful, versatile, nondestructive and non-intrusive analytical method, yielding meaningful structural and dynamical information.

It is an ideal complementary technique for other methods in a wide range of studies and application areas. Some important applications in chemistry, biology, engineering and medicine include:¹⁹⁹

- (i) Kinetics of radical reactions
- (ii) Spin trapping
- (iii) Triplet states of molecules and biradicals
- (iv) Drug detection, metabolism, and toxicity
- (v) Antioxidants, radical scavengers
- (vi) Oxygen based radicals
- (vii) NO in biological systems and
- (viii) Carcinogenic reactions
- (ix) Polymerization reactions
- (x) Organo-metallic compounds
- (xi) Catalysis
- (xii) Petroleum research

It is known that a molecule or atom has discrete quantized states with corresponding energies. The measurements and interpretations of energy differences (ΔE) between atomic and molecular states are known as spectroscopy. These energy differences are measured in relation to the absorption of electromagnetic radiation.

$$\Delta E = h\nu, \tag{2.1}$$

where h = plank's constant, ν = frequency of the radiation

EPR spectroscopy studies energy differences that are predominantly due to interaction of unpaired electrons in the sample with a magnetic field produced by a magnet. This effect is called the Zeeman effect. From quantum mechanics, we obtain the most basic equations of EPR:

$$E = g \mu_B B_0 M_S = \frac{1}{2} \pm g \mu_B B_0 \tag{2.2}$$

and

$$\Delta E = h\nu = g \mu_B B_0 \tag{2.3}$$

where g is the g-factor, which is a proportionality constant approximately equal to 2 for most samples, but varies, depending on the electronic configuration of the radical or ion. μ_B is the Bohr magneton, which is the unit of electronic magnetic moment and B_0 is the magnetic field. The unpaired electron, which gives the EPR spectrum, is very sensitive to its local surroundings. The nuclei of the atoms in a molecule often have a magnetic moment, which produces a local magnetic field at the electron. The interaction between the electron and the nuclei is called the hyperfine splitting.

The simplest possible spectrometer has three essential components, a source of

electromagnetic radiation, a sample and a detector. Electromagnetic radiation passes through the sample, then the amount of radiation which passes through the sample is measured and observed with a detector. For all the work that was done in this thesis, EPR measurements were carried out on Bruker™ Biospin's e-scan spectrometer designed to perform X-band EPR measurements. **Figure 2.3** shows the general outline of the instrument. The electromagnetic radiation source and the detector are located in a box called the microwave bridge. The sample is placed in the microwave cavity in a small box which helps to amplify weak signals from the sample. There is the magnet whose function is to tune the electronic energy levels. Lastly, there is the console which contains signal processing and controls electronics and a computer. The computer is used for analyzing data as well as co-coordinating all the units for acquiring a spectrum (**Figure 2.3**). The block diagram of the microwave bridge is shown in **Figure 2.4**.

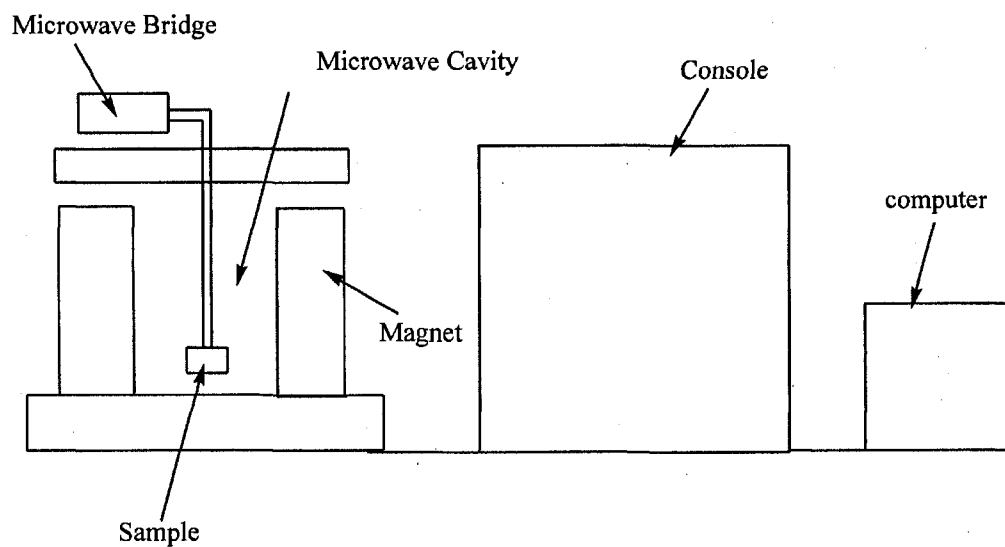


Figure 2.3: General outline of an EPR spectrometer

The instrument is interfaced to a computer with data acquisition and analysis carried out with WIN-EPR 2.22 rev. 5 acquisition software. Short-lived free radical intermediates of interests were detected by using spin trapping techniques^{200,201} This technique utilizes an addition reaction of a very reactive short-lived free radical with a diamagnetic compound (spin trap) to produce a relatively long-lived free radical adduct which can be studied by electron spin resonance. The radical traps of choice used in this research work are 5, 5-dimethyl-1-pyrroline N-oxide (DMPO) and N-tert-butyl-alpha-phenylnitron (PBN). The instrument comes with the following spectrometer settings: Microwave power: 31.55 mW; Receiver Gain: 8.93×10^2 ; Modulation frequency: 86.00 kHz; Modulation amplitude 1.99 G; Sweep time 2.62 sec; Time Constant: 5.120 ms; Sweep Width: 100 Gauss and centered about the $g = 2$ resonance position.

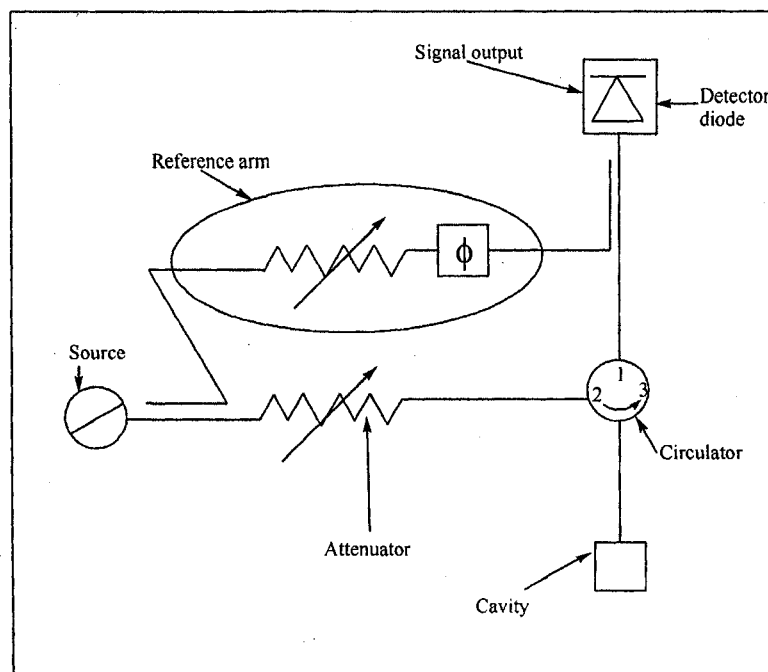


Figure 2.4: Block diagram of the microwave bridge.

2.2.4 Mass Spectrometry

A mass spectrometer (MS) is an apparatus which produces a beam of ions from a sample, sorts out the resulting mixtures of ions according to their mass-to-charge ratio, then provides an output signal on a read out. MS has developed over the years into a versatile analytical tool with wide applications ranging from geological to clinical and pharmaceutical samples. MS enables molecular weight determinations for large samples such as biomolecules, to within an accuracy of 0.01% of the actual molecular weight of the sample. This capability makes MS the most suitable technique for detecting minor mass changes in large biomolecules. Thus covalent modification of protein residues can be studied with ease. Generally, MS consists of four functional elements: (1) the source where a beam of ions, representative of the sample under study is generated; (2) the analyzer, where separation of ions is effected; (3) the detector, where the resolved ions are detected and their intensities are measured and (4) the vacuum system, which provides the environment for all these process.

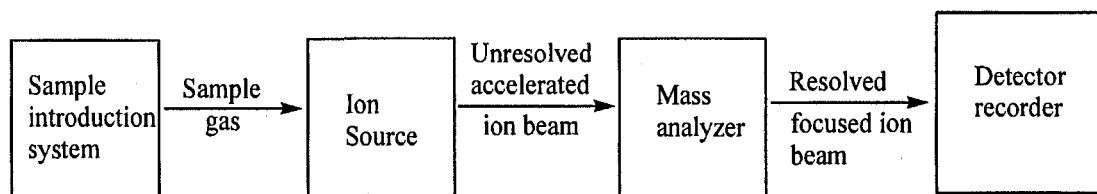


Figure 2.5: The main feature of a mass spectrometer

Specifically, the instrument used in sample analysis in this thesis, Micro TOF-Q is equipped with electrospray ionization (ESI) and orthogonal acceleration time-of-flight (TOF). Micro TOF-Q mass spectrometer provides exact mass measurements in an easy to use bench top package. Its applications include easy formula determination of small molecules, metabolic studies, analysis of complex mixtures, digests and in-depth evaluation of intact proteins. It targets previously characterised compounds in complex mixtures with a high specificity by defining both the molecular weight and a diagnostic fragment of the molecule simultaneously. Components are highlighted in **Figure 2.6**.

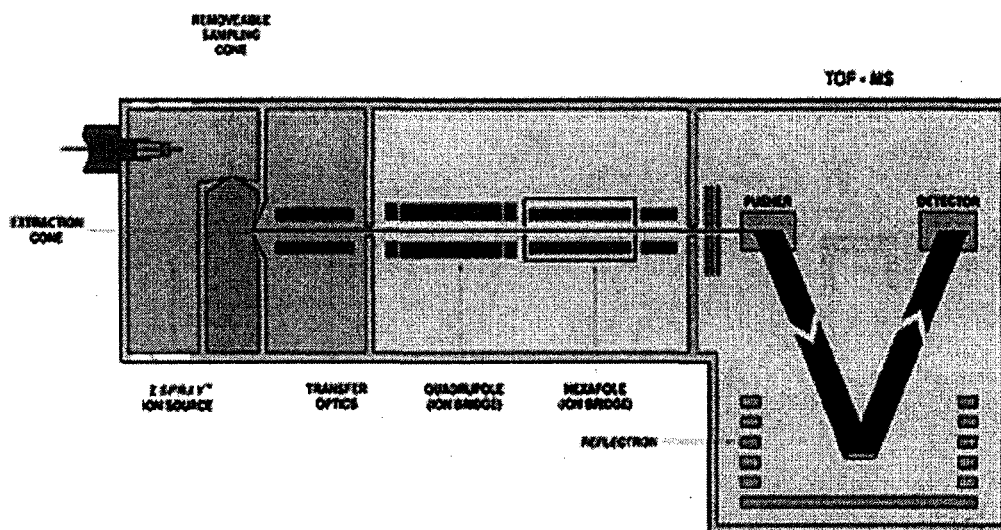
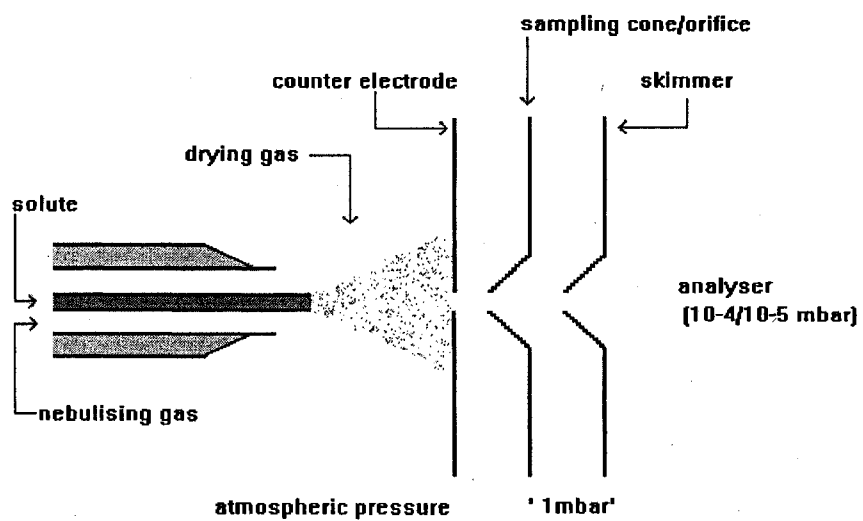
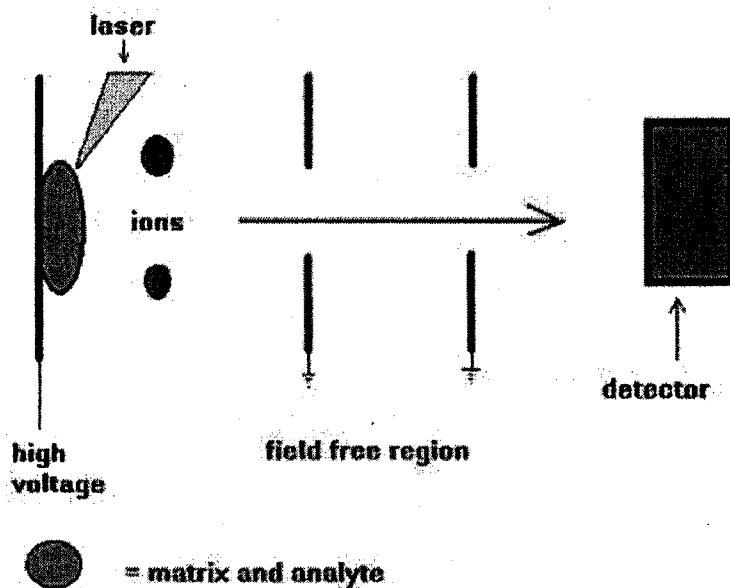


Figure 2.6: Schematic diagram of a Micro TOF Q spectrometer



(a)



(b)

Figure 2.7: Generation of ions by (a) Electrospray Ionization (ESI) and Matrix Assisted Laser Desorption Ionization (MALDI).

Analyte ions were generated by positive-mode electrospray ionization (ESI)²⁰²⁻²⁰⁵ which is depicted in **Figure 2.7(a)**. The sample is dissolved in a polar, volatile solvent and pumped through a narrow, stainless steel capillary (75 – 150 μm i.d.) at a flow rate of between 1 μL per min and 1 mL per min. A high voltage of 3 or 4 kV is applied to the tip of the capillary, which is situated within the ionisation source of the mass spectrometer, and as a consequence of this strong electric field, the sample emerging from the tip is dispersed into an aerosol of highly charged droplets, a process that is aided by a co-axially introduced nebulising gas flowing around the outside of the capillary (**Figure 2. 7(b)**). This gas, usually nitrogen, helps to direct the spray emerging from capillary tip towards the mass spectrometer.

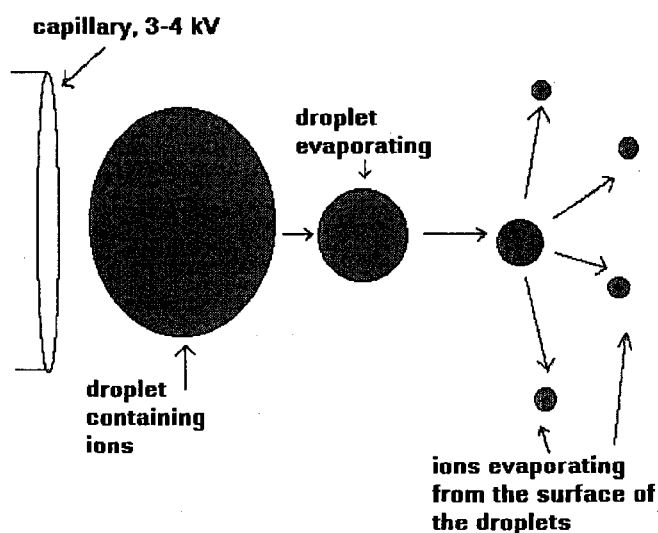


Figure 2.8: Diminishing of the size of the charged droplets with solvent evaporation

The charged droplets diminish in size by solvent evaporation, assisted by a warm flow of nitrogen (known as the drying gas), which passes across the front of the ionisation source. Eventually, charged sample ions, free from solvent, are released from the droplets (**Figure 2.8**), some of which pass through a sampling cone or orifice into an intermediate vacuum region, and from there through a small aperture into the analyser of the mass spectrometer, which is held under high vacuum. The lens voltages are optimised individually for each sample.

2.2.5 High Performance Liquid Chromatography (HPLC)

Liquid chromatography is a physical separation method in which the samples to be separated are distributed between two phases: the liquid mobile phase and the stationary phase. Sample separation is due to differences in distribution coefficients of the individual analytes in the sample. The sample is injected through the injection port into the mobile phase stream delivered by the high pressure pump and transported through the column where separation occurs (**Figure 2.9**). The use of high pressure in liquid chromatography gives this separation method its popular name, high performance liquid chromatography (HPLC). For an efficient separation, important issues such as particle size of stationary phase, column internal diameter, injection volume, constant flow rates and quality solvent mixtures are very important. The specific particle size, columns, injection volumes and flow rates used in this thesis are listed below.

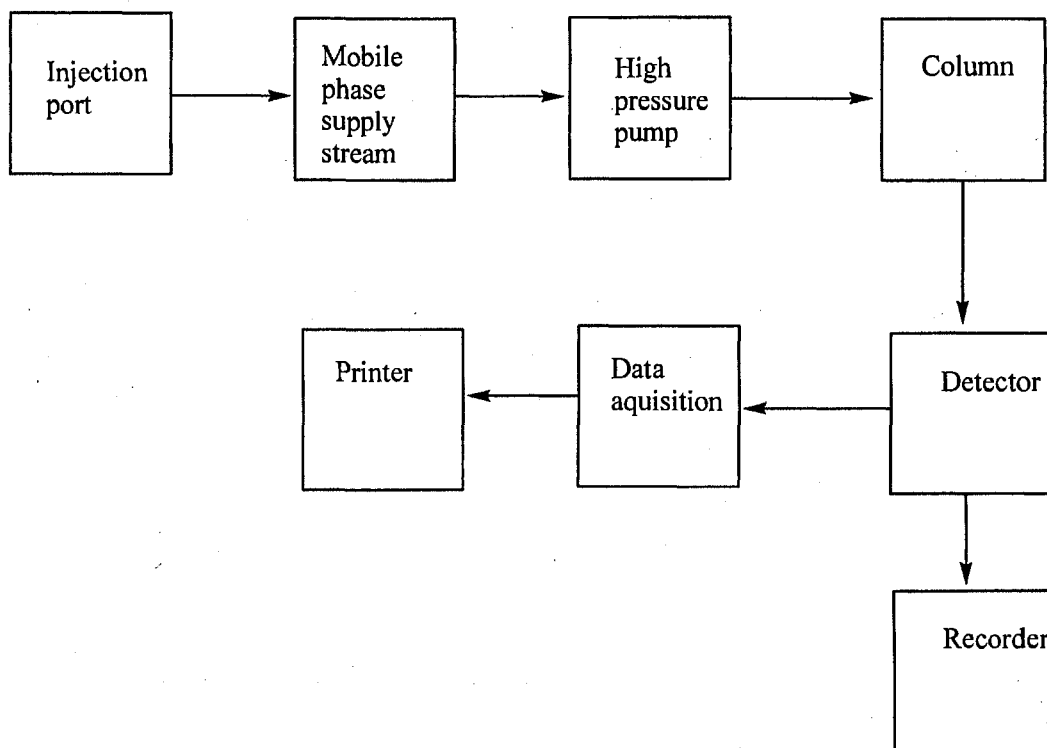


Figure 2.9: The basic liquid chromatography.

HPLC analysis was performed on a Shimadzu Prominence HPLC system controlled by a web browser through a static IP address using the CBM-20A Prominence BUS Communication Module (Columbia, MD). The system consisted of an LC-20AT Prominence LC (Kyoto, Japan) containing four LC-600 pumps, a DGU-20A5 Prominence degasser (Kyoto, Japan) and an SIL-10AD VP auto-injector (Columbia, MD). Detection was performed using an SPD-M10A Diode Array Detector (Columbia, MD) and an RF-10A XL fluorescence detector (Columbia, MD). HPLC grade solvents were filtered on 0.5 μm FHUP (organic) and 0.45 μm HATF (aqueous) Millipore isopore membrane filters (Bedford, MA) before they could be passed through the degasser. Injection volumes ranged from 10 μl to 100 μl and

separations were carried out on a 5 μm particle size, 250 x 4.6 mm Supelco Discovery (Bellefonte, PA) C18 column (reverse phase, 100 \AA pore size) at flow rates ranging from 0.5 to 1 ml per min. For protein modification reactions, separations were done using a 5 μm particle size, 250 x 4.6 mm Phenomenex Jupiter (Torrance, CA) C18 protein column (reverse phase, 300 \AA pore size). Solvents used were acetonitrile, methanol and water. 1 % trifluoroacetic acid (TFA), 1 % formic acid (FA) and other buffered solvents were incorporated whenever the need arose and either isocratic or gradient elutions were utilized. Data was acquired and analyzed using the EZ-Start 7.3 Chromatography Software for Windows (Columbia, MD).

2.2.6 Computer Simulations

A simulation can be referred to as a special type of mathematical model, which uses mathematical symbols to represent the interactions of the systems components at different points in time. We can also say that simulation models are dynamic models which involve changes in the state of the system through time. Simulation models express the dynamic relationships among variables, constants and parameters. When applied to the study of numerical research, simulations can serve as a complementary technique for constructing and understanding chemical research. Simulations use models which imitate and represent a system by trying to imitate the behavior of a system in a step by step basis over time. Some simulation models may be deterministic, stochastic or probabilistic²⁰⁶. In a deterministic model one assumes that the exact values of all parameters are known, while in stochastic model exact values cannot be computed and are not known. Simulations are useful for²⁰⁷

(1) improving understanding of basic research principles and analytic techniques: (2) investigating the effects of problems that arise in the implementation of research; and (3) exploring the accuracy and utility of novel analytic techniques applied to problematic data structures. In a simulation, the analyst first creates data according to a known model and then examines how well the model can be detected through data analysis. An important characteristic of simulation model is the level to which it can aggregate the real system. The model can be a “micro” level model and deal with small units (variable) of the system or it can be a “macro” level model and group the small units into the fairly large units.

2.2.6.1 Role of the computer in modeling

Digital electronic computers are the instruments of choice in computer simulations. Computers rapidly process massive information, data and calculate answers to complex mathematical problems. When the entire data crunching of a simulation is done on a computer it is known as all-computer simulation or more popularly as computer simulation. In computer simulation the computer program represents the system. The experimenter runs this program by supplying values to the variables and parameters in the equations and specifying the experimental controls. The experimenter can re-run this experiment by modifying the controls, by assigning different values to the variables and parameters or changing both the controls and values.

In this thesis *Kintecus*²⁰⁸ was utilized. It is a simulation software package developed by James C. Ianni. *Kintecus* is a compiler to model the reactions of chemical, biological, nuclear and atmospheric processes using three input spreadsheet files: a reaction spreadsheet, a species description spreadsheet and a

parameter description spreadsheet. *Kintecus* uses both the deterministic and the stochastic approaches. The most widely used approach is the deterministic model. In this work, we have used deterministic models for simulating reaction mechanisms. Reaction variables are entered into a model spreadsheet file and *Kintecus* is able to search for these model files and creates species spreadsheet file with all the values already entered and these file are loaded and scanned (run). Output files containing the concentration profiles of all species that are being displayed are then saved. Simulation time is set which could be days, hours, minutes, seconds and picoseconds. *Kintecus* can fit any numerical value (rate constants, third body enhancements, energy of activation, starting temperature etc) against an experimental or fabricated dataset. One might wish to use fabricated data sets to optimize numerical values such as initial concentrations of species to values which would minimize the presence of some harmful intermediate species, maximize certain products reduce and increase temperature and etc. *Kintecus* can fit the parameters at EXACTLY the time the data was measured. *Kintecus* does not interpolate a function against data and then fit the values against this interpolation. There is absolutely no need to neither wipe out data and suggest interpolation methods nor specify timing meshes against experimental data since *Kintecus* calculates values at exactly the times specified in the experimental data file.

2.3 MATERIALS

2.3.1 Analytical chemicals

The following analytical chemicals were used without further purification: sodium nitrite, 99.5 %, Hydrogen peroxide solution 30 % w/w, D-Mannitol sigmaUltra (Sigma Aldrich), sodium hydroxide, certified A.C.S., perchloric acid 70-72 %, sodium perchlorate, disodium ethylenediamine tetraacetate, certified A.C.S., sodium phosphate monobasic, certified A.C.S., glutathione reduced, cystine, glutathione oxidized, sodium bicarbonate, certified A.C.S., L-Ascorbic acid, certified A.C.S., (Fisher scientific), L-Cysteine, 99+ % (Acros-organics), 5,5-Dimethyl-1-pyrroline-N-oxide, high purity (DMPO), N-tert-butyl-alpha-phenylnitron (PBN), (Alexis biochemicals).

2.3.2 Tests for adventitious metal ion catalysis

Reagent solutions were prepared with distilled deionized water (Nanopure) from Barnstead Sybron Corporation water purification unit. Water sample from this unit was analyzed using inductively coupled plasma mass spectrometry (ICPMS). ICPMS analysis showed negligible concentrations of iron, copper, and silver and approximately 1.5 ppb of cadmium and 0.43 ppb in lead as the highest metal ion concentrations²⁰⁹.

2.3.3 Oxidant

The major oxidant used in this study is peroxyxynitrite.

2.3.4 Peroxynitrite synthesis

Peroxynitrite was synthesized in a quenched flow reactor purchased from Cole-Parmer. Solutions of 0.7 M HClO₄, 0.7 M H₂O₂ and 0.6 M NaNO₂ were pumped into T junction tygon tubing and mixed in a 1.6-mm-inside diameter by 10.0 cm tygon chemical tubing. The acid-catalyzed reaction of nitrous acid with H₂O₂ to form yellow peroxynitrous acid was quenched by pumping 1.5 M NaOH at the same rate into a second T junction at the end of the tygon tubing. Excess H₂O₂ was removed by treatment of peroxynitrite solution with granular manganese dioxide. Peroxynitrite was made fresh everyday, before use. Standardization of synthesized peroxynitrite was made both spectrophotometrically and iodometrically. Spectroscopic determination was made using wavelength absorbance maximum of peroxynitrite at 302 nm, with a molar absorptivity coefficient of 1670 M⁻¹ cm⁻¹. In the case of iodometric determinations, the oxidizing power of peroxynitrite was determined by titration with excess acidified iodide. Released iodine was titrated against standard thiosulfate solution. The end point of titration was enhanced by starch indicator spiked with micromolar concentration of iodide ions as a preservative. Concentration of peroxynitrite was then back calculated from moles of thiosulfate.

2.3.5 Thiols

All the thiol compounds used in this work were used without further purification.

The thiol based compounds used were chosen based on the following criteria after solubility in water: (a) their structural similarity to endogenous thiols, (b) possible drug use

and /or effects, (c) confirmed toxicity effects, (d) commercial availability from vendors, (e) storage and stability and (f) kinetic lability. The thiols used are cysteine (CYSH) and glutathione (GSH).

2.3.6 Ionic Strength

Sodium perchlorate was used to maintain an ionic strength of 0.5 M in all kinetic experiments.

2.4 EXPERIMENTAL METHODS

2.4.1 Stoichiometric determination

Stoichiometric determinations of PN-GSH/CYSH reactions were performed in excess oxidant (PN) concentrations. Varying amounts of PN in alkaline pH were first incubated with constant concentration of the reducing substrate. Then, excess acidified iodide was added to the reaction solutions for quantification of iodine by iodometric technique. Since the rate of formation of iodine is faster than the rate of self-decomposition of PN, iodine was quantitatively formed as a function of excess unreacted PN. The released iodine was titrated against standardized thiosulfate.

The end point of titration was enhanced by starch indicator spiked with micromolar concentration of iodide ions as a preservative. Concentration of peroxynitrite was then back calculated from moles of thiosulfate. A plot of the titer volume of thiosulfate versus initial PN concentration was linear. Extrapolating this linear plot to the PN concentration axis gives the exact amount of PN needed to

completely consume the substrate with nothing left to participate in the iodometric titration. This stoichiometry is shown in reaction R4.5 and R5.7. The concentration of excess unreacted PN was also determined spectrophotometrically by its absorbance at 302 nm with molar absorptivity coefficient of $1670 \text{ M}^{-1} \text{ cm}^{-1}$.

2.4.2 Reaction kinetics

Reactions where nitrosothiol was the major product were run at a constant ionic strength of 0.5 M by adding the required amount of sodium perchlorate. Constant ionic strength was maintained in the high acid concentrations (perchloric acid) used in reaction mixtures. Other reaction mixtures were constituted in sodium phosphate buffer without the use of sodium perchlorate. All reaction temperature was maintained at $25 \pm 0.5^\circ\text{C}$ using a Neslab RTE 101 thermostat bath. The kinetics of reaction systems studied, $\text{HNO}_2/\text{H}_2\text{O}_2$, $\text{ONOO}^- / \text{ONOOH} - \text{CYSH}$ and $\text{ONOO}^- / \text{ONOOH} - \text{GSH}$, were followed on a Hi-Tech Scientific Double-Mixing SF61-DX2 stopped-flow spectrophotometer. Digitization and amplifying were done via an Omega Engineering DAS-50/1 16-bit A/D board interfaced to a Pentium IV computer. The progress of these reaction systems was followed spectrophotometrically on the stopped flow at wavelength of 302 and 544 nm.

2.4.3 Electron Paramagnetic Resonance (EPR)

EPR spectra were recorded at room temperature on a Bruker BioSpin's e-scan EPR spectrometer designed to perform X-band EPR measurements. DMPO and PBN were reconstituted in phosphate buffer pH and 7.4, treated with EDTA.

2.4.3.1 Peroxynitrite decomposition: Peroxynitrite was rapidly mixed with DMPO and PBN in buffer pH 7.4 at room temperature and aspirated into VWR's calibrated micro pipette. The pipette was then transferred into quartz EPR tube and the spectra recorded.

2.4.3.2 Cysteine/glutathione oxidation by peroxynitrite: Experiments with cysteine or glutathione were conducted as above by adding specific amounts of thiols to buffer solution containing DMPO/PBN before the addition of peroxynitrite.

2.4.4 High Performance Liquid Chromatography (HPLC)

All samples were loaded onto the Discovery C18 column. They were run isocratically at 5% ACN/H₂O and all eluents were detected at a UV absorbance of 335 nm (for selective scans) with the maximum spectral scan mode employed to detect all eluents. A flow rate of 1 ml/min was maintained. All solutions for HPLC analysis were made with Milli-Q Millipore purified water and filtered with the 0.45 μ m pore-sized PVDP Whatman Polypropylene filter devices (Whatman Inc, Florham Park, NJ) before injection (10 μ l) onto the column using the auto injector. To curb the interaction of the protonated amines on the analytes with the silanol groups on the stationary phase

(which was causing tailing of the peaks) the sodium salt of 1-octanesulfonic acid (0.005 M) was incorporated into the aqueous mobile phase. This was sufficient to neutralize the protonated amines and produce good resolution while eliminating peak tailing.

2.4.5 Mass Spectrometry (MS)

Eluent of reaction mixture of acidified thiols and PN from HPLC system were dissolved in 50/50 acetonitrile: water for mass spectral analysis. Analytes were analyzed using positive-mode electrospray ionization (+ESI) at a capillary voltage of 2.8 kV and a flow rate of 5 μ l/min. The source block was maintained at 80 °C and the nitrogen desolvation gas was maintained at 150 °C and a flow rate of 400 L/h. MS/MS data was generated via CID in argon at collision energy of 15 eV.

CHAPTER 3

KINETICS OF PEROXYNITRITE FORMATION AND DECOMPOSITION IN PERCHLORIC ACID AND SODIUM PHOSPHATE BUFFER SOLUTIONS

3.1 INTRODUCTION

Peroxynitrite; ONOO^- (PN) may be produced in the physiological system at the micromolar concentration range when in close contact with superoxide anion, if it is also in the micromolar concentration range^{210,211}. The chemistry of PN has received a lot of attention in the scientific community due to its complex reactivity and cytotoxicity. PN is known to be both a nitrating and oxidizing compound, it is harmful to biological tissue membranes, proteins and nucleic acids^{212,213}. PN reacts with acids to form peroxynitrous acid (ONOOH):



ONOOH is very unstable and readily decomposes in aqueous solutions but ONOO^- is relatively stable in basic environments. This characteristic complex chemistry of PN has elicited a lot of research which has also brought about a lot of controversy among researchers in the chemistry of PN. It is believed by some workers that PN decomposition pathway goes through a non radical mechanism²¹⁴. Others believe in the homolysis of the O-O in peroxynitrous acid ($\text{O}=\text{N}-\text{O}-\text{OH}$), with subsequent formation of $\cdot\text{NO}_2$ and $\cdot\text{OH}$ radicals⁶³:



The objective of this chapter is to (a) provide evidence showing the decomposition products of PN as a function of pH (b) provide evidence of radical formation in the decomposition of PN and (c) propose a plausible mechanism for the formation and decomposition of PN.

3.2 PRODUCT DETERMINATION FOR PN FORMATION AND DECOMPOSITION

3.2.1 Formation reaction

Formation of PN can be derived from reaction mixtures of nitrite (NO_2^-), perchloric acid (HClO_4), and hydrogen peroxide (H_2O_2). Nitrite, in the presence of HClO_4 , rapidly forms nitrous acid, which rapidly reacts with hydrogen peroxide to produce PN. NO_2^- was initially acidified with HClO_4 and then reacted with H_2O_2 using the single mixing mode of the SF-61 DX2 double mixing spectrophotometer and the UV-vis spectrophotometer.

The stoichiometry of the formation reaction of PN was determined to be 1 mole of H_2O_2 : 1 mole HNO_2 , as shown in reaction R 3.3:



PN, once formed, is very unstable in acidic media with a half life of about 1 s

(Figure 3.1) but relatively stable in basic media. Stabilization is thus achieved by adding sodium hydroxide to the peroxyntirite product solution (see reaction R3.4):



The product of reaction, PN, was characterized spectrophotometrically at its wavelength of absorption of 302 nm (Figure 3.2).

Formation and decomposition of Peroxynitrite

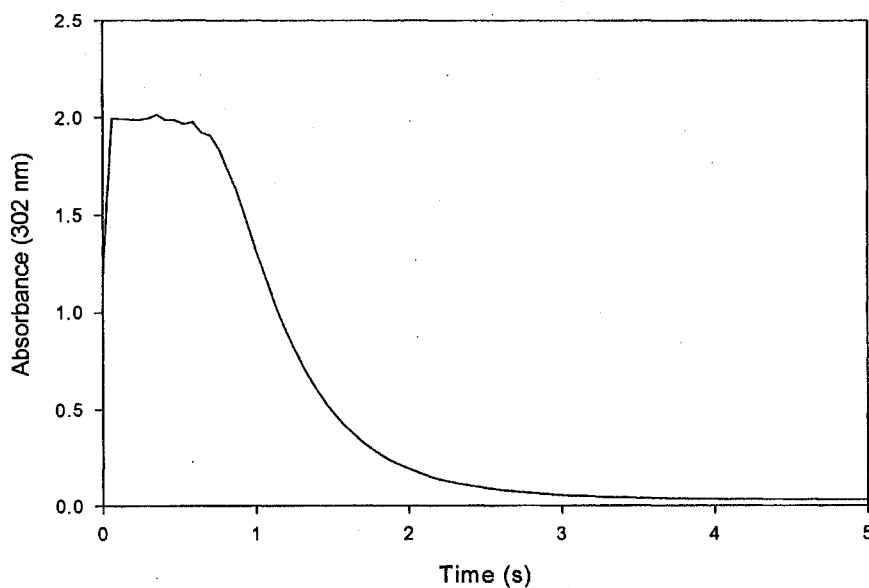


Figure 3.1: $[\text{HClO}_4] = 1.2 \times 10^{-2} \text{ M}$, $[\text{H}_2\text{O}_2] = 2.0 \times 10^{-1} \text{ M}$, $[\text{NaNO}_2] = 1.3 \times 10^{-3} \text{ M}$.
 $[\text{ONOOH}] = 1.2 \times 10^{-3} \text{ M}$ at $1670 \text{ cm}^{-1} \text{ M}^{-1}$

UV-vis spectral of peroxyxynitrite at pH 12

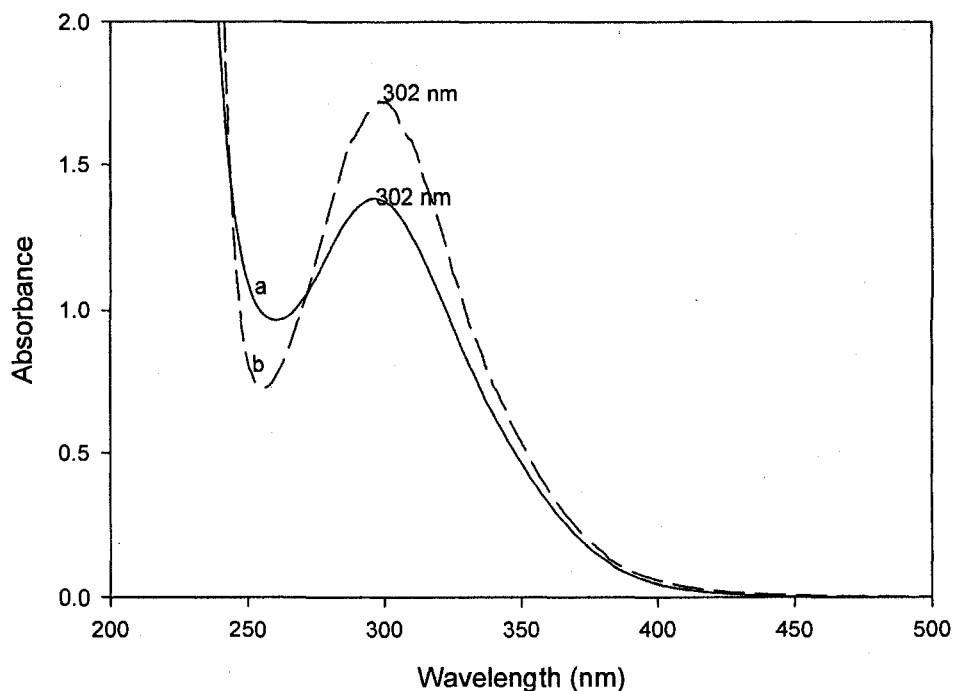


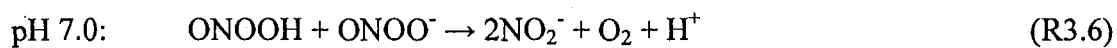
Figure 3.2: a) $[\text{ONOO}^-] = 8.1 \times 10^{-4} \text{ M}$, b) $[\text{ONOO}^-] = 1.0 \times 10^{-3} \text{ M}$ molar absorptivity coefficient of $1670 \text{ cm}^{-1} \text{ M}^{-1}$

3.2.2 Decomposition reaction

Since PN is highly unstable in strongly acidic medium and spontaneously decomposes, the products of decomposition as a function of pH were investigated using UV-vis spectrophotometry. Our results show that at pH of 1.0, the major product of decomposition is nitrate which absorbs at the same wavelength of 302 nm as PN. Standard sodium nitrate from the chemical manufacturers was used as standard for the determination of wavelength of absorption. At pH 7.0 there is a mixture of ONOO^- and ONOOH , and the product of decomposition was determined as nitrite and oxygen. Nitrite has a wavelength of 355 nm in the UV-vis region. At pH's 8.0 and 9.0 the major

product of decomposition is nitrite at the expense of nitrate and oxygen (**Figure 3.3**).

The stoichiometry of decomposition reaction was determined to be:



Products of decomposition of peroxynitrite in buffer pH 1.0, 7.0, 8.0 and 9.0 (1 hour after incubation)

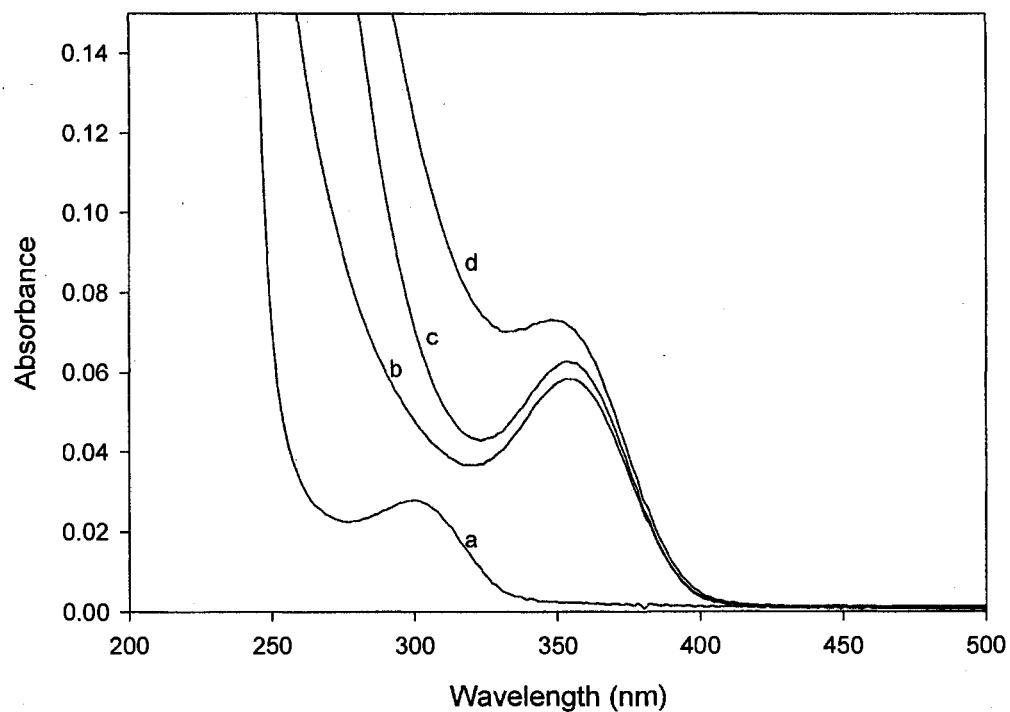


Figure 3.3: Fixed: Initial [PN] = 8.1×10^{-4} M, [phosphate buffer pH 1.0, 7.0, 8.0 and 9.0] = 0.15 M

Traces a-d are mixtures of PN with buffer a) = buffer pH 1.0, b) pH 7.0, c) pH 8.0, d) pH 9.0.

3.3 REACTION DYNAMICS

3.3.1 Formation of PN:

The formation traces of PN monitored at 302 nm exhibit a quick and instantaneous absorbance at time $t = 0$ which quickly saturates and decays with time (see **Figure 3.1**). The half-life of PN was found to be a function of the initial concentrations of the reactants.

3.3.1.1 Effect of acid: Acid is strong catalytic in the formation of PN from H_2O_2 , and NO_2^- . Higher acid concentrations increase the rate of formation of PN. Acid is not a reactant and so does not influence the maximum amount of PN formed only the time taken to attain this maximum. This catalytic action is more noticeable at lower acid concentrations (**Figure 3.4**), where there is an increase in PN formation with increase in acid concentrations. Further increase in acid concentrations seems to deliver a more complex acid dependence. At high enough acid concentrations formation of PN saturates and further increase in acid concentrations show that decomposition of PN occurs before its full quantitative formation. The decomposition of PN can be delayed at lower acid concentrations and higher concentrations of hydrogen peroxide and nitrite. The acid dependence plot shown in **Figure 3.5** is first order at low acid concentrations and seems to saturate at high acid concentrations. This would suggest a simple one-term rate law at low acid and a more complex rate law with respect to acid at higher concentrations.

Acid variation in the formation of PN

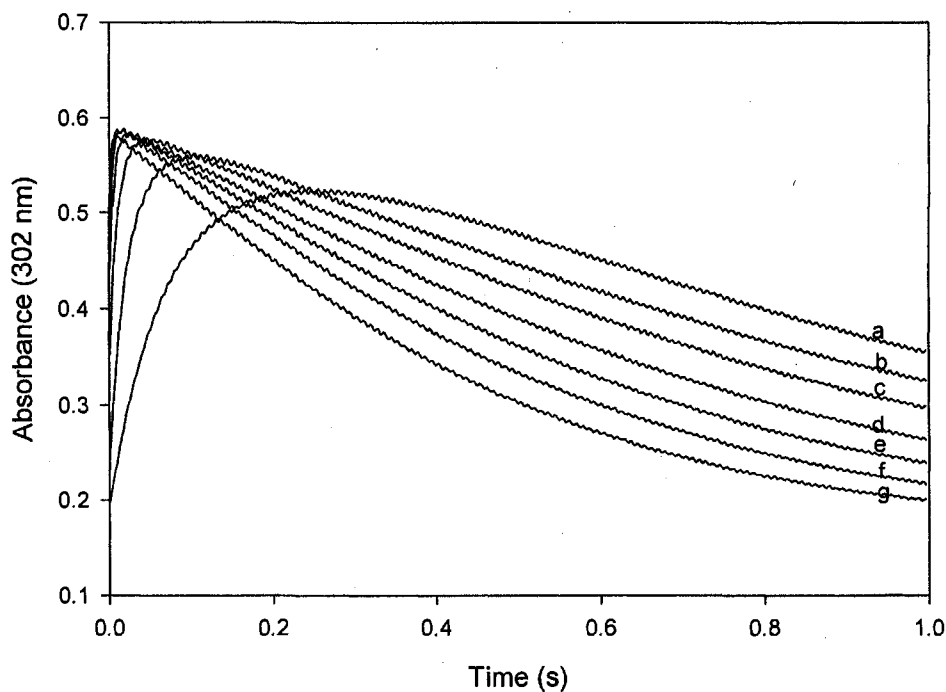


Figure 3.4 : Fixed: $[\text{NO}_2^-] = 3.5 \times 10^{-4} \text{ M}$, $[\text{H}_2\text{O}_2] = 3.0 \times 10^{-2} \text{ M}$, $I_{\text{NaClO}_4} = 0.5 \text{ M}$
 $[\text{HClO}_4] =$ a) $1.6 \times 10^{-3} \text{ M}$, b) $3.1 \times 10^{-3} \text{ M}$, c) $6.3 \times 10^{-3} \text{ M}$, d) $1.3 \times 10^{-2} \text{ M}$, e) $1.9 \times 10^{-2} \text{ M}$,
f) $2.5 \times 10^{-2} \text{ M}$, g) $3.1 \times 10^{-2} \text{ M}$.

3.3.1.2 Effect of nitrite: The effect of varying nitrite is shown in **Figure 3.6**.

Hydrogen peroxide concentrations are maintained at overwhelming excess over nitrite concentrations. As the concentrations of nitrite are increased, the absorbance of PN also increases. The lowest nitrite concentrations have the highest rates of decay, while the highest nitrite concentrations have the slowest decay rate, and thus, rate of decay can be said to be concentration dependent.

PN produced with excess hydrogen peroxide generates nitrite - free peroxyxynitrite.

Initial rate plot for acid variation in the formation of PN

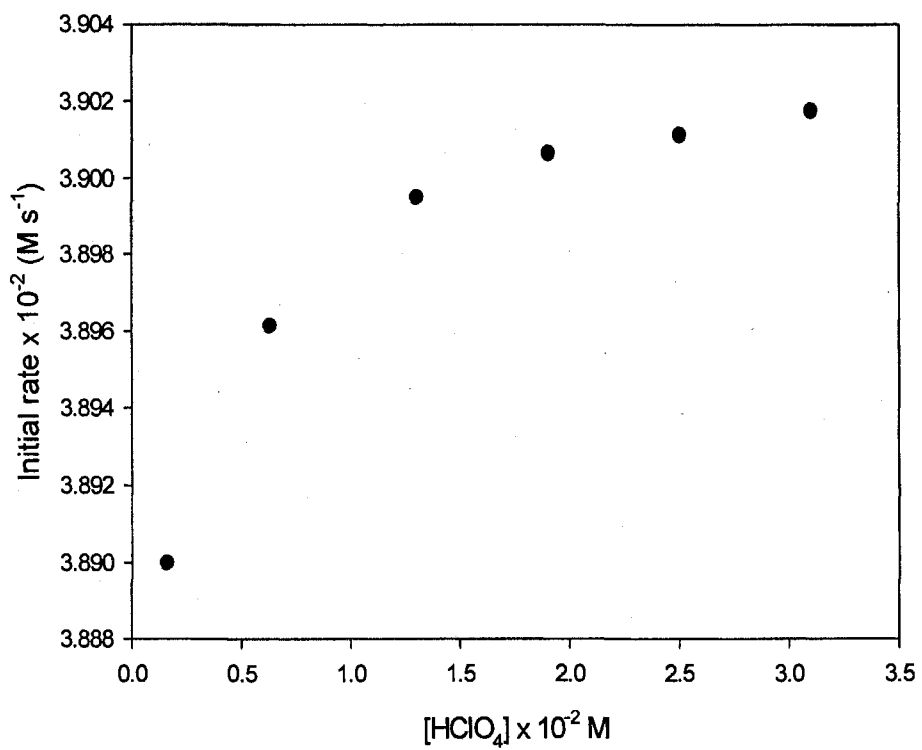


Figure 3.5: Fixed: $[\text{NO}_2^-] = 3.5 \times 10^{-4} \text{ M}$, $[\text{H}_2\text{O}_2] = 3.0 \times 10^{-2} \text{ M}$, $[\text{NaClO}_4] = 0.5 \text{ M}$

$[\text{HClO}_4] = \text{a) } 1.6 \times 10^{-3} \text{ M, b) } 3.1 \times 10^{-3} \text{ M, c) } 6.3 \times 10^{-3} \text{ M, d) } 1.3 \times 10^{-2} \text{ M, e) } 1.9 \times 10^{-2} \text{ M, f) } 2.5 \times 10^{-2} \text{ M, g) } 3.1 \times 10^{-2} \text{ M.}$

Nitrite variation in formation of PN.

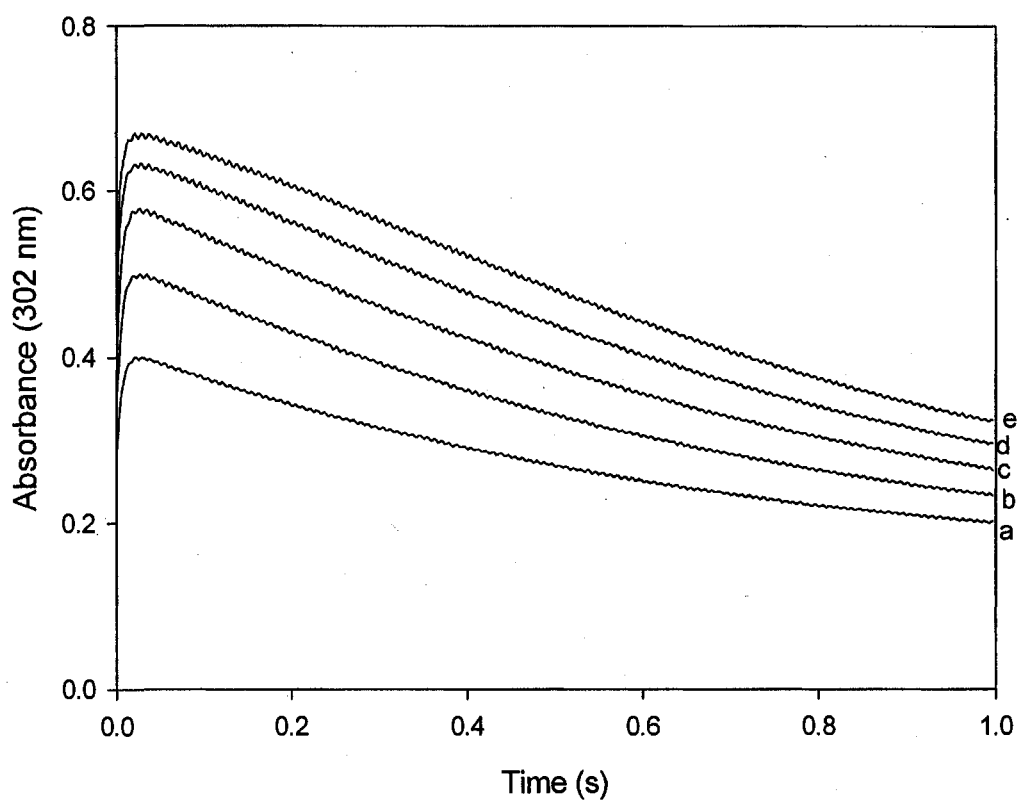


Figure 3.6: Fixed: $[\text{H}_2\text{O}_2] = 3.0 \times 10^{-2} \text{ M}$, $[\text{HClO}_4] = 1.3 \times 10^{-2} \text{ M}$, $I_{\text{NaClO}_4} = 0.5 \text{ M}$.

$[\text{NO}_2^-] =$ a) $2.5 \times 10^{-4} \text{ M}$, b) $3.0 \times 10^{-4} \text{ M}$, c) $3.5 \times 10^{-4} \text{ M}$, e) $4.0 \times 10^{-4} \text{ M}$, f) $4.5 \times 10^{-4} \text{ M}$, g) $5.0 \times 10^{-4} \text{ M}$.

The initial rate plot for nitrite variation shows that the rate of formation of PN with respect to nitrite concentrations is first order. This is shown in **Figure 3.7**.

Initial rate plot for nitrite variation in formation of PN.

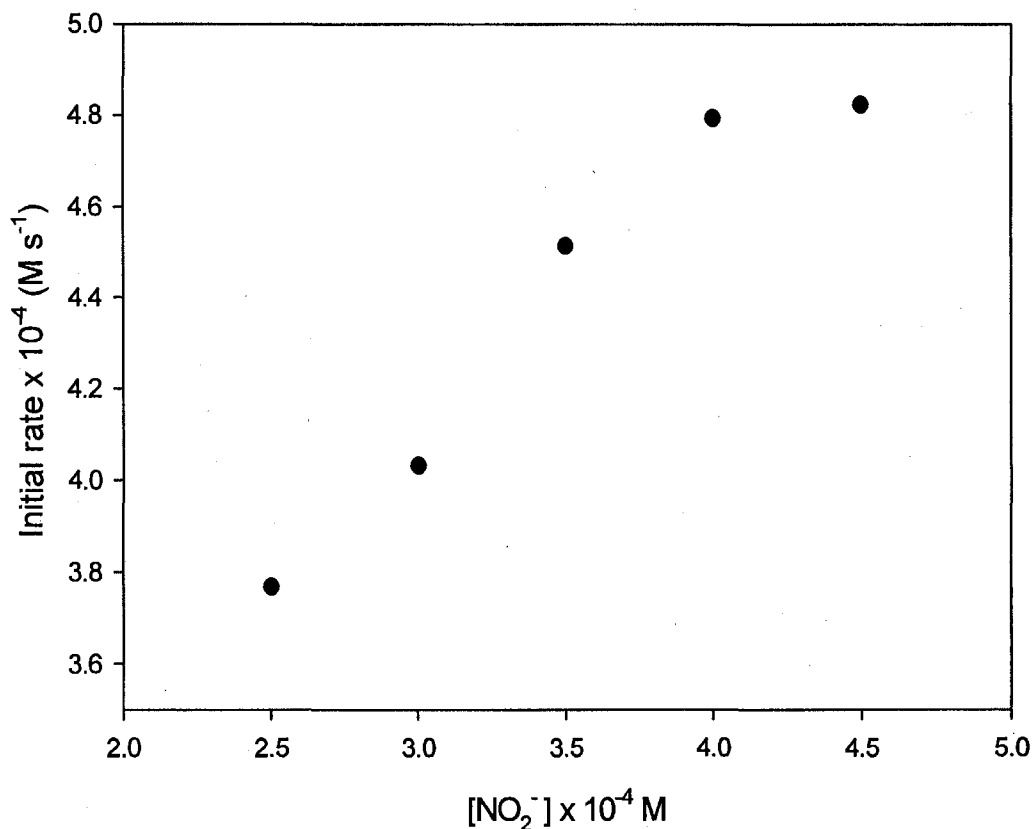


Figure 3.7 : Fixed: $[\text{H}_2\text{O}_2] = 3.0 \times 10^{-2} \text{ M}$, $[\text{HClO}_4] = 1.3 \times 10^{-2} \text{ M}$, $I_{\text{NaClO}_4} = 0.5 \text{ M}$.

$[\text{NO}_2^-] =$ a) $2.5 \times 10^{-4} \text{ M}$, b) $3.0 \times 10^{-4} \text{ M}$, c) $3.5 \times 10^{-4} \text{ M}$, e) $4.0 \times 10^{-4} \text{ M}$, f) $4.5 \times 10^{-4} \text{ M}$.

3.3.1.3 Effect of hydrogen peroxide: Under conditions in which hydrogen peroxide ratio to nitrite ratio is less than 1:1, an increase in hydrogen peroxide concentration increases the absorbance of PN produced at 302 nm with the rate of decomposition

of PN inversely proportional to absorbance of PN. Continual increase of hydrogen peroxide concentration past the initial nitrite concentrations results in saturation as seen in **Figure 3.8**.

Hydrogen peroxide variation in formation of PN

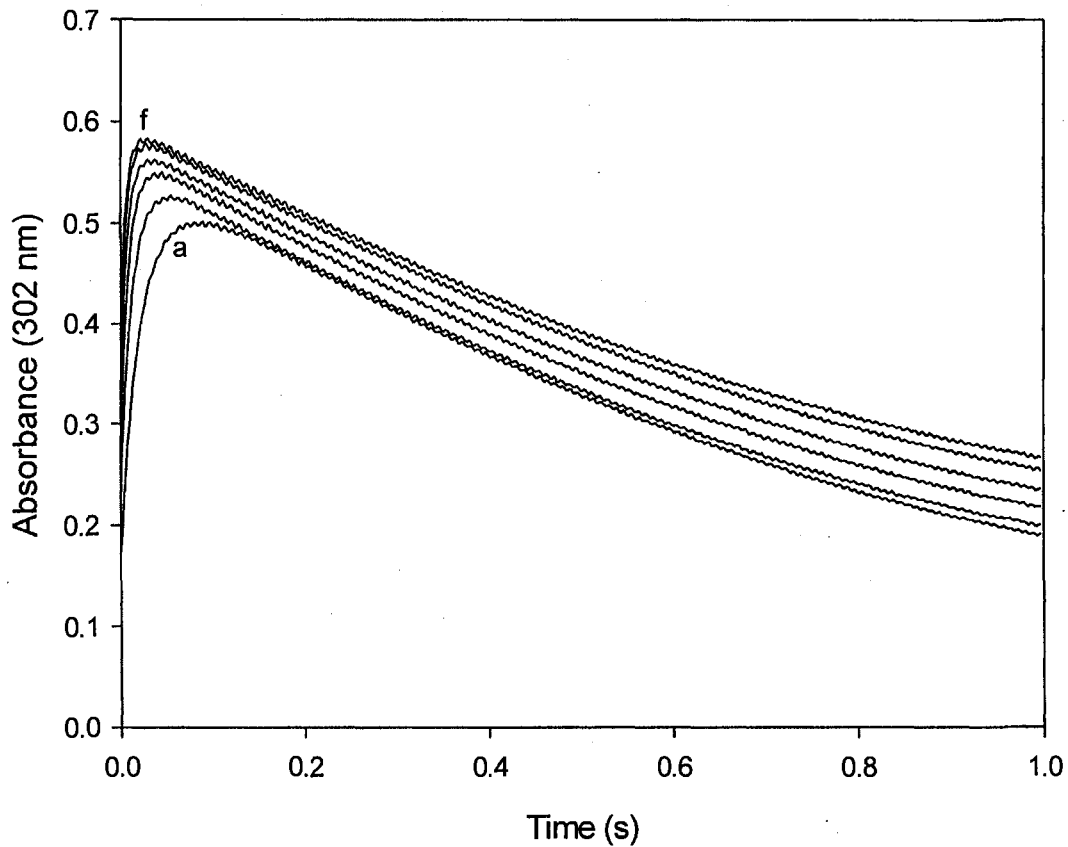


Figure 3.8 :Fixed: $[\text{NO}_2^-] = 3.5 \times 10^{-4} \text{ M}$, $[\text{HClO}_4] = 1.3 \times 10^{-2} \text{ M}$, $I_{\text{NaClO}_4} = 0.5 \text{ M}$

$[\text{H}_2\text{O}_2] = \text{a) } 1.5 \times 10^{-4} \text{ M, b) } 2.0 \times 10^{-4} \text{ M, c) } 2.5 \times 10^{-4} \text{ M, d) } 3.0 \times 10^{-4} \text{ M, e) } 3.5 \times 10^{-4} \text{ M, f) } 4.0 \times 10^{-4} \text{ M.}$

The initial rate plot for hydrogen peroxide dependence at lower concentrations of hydrogen peroxide before saturation sets in shows that the rate of formation of PN with respect to hydrogen peroxide concentrations is first order. This is shown in **Figure 3.9**.

Initial rate plot for hydrogen peroxide variation in formation of PN

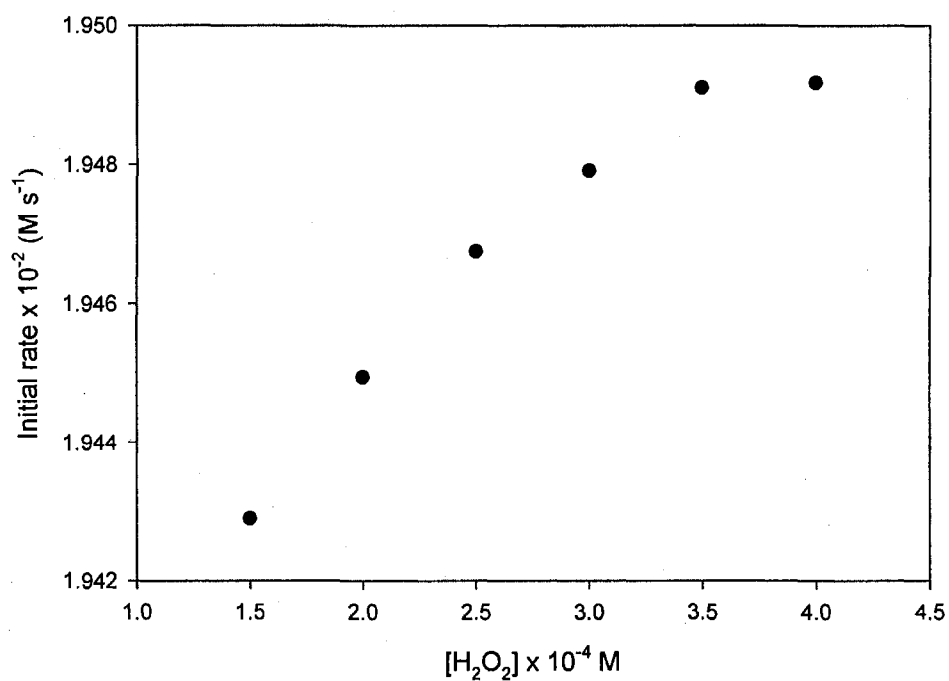


Figure 3.9 : Fixed: $[\text{NO}_2^-] = 3.5 \times 10^{-4} \text{ M}$, $[\text{HClO}_4] = 1.3 \times 10^{-2} \text{ M}$, $I_{\text{NaClO}_4} = 0.5 \text{ M}$

$[\text{H}_2\text{O}_2] =$ a) $1.5 \times 10^{-4} \text{ M}$, b) $2.0 \times 10^{-4} \text{ M}$, c) $2.5 \times 10^{-4} \text{ M}$, d) $3.0 \times 10^{-4} \text{ M}$, e) $3.5 \times 10^{-4} \text{ M}$, f) $4.0 \times 10^{-4} \text{ M}$.

3.3.2 Decomposition of PN:

PN decomposition was followed using its wavelength of maximum absorbance at 302 nm. Decomposition is catalysed in the presence of protons. This was effected at different pH conditions using sodium phosphate buffer. The pH of each solution was determined after decomposition reactions by taking pH measurements of the waste from the stopped flow instrument. All reactions were run in phosphate buffer of strength 0.15 M.

3.3.2.1 Effect pH: For the effect of pH on PN decomposition, PN concentrations were kept constant while buffer solution pHs at the same concentrations were varied (**Figure 3.10**). A monotonous decrease in absorbance was observed with rate of decrease in absorbance at low pH being faster than rate of decrease at high pH. The decrease in absorbance at 302 nm was used to determine initial rate. The initial rate plot against pH was linear for pH 6.5-8.0 which implies that the decomposition of PN as a function of pH in this range is first order. The same plot for pH 3.0-5.5, however, deviated from linearity (**Figure 3.11**). The rate constants of decomposition of PN in the absence of a substrate at pH 3.0-8.0 are shown in **Figure 3.12**.

Effect of pH on PN decomposition (buffer pH 3-8 at 0.15 M)

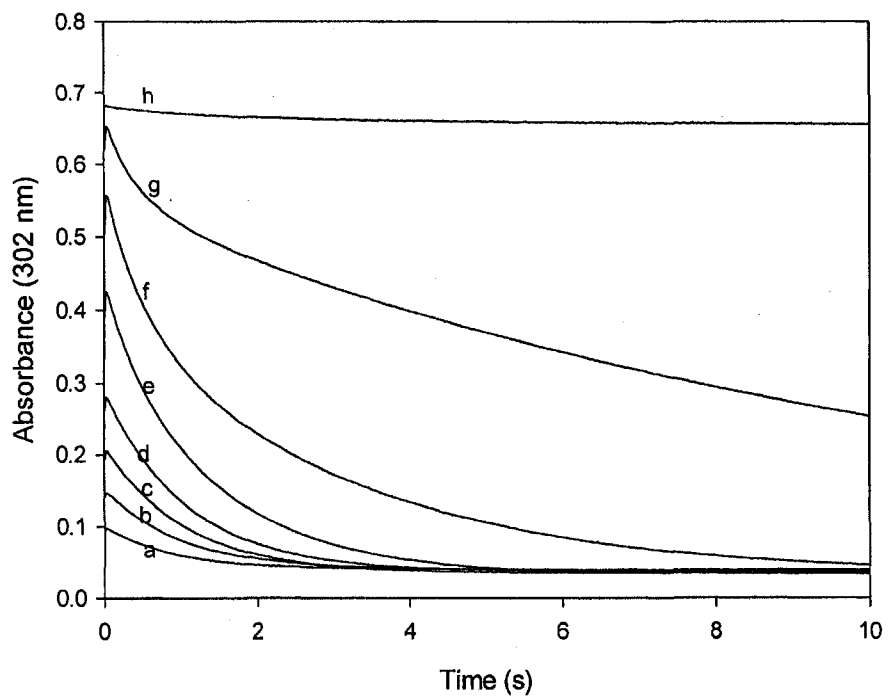


Figure 3.10: Fixed [PN] = 4.6×10^{-4} M, [EDTA] = 1.0×10^{-4} M, [Phosphate buffer 0.15 M] = a) pH 3.0, b) pH 4.0, c) pH 5.0, d) pH 6.0, e) pH 6.5, f) pH 7.0, g) pH 7.4, h) pH 8.0

Initial rate plot for decomposition of PN in phosphate buffer pH 3-8

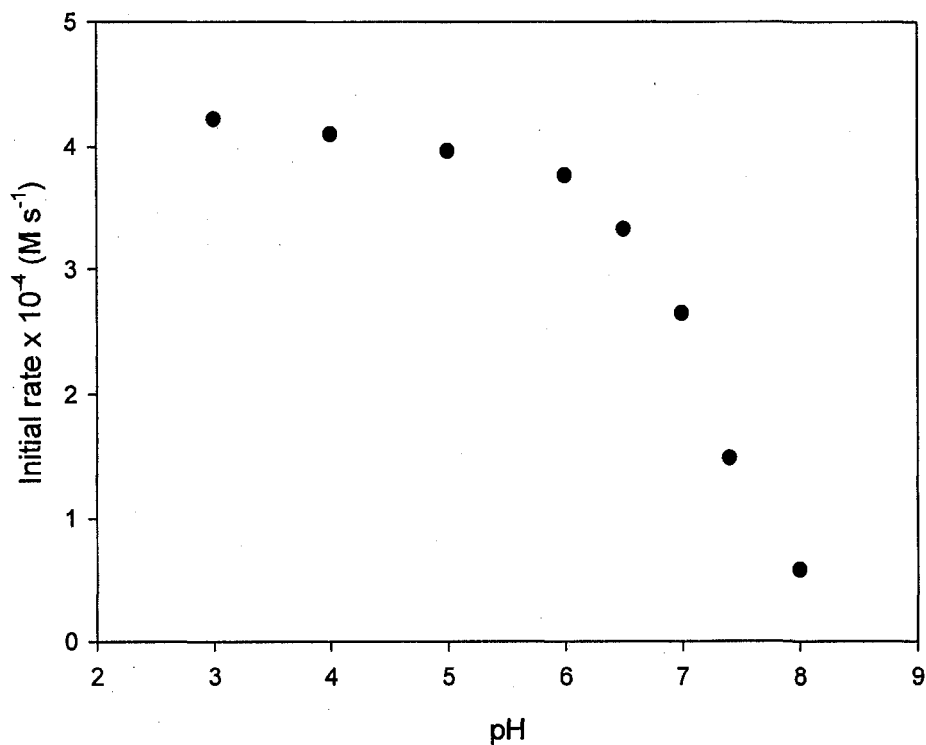


Figure 3.11: Fixed $[PN] = 4.6 \times 10^{-4} M$, $[EDTA] = 1.0 \times 10^{-4} M$,
[Phosphate buffer 0.15 M] = a) pH 3.0, b) pH 4.0, c) pH 5.0, d) pH 6.0, e) pH 6.5, f) pH 7.0, g) pH 7.4, h) pH 8.0

Rate constants for effect of pH on PN decomposition (buffer pH 3-8 at 0.15 M)

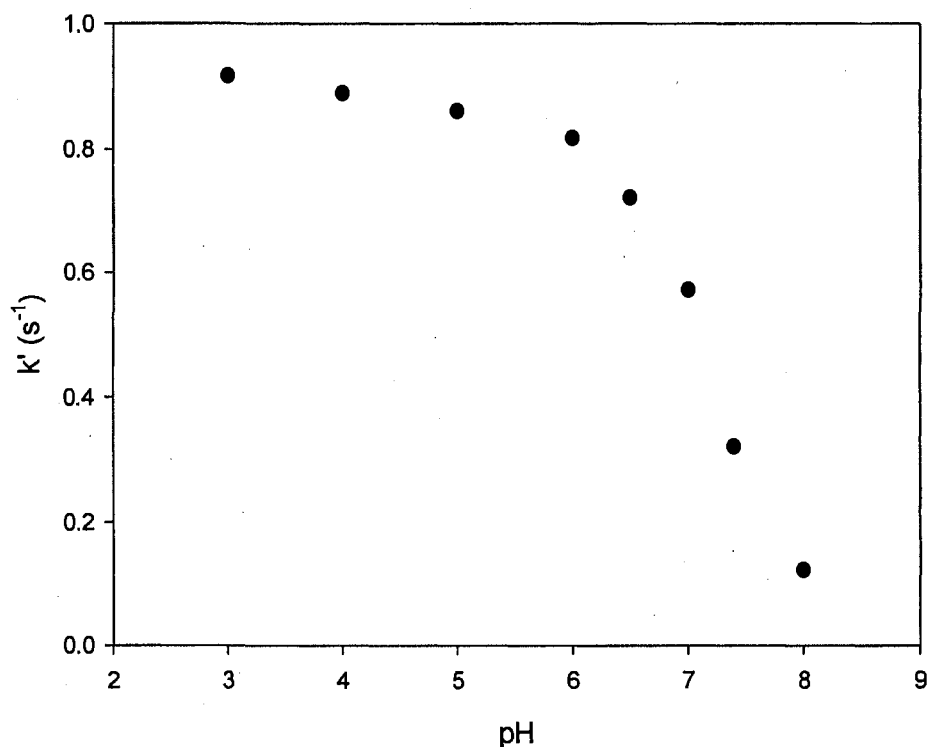


Figure 3.12: Fixed: [PN] = 4.6×10^{-4} M, [EDTA] = 1.0×10^{-4} M,
[Phosphate buffer 0.15 M] = a) pH 3, b) pH 4, c) pH 5, d) pH 6, e) pH 6.5, f) pH 7, g) pH 7.4, h) 8

3.3.2.2 Effect HCO_3^- : Carbon dioxide is found in significant concentrations

(14.7-25 mM) in physiological tissues in equilibrium with bicarbonate at pH of 7.4²¹⁵.

The study of the effect of HCO_3^- on PN decomposition is therefore very relevant.

Figure 3.13 shows the depletion of PN at 302 nm by HCO_3^- at pH 6.5. The rate of depletion is directly proportional to concentration of HCO_3^- . The initial rate plot (see **Figure 3.13 insert**) for effect of HCO_3^- on PN depletion was determined to be first order.

Effect of HCO_3^- on PN decomposition done varying HCO_3^- at pH 6.5

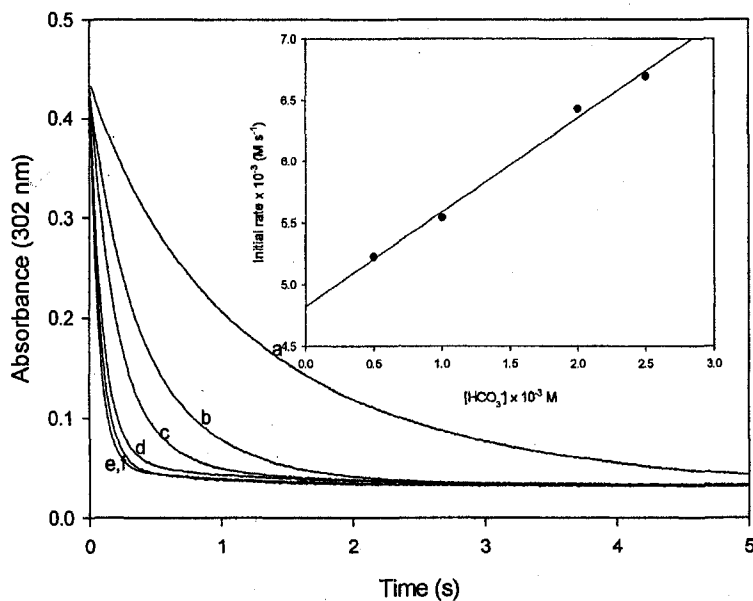


Figure 3.13: Fixed: $[\text{PN}] = 4.6 \times 10^{-4} \text{ M}$, $[\text{EDTA}] = 1.0 \times 10^{-4} \text{ M}$, $[\text{Phosphate buffer at pH 6.5}] = 1.5 \times 10^{-1} \text{ M}$
 $[\text{HCO}_3^-]$ = a) 0 M, b) $5.0 \times 10^{-4} \text{ M}$, c) $1.0 \times 10^{-3} \text{ M}$, d) $2.0 \times 10^{-3} \text{ M}$, e) $2.5 \times 10^{-3} \text{ M}$, f) $3.0 \times 10^{-3} \text{ M}$.

Effect of HCO_3^- on PN decomposition done varying HCO_3^- at pH 7.4

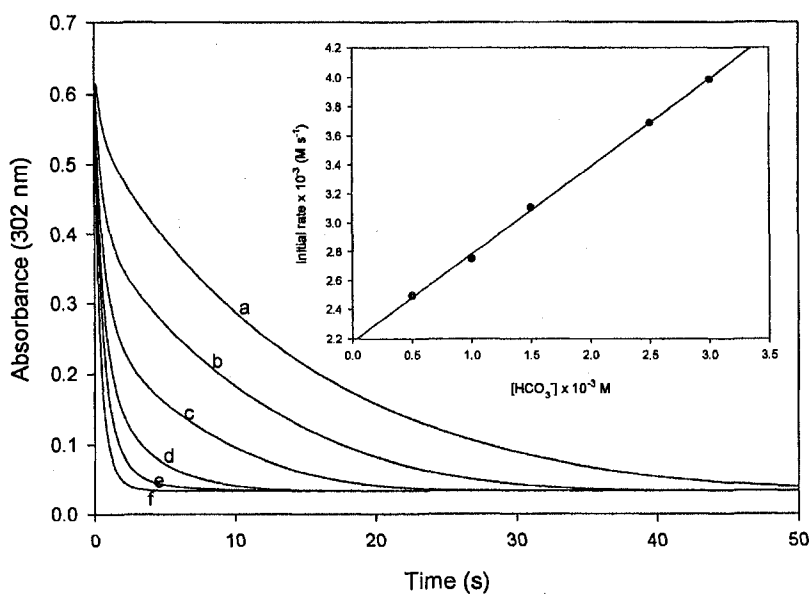


Figure 3.14: Fixed: $[\text{PN}] = 4.2 \times 10^{-4} \text{ M}$, $[\text{EDTA}] = 1.0 \times 10^{-4} \text{ M}$, $[\text{Phosphate buffer at pH 7.4}] = 1.5 \times 10^{-1} \text{ M}$
 $[\text{HCO}_3^-]$ = a) 0 M, b) $5.0 \times 10^{-4} \text{ M}$, c) $1.0 \times 10^{-3} \text{ M}$, d) $1.5 \times 10^{-3} \text{ M}$, e) $2.5 \times 10^{-3} \text{ M}$, f) $3.0 \times 10^{-3} \text{ M}$.

The effect of pH on HCO_3^- reaction with PN was investigated by altering the pH of the buffer solution to 7.4 while HCO_3^- concentrations were varied with a fixed concentration of PN (**Figure 3.14**). The rate of decomposition of PN in the presence of HCO_3^- at pH 6.5 was faster than the rate of decomposition at pH 7.4. The initial rate of decomposition at pH 7.4 was also determined to be first order (**Figure 3.14 insert**).

3.4 EPR STUDIES

3.4.1 Radical formation in decomposition of PN: 5, 5-dimethyl-1-pyrroline N-oxide (DMPO) was used for trapping short lived radicals in reaction media by formation of an adduct with the short lived radicals. These adducts are paramagnetic and so generate EPR signals. DMPO was dissolved in 0.15 M sodium phosphate buffer at pH 7.4, the DMPO solution was then mixed with diluted alkaline stock solution of PN. The solution was allowed to incubate for about 1 minute and then scans were obtained. At pH 7.4 PN decomposes with the decomposition products of PN forming adducts with DMPO. Fenton's reaction, reaction R3.8, was used as control experiment for generation of hydroxyl radicals (**Figure 3.15 (a)**):

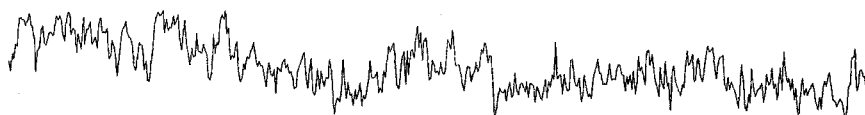


Trace (a) generated 1:2:2:1 quartet with splitting of $a_{\text{N}}=a_{\text{H}}=14.9 \text{ G}^{216}$

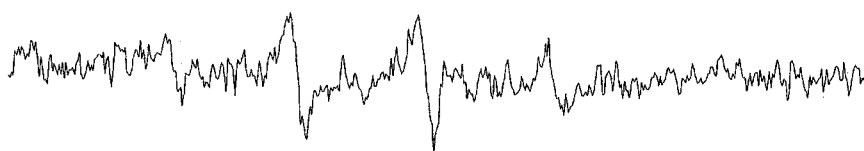
characteristic of DMPO-OH radical adduct. Trace (b) indicates that DMPO dissolved in buffer pH 7.4 does not generate any radicals. Trace (c) also shows the 1:2:2:1 quartet with splitting of $a_N = a_H = 14.9$ G, but radical adduct yields were low. Increase in PN concentration in trace (d) resulted in stronger signal generation. The comparison of traces obtained in **Figure 3.15 c and d** to the control indicates that radical adduct detected during the decomposition of peroxyxynitrite in the presence of DMPO was DMPO-hydroxyl radical adduct. Furthermore, spin trap studies were done with Mannitol, which is a well known hydroxyl radical scavenger. Identical experimental conditions were used as in decomposition of PN. The yield of DMPO hydroxyl radical adduct was greatly reduced with the subsequent EPR signal being very faint (**Figure 3.15 e**). This is indicative of scavenging of hydroxyl radicals produced by PN in the process of decomposition at pH 7.4.



a) Fenton's reaction: $[\text{H}_2\text{O}_2] = 0.2 \text{ mM}$, $[\text{FeSO}_4] = 0.05 \text{ mM}$, $[\text{DMPO}] = 80 \text{ mM}$



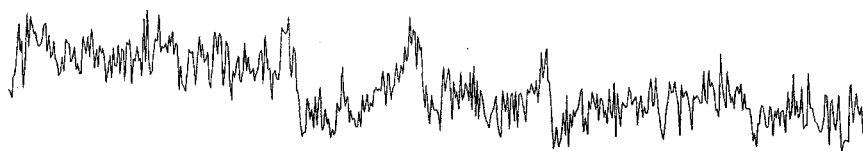
b) DMPO trace at pH 7.4: $[\text{DMPO}] = 80 \text{ mM}$, $[\text{PN}] = 0 \text{ }\mu\text{M}$ peroxynitrite



c) PN decomposition at pH 7.4: $[\text{DMPO}] = 80 \text{ mM}$, $[\text{PN}] = 10 \text{ }\mu\text{M}$ peroxynitrite



d) PN decomposition at pH 7.4: $[\text{DMPO}] = 80 \text{ mM}$, $[\text{PN}] = 20 \text{ }\mu\text{M}$ peroxynitrite

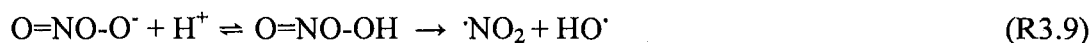


e) Effect of Mannitol on PN decomposition at pH 7.4: $[\text{DMPO}] = 80 \text{ mM}$, $[\text{PN}] = 20 \text{ }\mu\text{M}$, $[\text{Mannitol}] = 0.25 \text{ mM}$

→
3436-3536 G

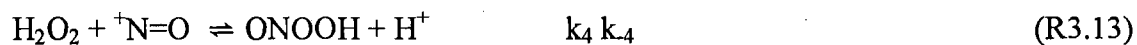
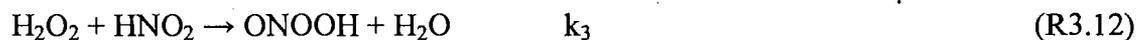
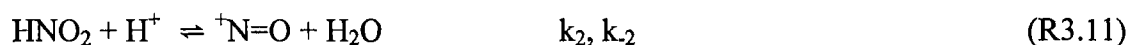
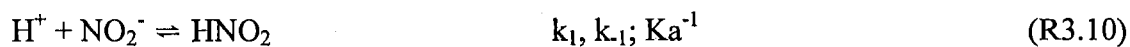
Figure 3.15: EPR spectra of DMPO radical adducts obtained during peroxynitrite (PN) decomposition. Spectra were obtained after about 1 minute incubation period at room temperature with 80 mM DMPO dissolved in 0.15 M phosphate buffer at pH 7.4 with 0.1 mM EDTA a) Fenton's reaction for generation of $\cdot\text{OH}$ radical, b) 0 μM PN, c) 10 μM PN, d) 20 μM PN, e) 20 μM PN + 0.25 mM Mannitol.

Formation of DMPO-OH adduct from PN decomposition is metal ion independent since all EPR experiments in **Figure 3.15** were performed with EDTA in the reaction mixture. Based on the results from **Figure 3.15**, products of the decomposition of PN at pH 7.4 may be deduced to be²¹⁶:



3.5 Mechanism of formation of PN

The reaction dynamics suggest only four reactions as being relevant in the production of PN. They involve the protonation of nitrite to produce nitrous acid followed by the production of the nitrosyl ion²¹⁷ and the reaction of both nitrous acid and nitrosyl cation with hydrogen peroxide:



The rate of reaction, based on the formation of ONOOH, is given by:

$$\frac{d[\text{ONOOH}]}{dt} = k_3[\text{H}_2\text{O}_2][\text{HNO}_2] + k_4[\text{H}_2\text{O}_2][^+\text{N}=\text{O}] - k_{-4}[\text{ONOOH}][\text{H}^+] \quad (1)$$

At the beginning of the reaction, before accumulation of ONOOH (at time $t = 0$), the last term in eq 1 can be ignored. All the nitrogen (III) species in the reaction solution are bound by the following mass balance equation:

$$[\text{N(III)}]_{\text{T}} = [\text{NO}_2^-] + [\text{HNO}_2] + [\text{ONOOH}] + [^+\text{N}=\text{O}] \quad (2)$$

The total N (III) species in this case would be the nitrite added to the reaction mixture. Since we expect the nitrosyl ion to be a transient reactive intermediate, its concentration can be assumed to be negligible. For initial rate measurements, concentration of product ONOOH can also be ignored. We can apply a steady-state approximation on the nitrosyl ion to simplify eq 1 into measurable concentrations.

$$\frac{d[\text{NO}^+]}{dt} = k_2[\text{HNO}_2][\text{H}^+] - k_{-2}[\text{NO}^+] - k_4[\text{H}_2\text{O}_2][\text{NO}^+] + k_{-4}[\text{ONOOH}][\text{H}^+] \quad (3)$$

$$[\text{NO}^+] = \frac{k_2[\text{HNO}_2][\text{H}^+]}{k_{-2} + k_4[\text{H}_2\text{O}_2]} \quad (4)$$

By using the dissociation constant of nitrous acid:



and the mass balance balance eq 2, the initial rate law can now be rewritten as the following complex function of acid concentrations:

$$\text{rate} = \frac{d[\text{ONOOH}]}{dt} = \frac{[\text{H}_2\text{O}_2][\text{N(III)}]_{\text{T}}[\text{H}^+]}{K_a + [\text{H}^+]} \left(k_3 + \frac{k_2 k_4 [\text{H}^+]}{k_2 + k_4 [\text{H}_2\text{O}_2]} \right) \quad (5)$$

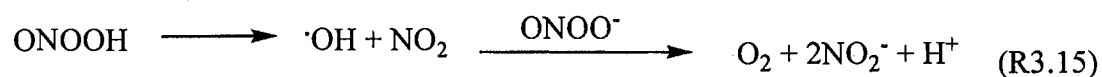
Equation 5 is supported by the kinetics data shown in Figures 3.4-9. Specifically, it predicts first-order kinetics with respect to H_2O_2 and nitrite. It also predicts first-order kinetics in acid at low concentrations. When $[\text{H}^+]_0$ is low the second term in (5) becomes negligible and the reaction retains first-order kinetics on the basis of the first term only. Rate law equation written in equation 5 is complex and can be made simple if equilibrium constant for reaction R3.11 (K_2) is known with certainty for these experimental conditions. Since reactions R3.12 and R3.13 are the rate-determining steps, an initial approximation would be that $k_{-2} \gg k_4$. This would simplify eq 5 to read:

$$\text{rate} = \frac{d[\text{ONOOH}]}{dt} = \frac{[\text{H}_2\text{O}_2][\text{N(III)}]_{\text{T}}[\text{H}^+]}{K_a + [\text{H}^+]} (k_3 + k_2k_4 [\text{H}^+]) \quad (6)$$

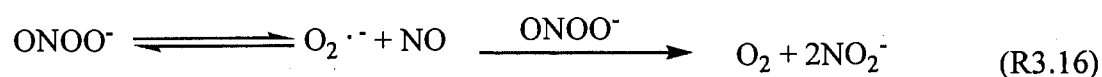
3.6 Conclusion

PN is formed in strongly acidic media by the reaction of HNO_2 , NO^+ with H_2O_2 (**Figure 3.1**). PN formed in acidic medium can be regarded as an intermediate formed before rearrangement or isomerisation into the final product, nitrate (NO_3^-). The formation of PN in highly acidic concentrations, as in the concentrations used in **Figure 3.4, 6 and 8**, involve the nitrosation of H_2O_2 (reaction R3.10-13). The formation of PN in perchloric acid before decay with respect to HNO_2 , NO^+ and H_2O_2 was determined to be first order; acid is a catalyst which catalyzes the rate of formation of PN. Rearrangement/isomerisation of PN has a half life of approximately 1 sec to more stable NO_3^- which also absorbs at 302 nm. The life-time of isomerization is directly dependent on concentration of initial reactants (**Figure 3.6**). The bimolecular rate constant for the reaction of H_2O_2 and HNO_2 at 25 °C was determined to $3.7 \times 10^3 \text{ M}^{-1} \text{ s}^{-1}$. Decomposition of PN is highly pH-dependent. In neutral to slightly alkaline pH, nitrite and oxygen are formed at the expense of nitrate in a 2:1 stoichiometric ratio. Decomposition reactions showed first order dependence with respect to pH. The rate constant of decomposition of PN in the absence of a substrate at pH 3.0 is 0.98 s^{-1} and 0.10 s^{-1} at pH 8.0 (see **Figure 3.12**). Bicarbonate rapidly forms a complex with PN thereby increasing the rate of decomposition of PN. The rate of decomposition of PN in the presence of bicarbonate has an inverse dependence on pH. Bimolecular rate

constant for decomposition of PN at pH 6.5 in the presence of bicarbonate is $2.0 \times 10^4 \text{ M}^{-1} \text{ s}^{-1}$ and $1.0 \times 10^4 \text{ M}^{-1} \text{ s}^{-1}$ at pH 7.4. Data generated from EPR studies seems to indicate the generation of $\cdot\text{OH}$ radical as a decomposition product of PN. From the EPR data it may be plausible to say that homolysis of the O-O bond in $\text{ONOOH}/\text{ONOO}^-$ at pH 7.4 leads to initial formation of $\cdot\text{NO}_2$ and $\cdot\text{OH}$ radical pairs. These radical species can then undergo bimolecular reactions with more ONOO^- in solution to form nitrite and oxygen. This is shown in reaction (R3.14), while formation of nitrite, at pH 7.4, as a product of decomposition is shown in **Figure 3.3**:



In similar fashion, nitrite and oxygen are formed in strongly basic pH (pH 9-12) conditions (**Figure 3.3**).



In summary, decomposition reactions of PN produce products which are determined by the pH of the reaction media, this is shown in **Figure 3.16**.

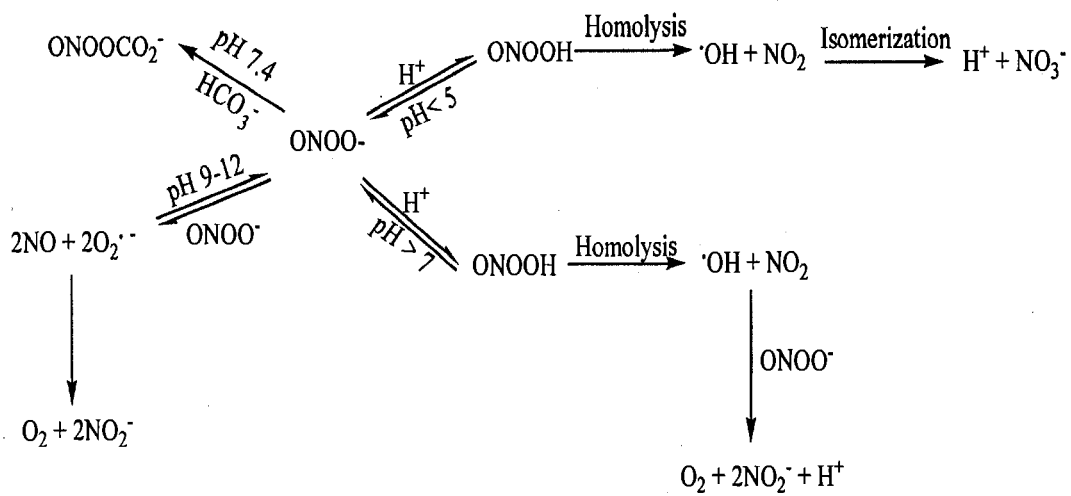


Figure 3.16: Products of decomposition of PN as a function of pH.

CHAPTER 4

MECHANISTIC BASIS OF PEROXYNITRITE (PN) DEACTIVATION BY GLUTATHIONE

4.1 INTRODUCTION

The oxidation chemistry by peroxynitrite is highly pH dependent. Thiols are some of the most well known substrates that can be oxidized by PN in the physiological environment. The oxidation of substrates by PN can occur through various pathways which are at present poorly understood. There are generally two main pathways (i) direct oxidations (ii) indirect oxidations. Direct oxidations usually occur through a two electron transfer from oxidant to reductant with formation of sulfenic acid which is an unstable intermediate. Sulfenic acid formed is rapidly reduced to the disulfides corresponding to the initial thiol. PN may, in other pH conditions, decompose into highly reactive species and the decomposition products then oxidizes the substrates. This pathway of oxidation is known as the indirect pathway of PN oxidation. Oxidations by the indirect pathway may occur through reaction of radicals with the substrate, in other words, by one electron mechanisms (**Figure 4.1**). The final stable product of oxidation for both the direct and indirect oxidation pathways is disulfide of the parent thiol. Disulfide formation as the final stable product cannot distinguish between one or two electron oxidation pathways. There may be different intermediates formed, depending on the number of electrons transferred in the process of oxidation, which is a function of the pH of the reaction medium. Many intermediates have been proposed as the intermediates formed in the PN mediated one or two electron oxidation of thiols.

Examples are sulfenic acids²¹⁸, sulfanyl radicals²⁰¹, thionitrites or nitrosothiols²¹⁹ and sulfenyl nitrites²¹⁸. Some articles have also proposed that at physiological pH conditions, peroxynitrites oxidize thiols to give small amounts of S-nitrosothiols, which can be effective NO donors in the physiological system. The mechanisms of thiol oxidation and the exact pathway of oxidation remain unclear in spite of numerous research works that have been done so far.

In this chapter, the oxidation mechanisms of glutathione by PN will be examined, S-nitrosothiol formation of glutathione in the presence of PN will be studied and the final product (s) of oxidation will be established.

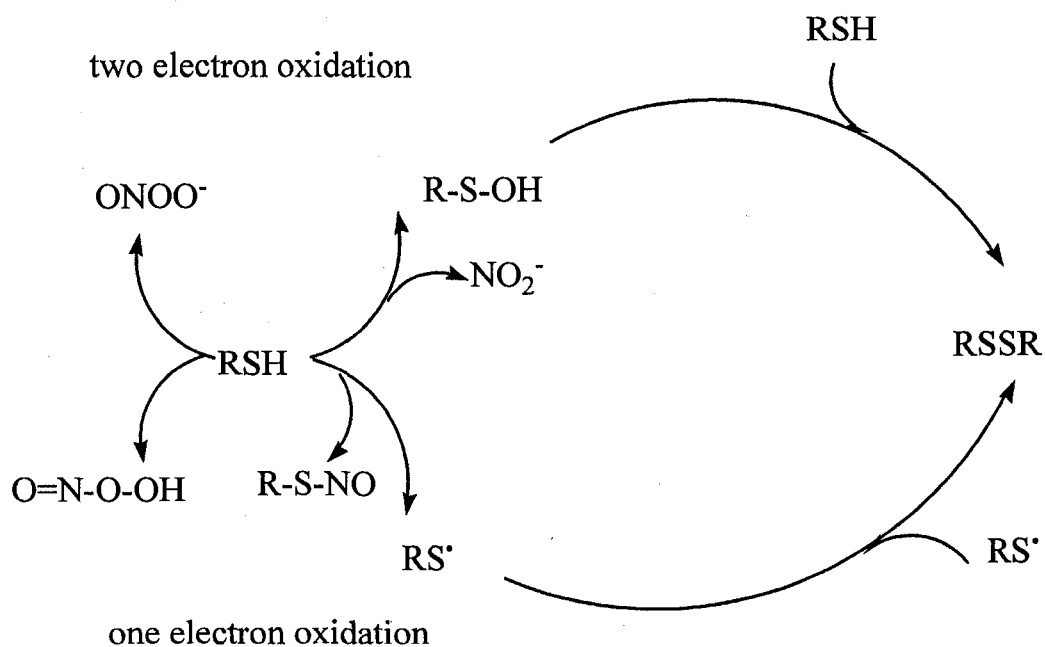
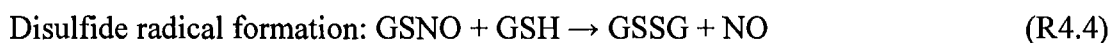
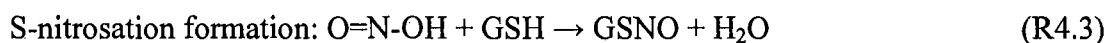


Figure 4.1: Pathways of thiol oxidation.

4.2 Stoichiometry and product determination

The stoichiometry of the S-nitrosation reaction of glutathione (GSH) with PN in acidic pH conditions was determined as:



In high pH conditions the stoichiometry of oxidation reaction of PN with GSH was determined as:



Reaction R4.5 is a stepwise reaction that involved initially, the formation of a sulfenic acid intermediate (reaction R4.6) followed by a dimerization/condensation reaction to form the disulfide (see reaction R4.7).



GSNO and GSSG formed in reactions (R 4.3 and 4.5) were characterized using

mass spectrometry and HPLC methods (**Figure 4.2**). HNO_2 and NO_2^- formed in reactions (R 4.2 and 4.5) were characterized by the wavelength of absorption of 355 nm.

4.3 Reaction dynamics

The study of the oxidation of GSH by PN was split into the following three general sections: (i) S-nitrosation reactions (ii) direct GSSG formation at 302 nm, and (iii) EPR studies

4.3.1 S-nitrosation reactions: These reactions involve electrophilic addition of a nitrosyl (NO^+) ion (formed in low pH conditions) from PN to the sulfur atom of glutathione thiolate anion in a process called S-nitrosation. PN was made fresh every day from the reaction of acidified hydrogen peroxide with nitrite. The single mixing mode of the stopped flow was used such that PN at pH 12 was mixed with sodium perchlorate and diluted with deionised water. This mixture was then transferred into a feed stream of the stopped flow and the other feed stream contains the mixture of GSH and perchloric acid. The injection of acid and PN into separate feed streams precludes the possibility of PN decomposing before nitrosation starts. The progress of the reaction was followed on the stopped flow at the wavelength of absorption of glutathione nitrosothiol (GSNO). GSNO absorbs at two distinct wavelengths, one in the near UV region (335 nm) and the other in the visible (544 nm). The absorbance in the visible region does not have interference from the absorbance contributions from nitrite at 355 nm and absorption of PN at 302 nm.

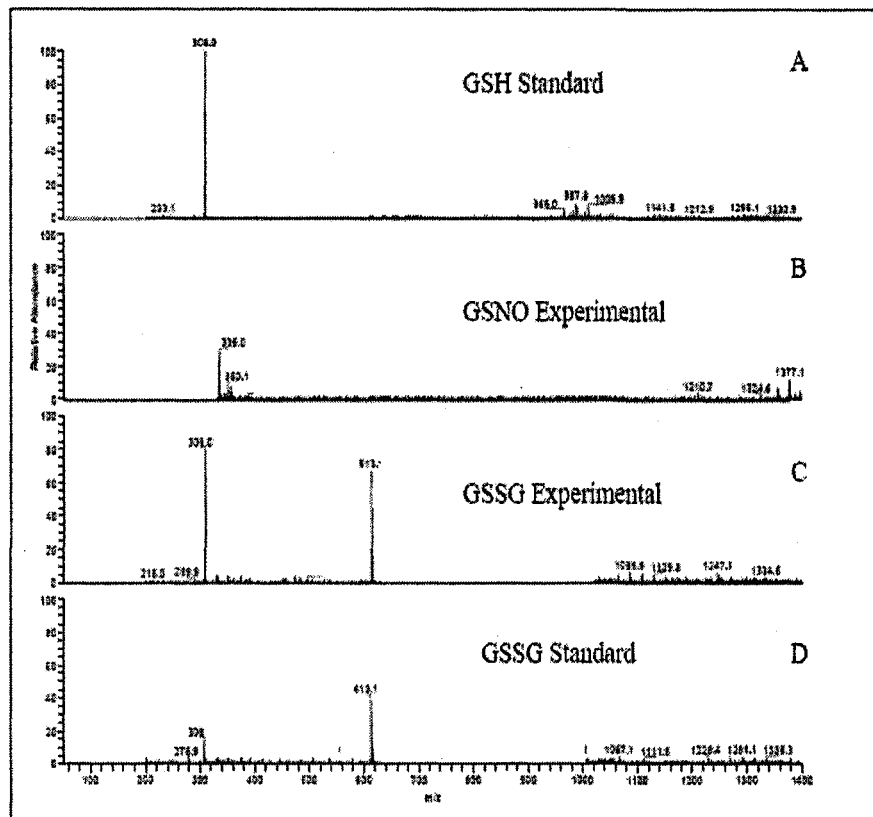


Figure 4.2: Product determination of the nitrosation and direct disulfide formation reactions of GSH by PN, a) 0.98 mM standard GSH, b) 150 mM GSH + 50 mM PN + 12.5 mM H^+ , c) 8.0 mM GSH + 0.8 mM PN in buffer pH 7.4 d) 0.098 mM standard GSSG. Spectra in (b) with m/z of 335 identifies GSNO and the appearance of a single spectra with m/z of 613.1 in spectra (c) which is the exact m/z of 613.1 for GSSG standard, identifies GSSG.

Clearly from **Figure 4.3**, the best wavelength to follow the progress of this reaction was at 544 nm. Most of the reactions were run with PN as the limiting reagent.

Spectra of GSH, PN and the reaction of GSH, H⁺ and PN to form GSNO

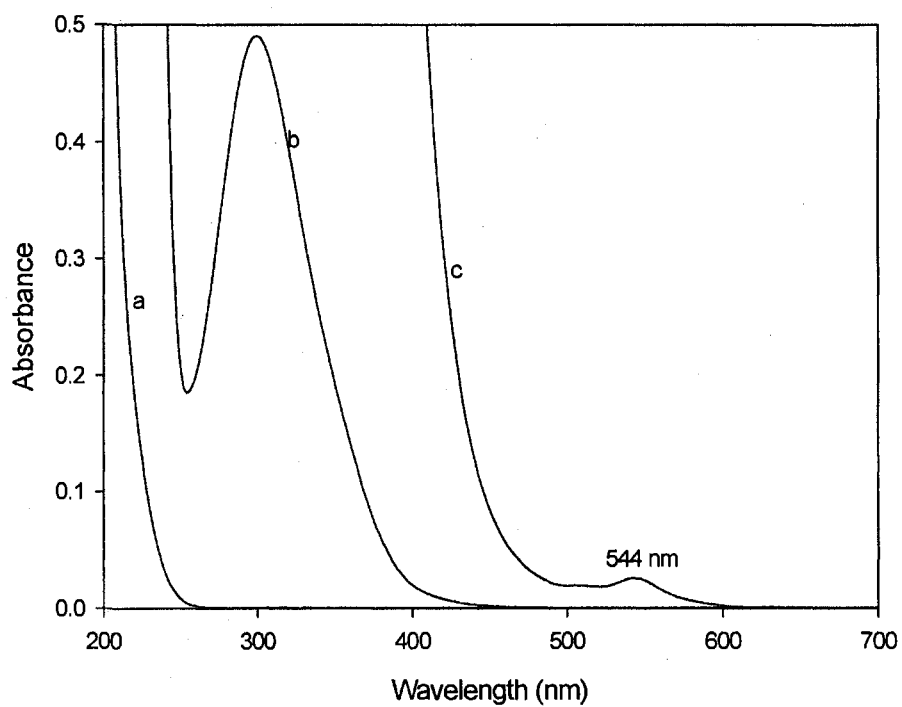


Figure 4.3: a) [GSH] = 1.0×10^{-3} M, b) [PN] = 2.9×10^{-4} M, c) GSH + HClO₄ + PN at 544 nm

For c) [GSH] = 2.5×10^{-2} M, [HClO₄] = 0.175 M, [PN] = 1.7×10^{-3} M.

4.3.1.1 Acid dependence

Kinetics of formation of GSNO seems to have a complex dependence on acid.

Figure 4.4 shows the effect of adding acid at concentrations greater than those of PN. This shows a catalytic effect on the formation of GSNO at 544 nm. As concentrations of perchloric acid are increased so does the formation of GSNO and its rate of formation. Further increase in acid concentrations, however does not seem to increase formation of GSNO and saturation sets in. The continual increase in acid concentration is seen to catalyze the decay of GSNO (see **Figure 4.4**, traces e, f and g).

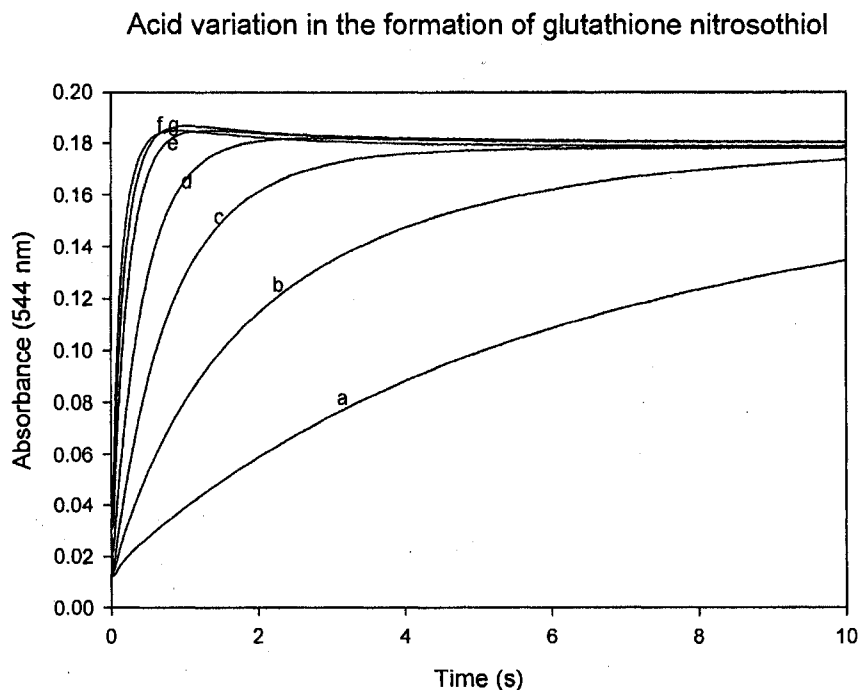


Figure 4.4: Fixed: [PN] = 1.2×10^{-2} M, [GSH] = 9.0×10^{-2} M, [EDTA] = 1.0×10^{-4} M, I_{NaClO_4} = 0.5 M.

[HClO₄] a) 2.9×10^{-1} M, b) 3.1×10^{-1} M, c) 3.4×10^{-1} M, d) 3.6×10^{-1} M, e) 3.9×10^{-1} M, f) 4.1×10^{-1} M, g) 4.4×10^{-1} M.

The initial rate plot of acid dependence shown in **Figure 4.5** appears to be discontinuous with the first five acid concentrations showing linearity as a direct function of acid concentrations. It can be implied that at low acid concentrations the rate of formation of GSNO is first order with respect to PN. The plot, however, loses linearity at higher acid concentrations. This would suggest a simple one term rate law at low acid and a more complex multiterm rate law at higher acid concentrations.

Initial rate plot for acid variation in oxidation of GSH by PN

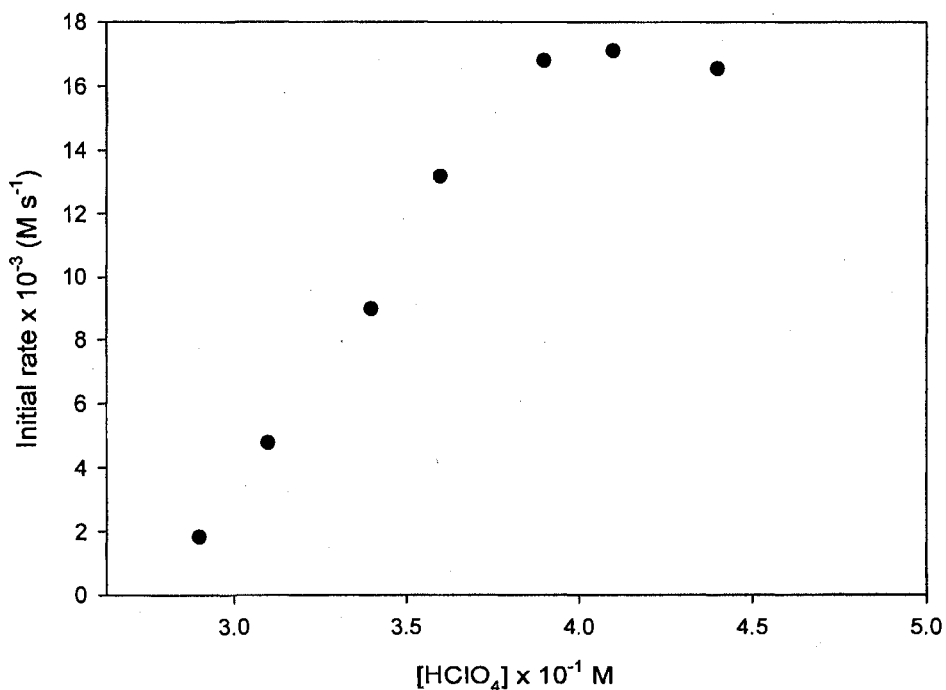


Figure 4.5: Fixed: [PN] = 1.2×10^{-2} M, [GSH] = 9.0×10^{-2} M, [EDTA] = 1.0×10^{-4} M, I_{NaClO_4} = 0.5 M.
 [HClO₄] a) 2.9×10^{-1} M, b) 3.1×10^{-1} M, c) 3.4×10^{-1} M, d) 3.6×10^{-1} M, e) 3.9×10^{-1} M, f) 4.1×10^{-1} M, g) 4.4×10^{-1} M.

4.3.1.2 GSH dependence

The effect of varying GSH in the presence of constant concentrations of PN and acid (HClO_4) is shown in **Figure 4.6**. As concentrations of GSH are increased, the rate of formation and the final concentration of GSNO also increase. Initial rate plot (**Figure 4.7**) with respect to GSH concentrations shows first order dependence in GSH for as long as $[\text{GSH}]_0 > [\text{PN}]_0$.

Glutathione variation in the formation of glutathione nitrosothiol (GSNO)

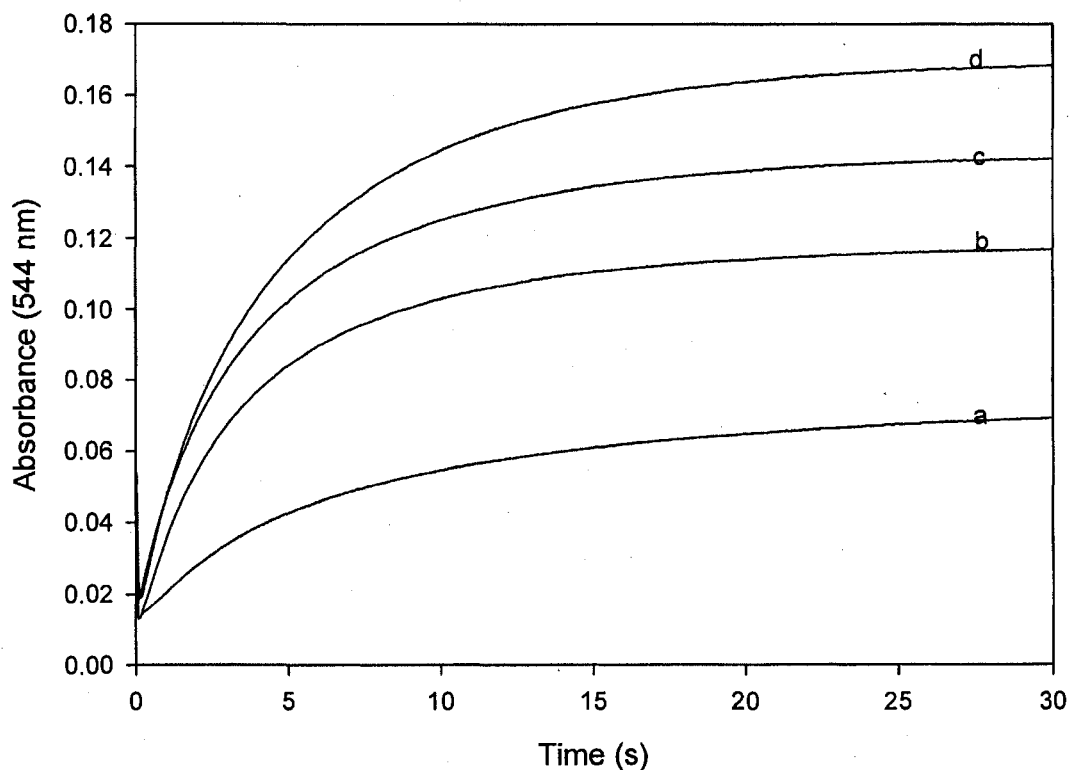


Figure 4.6: Fixed $[\text{PN}] = 9.0 \times 10^{-3} \text{ M}$, $[\text{HClO}_4] = 3.1 \times 10^{-1} \text{ M}$, $[\text{EDTA}] = 1.0 \times 10^{-4} \text{ M}$, $I_{\text{NaClO}_4} = 0.5 \text{ M}$. $[\text{GSH}] = \text{a) } 1.5 \times 10^{-2} \text{ M}$, $\text{b) } 3.0 \times 10^{-2} \text{ M}$, $\text{c) } 4.5 \times 10^{-2} \text{ M}$, $\text{d) } 6.0 \times 10^{-2} \text{ M}$.

Initial rate plot for the variation of GSH in the formation of GSNO

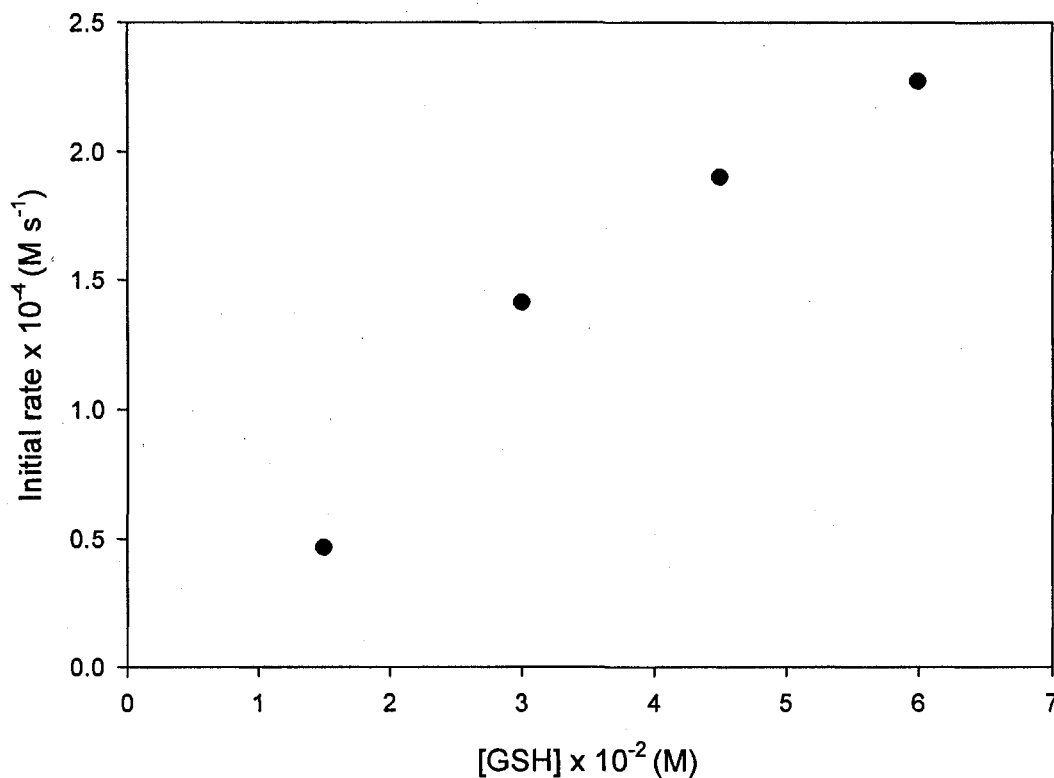


Figure 4.7: Fixed [PN] = 9.0×10^{-3} M, [HClO₄] = 3.1×10^{-1} M, [EDTA] = 1.0×10^{-4} M, I_{NaClO₄} = 0.5 M. [GSH] = a) 1.5×10^{-2} M, b) 3.0×10^{-2} M, c) 4.5×10^{-2} M, d) 6.0×10^{-2} M.

4.3.1.3 PN dependence

Variation of PN to determine the effect of PN on the formation of GSNO shows continuous increase in the amount and rate of GSNO formed as the concentration of PN increases (**Figure 4.8**). The initial rate plot shown in **Figure 4.9** shows that the rate of formation of glutathione nitrosothiol (GSNO) with respect to PN concentrations is first order.

Peroxynitrite variation in the formation of glutathione nitrosothiol

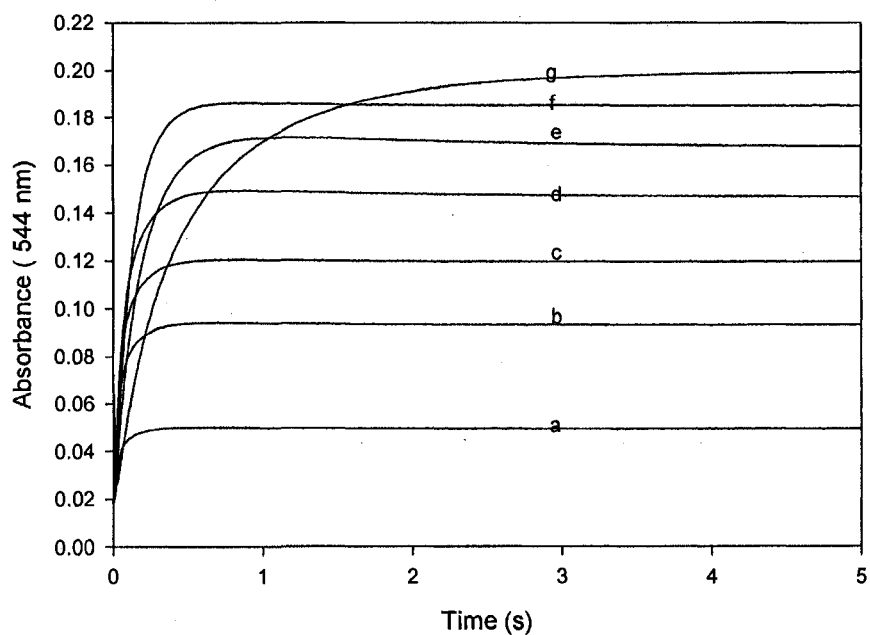


Figure 4.8: Fixed [GSH] = 9.0×10^{-2} M, [HClO₄] = 3.8×10^{-1} M, [EDTA] = 1.0×10^{-4} M, I_{NaClO₄} = 0.5 M.
[PN] = a) 2.8×10^{-3} M, b) 5.3×10^{-3} M, c) 6.9×10^{-3} M, d) 8.4×10^{-3} M, e) 9.7×10^{-3} M, f) 1.0×10^{-2} M, g) 1.1×10^{-2} M

Initial rate plot for the variation of PN in the formation of GSNO by PN

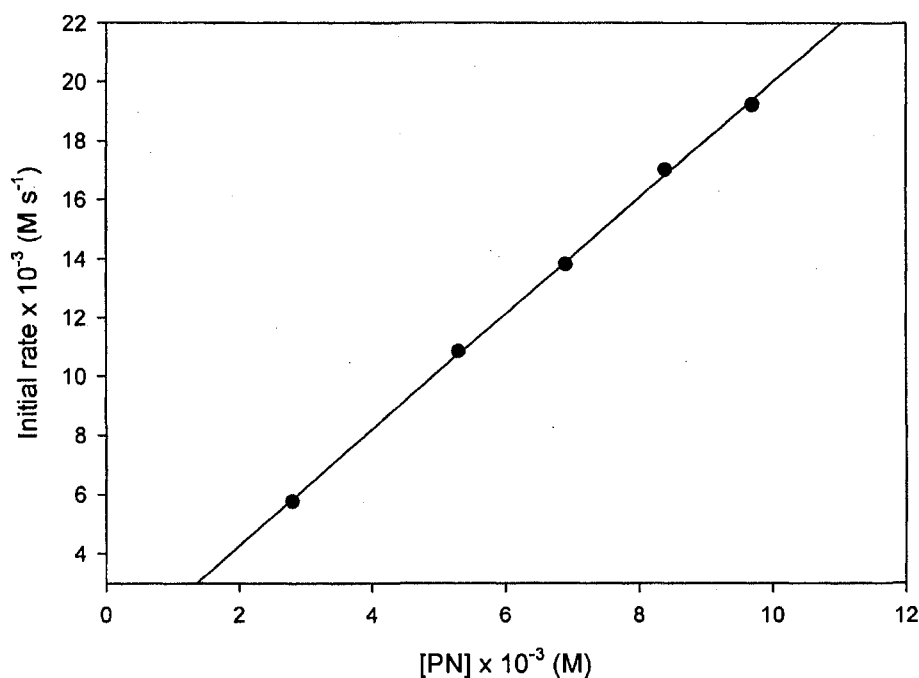


Figure 4.9: Fixed [GSH] = 9.0×10^{-2} M, [HClO₄] = 3.8×10^{-1} M, [EDTA] = 1.0×10^{-4} M, I_{NaClO₄} = 0.5 M.

[PN] = a) 2.8×10^{-3} M, b) 5.3×10^{-3} M, c) 6.9×10^{-3} M, d) 8.4×10^{-3} M, e) 9.7×10^{-3} M, f) 1.0×10^{-2} M, g) 1.1×10^{-2} M

4.3.2 Direct GSSG formation at 302 nm

Direct GSSG formation implies the oxidation of GSH directly to GSSG in a two-electron oxidation transfer from PN (ONOO⁻) through the formation of an unstable sulfenic acid (GSOH) as shown in reaction R4.7. Further reaction of GSOH with excess GSH finally forms GSSG, reaction R4.7. The oxidation reaction was monitored at 302 nm, which is the wavelength of absorption of PN. The consumption of PN was monitored using the single mixing mode of the stopped flow spectrophotometer. The choice of 302 nm for monitoring the progress of reaction

was ideal in that GSH does not absorb in the UV-vis region, and also that GSSG does not absorbance at 302 nm. Thus, the measured absorbance at 302 nm is due solely to spectrophotometric activity of PN. PN was mixed with ethylenediammine tetraacetic acid (EDTA), diluted with distilled water and fed into one of the reaction vessels of the stopped flow instrument while the second vessel contained GSH and sodium phosphate buffer at a specific pH. This arrangement helped to prevent premature reaction of GSH with PN before kinetic measurement by the stopped flow could commence. Reactions were performed at 25 °C, and equal volumes of PN and GSH solutions were taken each time for every acquisition on the stopped flow. Multiple acquisitions were made to ensure reproducibility.

4.3.2.1 GSH dependence

The role of GSH in the oxidation of GSH by PN was examined by varying concentrations of GSH and keeping the concentrations of PN constant. This is shown in **Figure 4.10**. Increasing GSH concentrations increases the rate of consumption of PN by GSH with the highest GSH concentration having the highest rate of PN consumption. Further increase in GSH concentration as seen in traces e, f, g tends to saturates because all the PN have been consumed by GSH. The initial rate plot for the consumption is shown in **Figure 4.11**, which shows that the rate of depletion of PN is first order with respect to GSH.

Oxidation of glutathione by peroxynitrite: Varying Glutathione

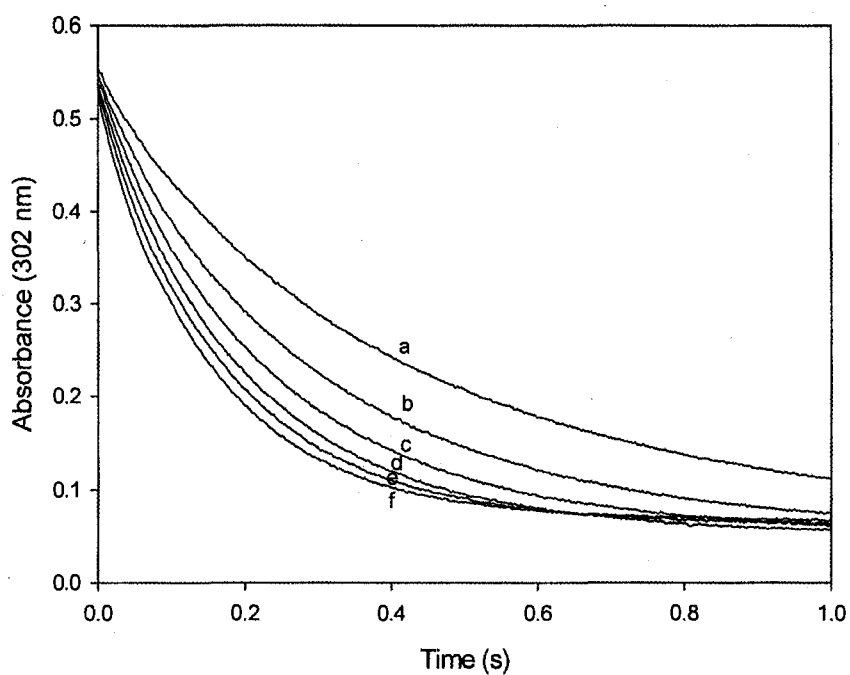


Figure 4.10: Fixed: [PN] = 3.96×10^{-4} M, [EDTA] = 1.0×10^{-4} M, [Phosphate buffer pH 7.0] = 1.5×10^{-3} M, [GSH] = a) 3.0×10^{-3} M, b) 4.0×10^{-3} M, c) 5.0×10^{-3} M, d) 6.0×10^{-3} M, e) 7.0×10^{-3} M, f) 8.0×10^{-3} M.

Initial rate plot for the oxidation of glutathione by PN

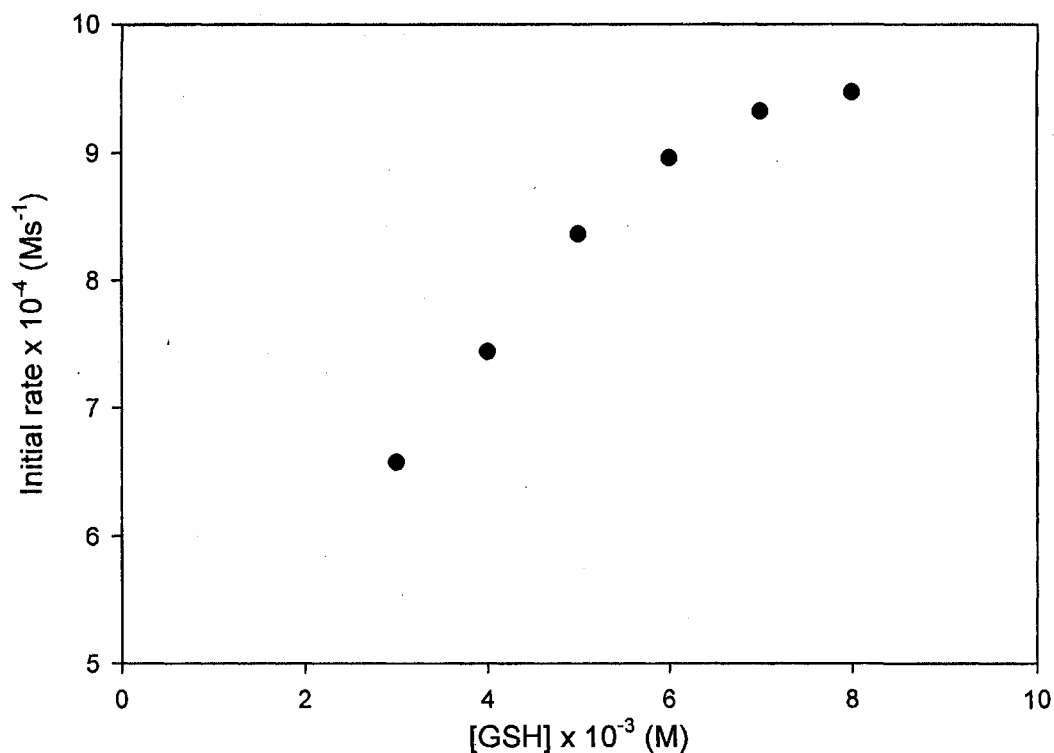


Figure 4.11: Fixed: [PN] = 3.96×10^{-4} M, [EDTA] = 1.0×10^{-4} M, [Phosphate buffer pH 7.0] = 1.5×10^{-1} M, [GSH] = 3.0 x 10⁻³ M, b) 4.0 x 10⁻³ M, c) 5.0 x 10⁻³ M, d) 6.0 x 10⁻³ M, e) = 7.0 x 10⁻³ M, f) 8.0 x 10⁻³ M.

4.3.2.2 PN dependence

To determine the effect of PN on the oxidation of GSH, PN concentrations were varied while the concentration of GSH was kept constant. Since absorbance is directly proportional to concentration, higher PN concentrations have higher initial absorbance readings and likewise low PN concentrations delivers lower PN absorbances at 302 nm with constant excess GSH concentration over PN (Figure 4.12). The lowest PN concentration has the lowest rate of depletion

while the highest PN concentration has the highest rate of depletion of PN by GSH. The initial rate of consumption is shown in **Figure 4.13**. The graph in **Figure 4.13** further shows that the rate of consumption of PN in the presence of a fixed concentration of GSH follows a first order dependence with respect to PN concentrations.

Oxidation of glutathione by peroxyntirite: Varying peroxyntirite

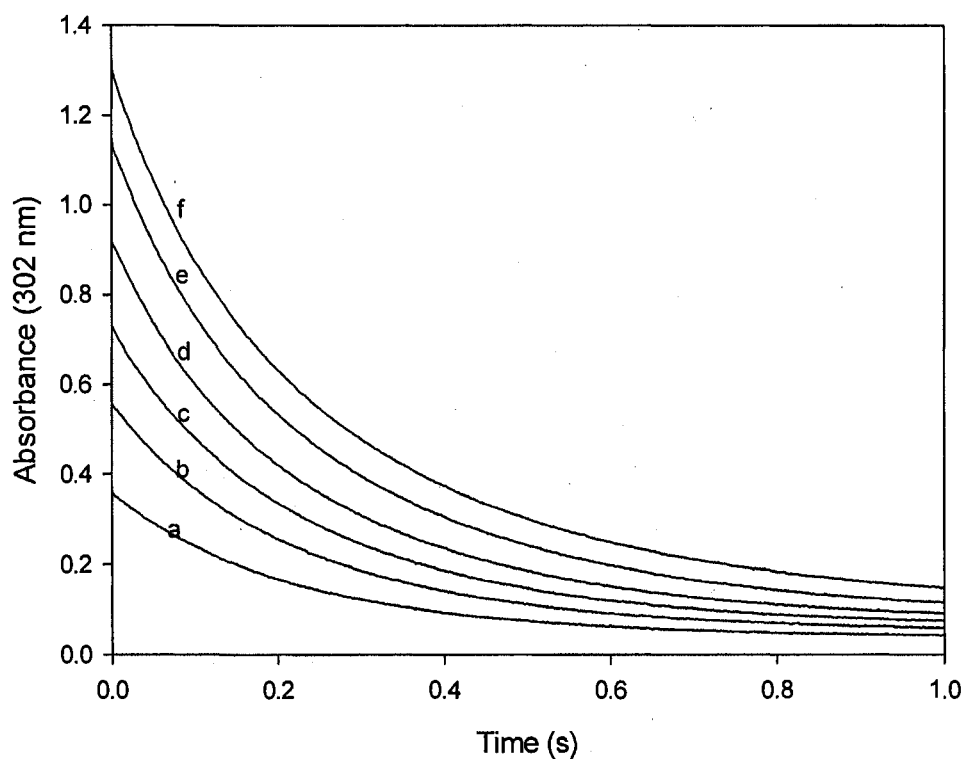


Figure 4.12: Fixed: [GSH] = 5.0×10^{-3} M, [EDTA] = 1.0×10^{-4} M, [Phosphate buffer pH 7.0] = 1.5×10^{-1} M, [PN] = a) 2.6×10^{-4} M, b) 3.9×10^{-4} M, c) 5.2×10^{-4} M, d) 6.5×10^{-4} M, e) 7.8×10^{-4} M, f) 9.1×10^{-4} M.

Initial rate plot for the oxidation of GSH by PN, done varying PN

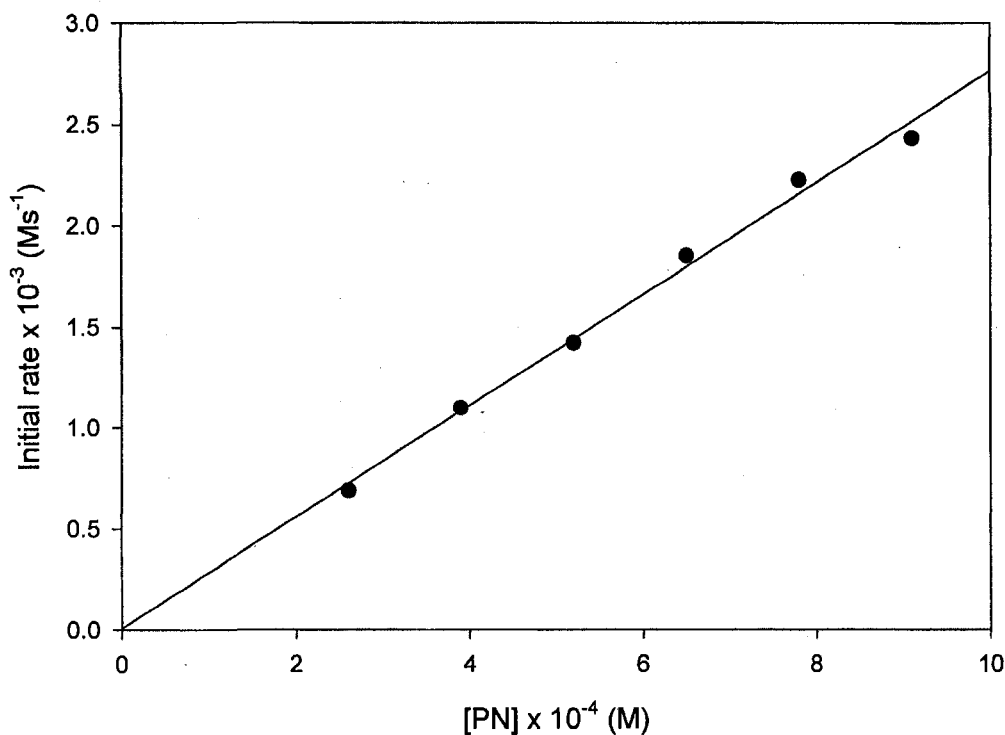


Figure 4.13: Fixed: [GSH] = 5.0×10^{-3} M, [EDTA] = 1.0×10^{-4} M, [Phosphate buffer pH 7.0] = 1.5 : [PN] = a) 2.6×10^{-4} M, b) 3.9×10^{-4} M, c) 5.2×10^{-4} M, d) 6.5×10^{-4} M, e) 7.8×10^{-4} M, f) 9.1×10^{-4} M.

4.3.2.3 Effect of pH on glutathione oxidation by PN

The depletion of PN at 302 nm as a function of pH in the presence of glutathione is shown in **Figure 4.14**. The graph shows that PN is quickly consumed in the presence of constant concentration of GSH at different pH. The highest rate of consumption of PN was observed at low pH conditions, while at high pH conditions the rate of consumption of PN decreased. Initial rate plot for data in

Figure 4.14 shows linear dependence in relation to pH 3.0-5.0, deviations from linearity were observed for pH 5.5-8.5 (**Figure 4.15**). Bimolecular rate constants for the oxidation of GSH at 25 °C in pH 3.0-8.0 are shown in **Figure 4.16**.

Effect pH on glutathione oxidation by PN

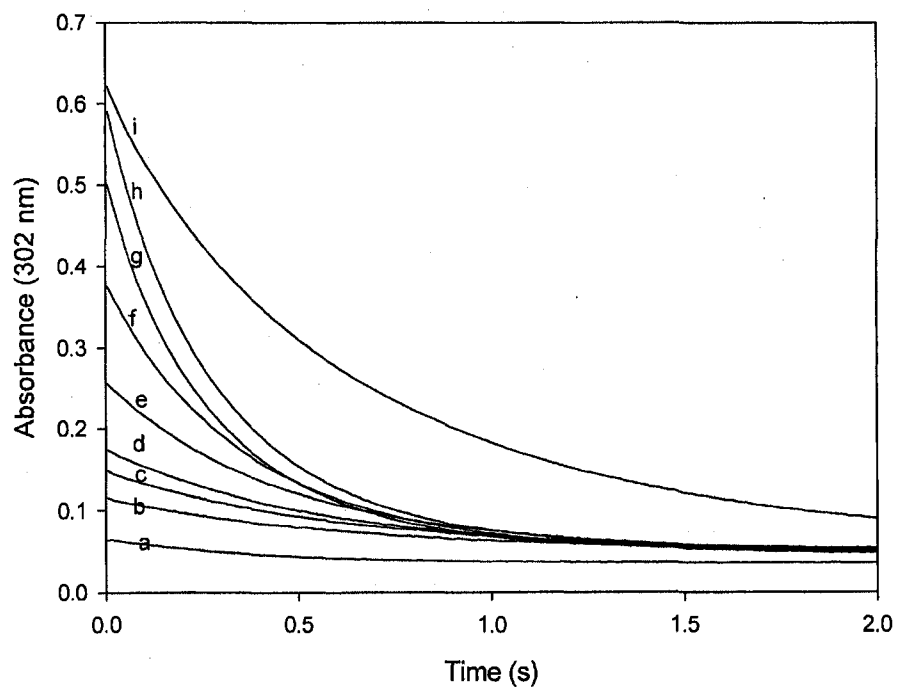


Figure 4.14: Fixed: [GSH] = 4.0×10^{-3} M, [PN] = 3.8×10^{-4} M, [EDTA] = 1.0×10^{-4} M, [Phosphate buffer] 1.5×10^{-1} M
Phosphate buffer pH = a) 3.0, b) 4.0, c) 5.0, d) 5.5, e) 6.0, f) 6.5, g) 7.0, h) 7.4, i) 8.0

Initial rate plot for the effect pH on glutathione oxidation by PN

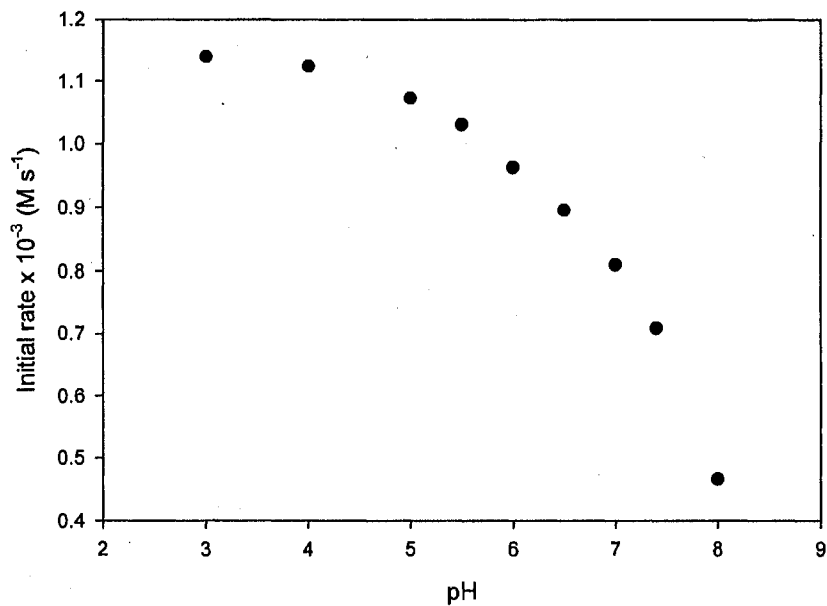


Figure 4.15 : Fixed: [GSH] = 4.0×10^{-3} M, [PN] = 3.8×10^{-4} M, [EDTA] = 1.0×10^{-4} M, [Phosphate buffer] 1.5×10^{-1} M
Phosphate buffer pH = a) 3.0, b) 4.0, c) 5.0, d) 5.5, e) 6.0, f) 6.5, g) 7.0, h) 7.4, i) 8.0

Rate constants for effect pH on glutathione oxidation by PN.

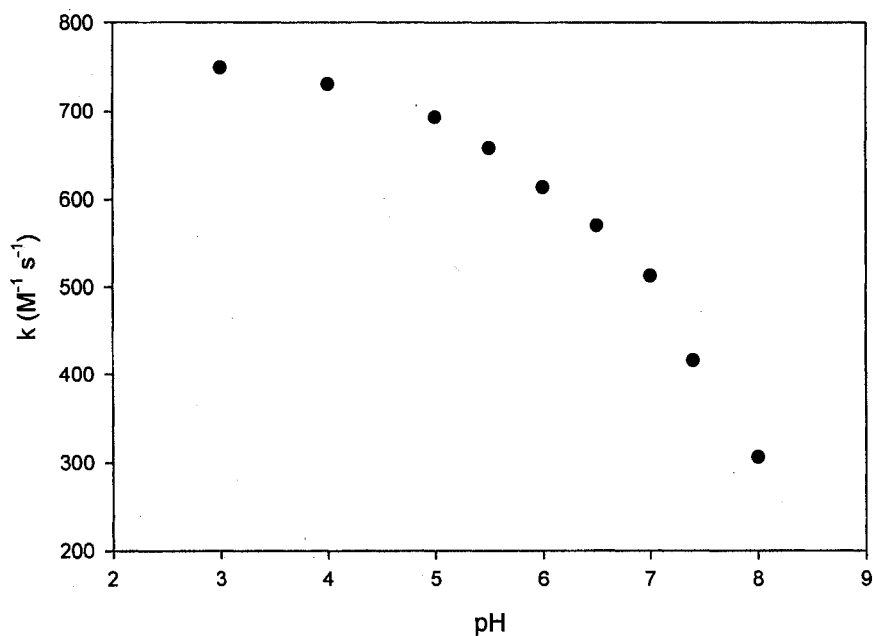


Figure 4.16: Fixed: [GSH] = 4.0×10^{-3} M, [PN] = 3.8×10^{-4} M, [EDTA] = 1.0×10^{-4} M, [Phosphate buffer] 1.5×10^{-1} M
Phosphate buffer pH = a) 3.0, b) 4.0, c) 5.0, d) 5.5, e) 6.0, f) 6.5, g) 7.0, h) 7.4, i) 8.0

4.3.2.4 Effect of sodium bicarbonate (HCO_3^-) on glutathione oxidation by PN

HCO_3^- is naturally produced by the gastric membrane in the stomach and helps in regulating the acid-base balance in the physiological system²²⁰. The mucus membrane of the human stomach has 30 million glands which produce gastric juice containing not only acids, but also bicarbonate²²¹. The flow of bicarbonate in the stomach amounts from 400 μmol per hour (24.4 mg/h) for a basal output to 1,200 μmol per hour (73.2 mg/h) for a maximal output²²². At least half a gram of bicarbonate is secreted daily in the human stomach. This rate of gastric bicarbonate secretion is 2-10 % of the maximum rate of acid secretion²²². In the stomach, bicarbonate participates in a mucus-bicarbonate barrier regarded as the first line of the protective and repair mechanisms²²⁰. On neutralization by acid, carbon dioxide is produced from bicarbonate:



Since PN is produced in the physiological system and has been implicated in many oxidative processes, the study of PN oxidation of thiols will be incomplete without studying the effect of HCO_3^- on PN oxidations.

Figure 4.17 shows the effect of varying GSH in the oxidation of GSH at a constant concentration of PN and HCO_3^- . PN is consumed at 302 nm in the presence of zero concentration HCO_3^- as shown in trace (a), while trace (b) shows the effect of added HCO_3^- on the rate of consumption of PN by GSH. As concentrations of GSH

are being increased with constant HCO_3^- ; increased rate of consumption is observed at constant PN and excess HCO_3^- over PN. It seems there is competition between the HCO_3^- and GSH for PN since both HCO_3^- and GSH are in excess concentration over PN. The initial rate plot shown in **Figure 4.18** shows that the rate of consumption of PN with respect to GSH is a first order reaction.

Effect HCO_3^- on glutathione oxidation: Varying glutathione

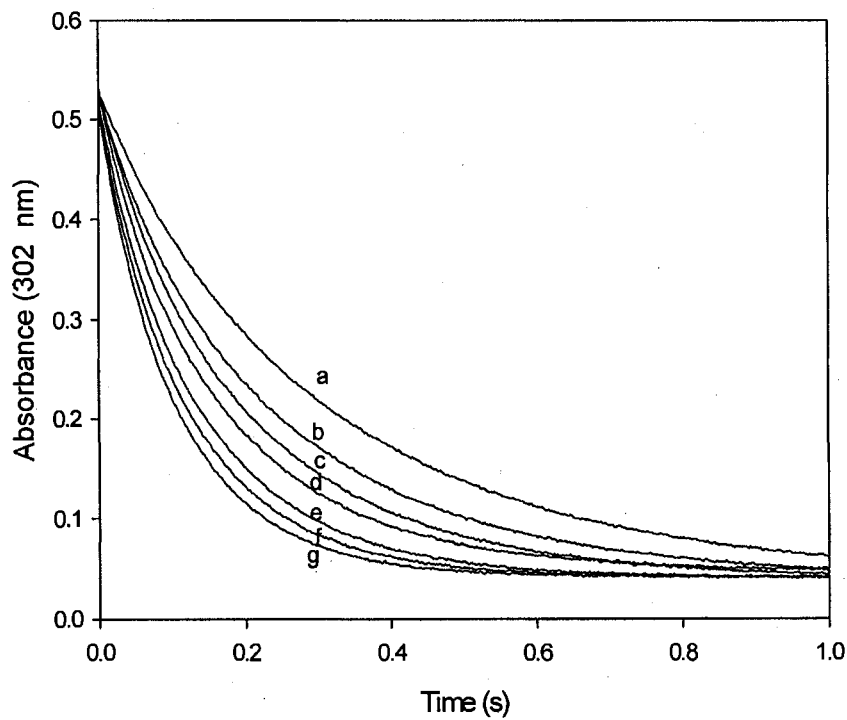


Figure 4.17: Fixed: $[\text{PN}] = 3.1 \times 10^{-4} \text{ M}$, $[\text{HCO}_3^-] = 1.5 \times 10^{-3} \text{ M}$, $[\text{EDTA}] = 1.0 \times 10^{-4} \text{ M}$, [Phosphate buffer pH 7.4] = $1.5 \times 10^{-1} \text{ M}$, $[\text{GSH}] =$ a) $4.0 \times 10^{-3} \text{ M} + 0 \text{ M HCO}_3^-$, b) $4.0 \times 10^{-3} \text{ M}$, c) $5.0 \times 10^{-3} \text{ M}$, d) $6.0 \times 10^{-3} \text{ M}$, e) $7.0 \times 10^{-3} \text{ M}$, f) $8.0 \times 10^{-3} \text{ M}$, g) $9.0 \times 10^{-3} \text{ M}$.

Initial rate plot for the effect of HCO_3^- on GSH oxidation: Varying GSH

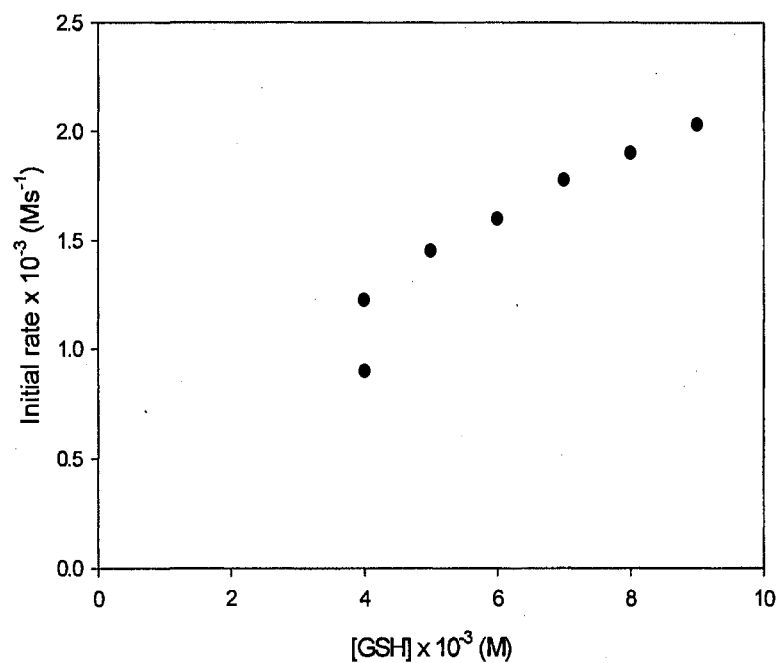


Figure 4.18: Fixed: $[\text{PN}] = 3.1 \times 10^{-4} \text{ M}$, $[\text{HCO}_3^-] = 1.5 \times 10^{-3} \text{ M}$, $[\text{EDTA}] = 1.0 \times 10^{-4} \text{ M}$, $[\text{Phosphate buffer pH 7.4}] = 1.5 \times 10^{-1} \text{ M}$
 $[\text{GSH}] = \text{a) } 4.0 \times 10^{-3} \text{ M} + 0 \text{ M HCO}_3^-$, b) $4.0 \times 10^{-3} \text{ M}$, c) $5.0 \times 10^{-3} \text{ M}$, d) $6.0 \times 10^{-3} \text{ M}$, e) $7.0 \times 10^{-3} \text{ M}$, f) $8.0 \times 10^{-3} \text{ M}$, g) $9.0 \times 10^{-3} \text{ M}$

4.4 EPR studies

The major aim of following the progress of oxidation of GSH by PN using EPR as a tool is to elucidate the pathway of oxidation; if it involves formation of radicals.

4.4.1 Oxidation of glutathione by PN

Graphical data obtained in **Figure 4.19** (shown later in the text) shows DMPO radical adduct of the oxidation products of GSH at pH 7.4. Trace (a) was generated from the standard Fenton's reaction which is a well known reaction for the generation of hydroxyl radicals. This trace shows the 1:2:2:1 quartet spectrum with splitting of $a_N = a_H = 14.9 \text{ G}^{216}$ characteristic of DMPO-OH radical adduct. Trace (b) is a mixture of PN and DMPO without the addition of GSH. At pH 7.4, PN is reasonably protonated and decomposition of PN is expected to occur according to reaction sequence R4.9 - 10:



Trace (b) also generated 1:2:2:1 quartet with splitting of $a_N = a_H = 14.9 \text{ G}^{216}$ characteristic of DMPO-OH radical adduct, but radical adduct yields were low.

Increase in PN concentration in trace (c) resulted in loss of signal. Trace (d) and (e) contained added concentrations of GSH, increase in added concentrations of GSH led to stronger signal intensity with a 1:2:2:1 quartet with splitting of $a_N = 15.4 \text{ G}$; $a_H = 16.2 \text{ G}^{216}$ which is characteristic of DMPO-glutathionyl radical adduct. GSH by itself in DMPO at pH 7.4 did not generate any EPR signal. Trace (f) shows the trace which

consists of mannitol, a well known hydroxyl radical scavenger, added to reactants with similar concentrations as in trace (b). The result shows an almost complete annihilation of signal. This result is evidence of generation of hydroxyl radical (trace (b)) from the decomposition products of PN, while trace (d) and (e) indicate the generation of glutathionyl radical. The fading of signal intensity observed in trace (c) could be due to direct reactions of PN with either DMPO, DMPO-OH adduct or both. Trace (f) shows the scavenging ability of mannitol for hydroxyl radicals, hence the decrease in signal intensity. To obtain unambiguous evidence for pathway of GSH oxidation by PN at pH 7.4 another spin trap, N-tert-butyl- α -phenylnitron (PBN), was employed. Trace (a) in **Figure 4.20** shows the standard Fenton's reaction with hyperfine splitting of $a_N = 15.46$ G; $a_H = 0.21$ G characteristics of PBN-OH radical adduct. Trace (b) shows incubation of PN and PBN without the addition of GSH showing the typical triple doublet characteristic of PBN-OH radical adduct with splitting of $a_N = 15.46$ G; $a_H = 0.21$ G. In trace (c), the same sample used in trace (b), was used except that the length of incubation was prolonged to test for stability of signal generated, and it was observed that up to a period of 30 minutes the signal intensity did not decay to any noticeable extent. Trace (d) and (e) have added GSH, spectrum generated shows the characteristic glutathionyl radical adduct with splitting of $a_N = 15.5$ G; $a_H = 0.31$ G.

4.4.2 Effect of sodium bicarbonate on oxidation of glutathione by PN

The effect of HCO_3^- on the oxidation of GSH by PN was mentioned in section 4.3.2.4, but the experimental tools (kinetics, using stopped flow spectrophotometer)

used in this section were not able to differentiate between two- and one-electron oxidation mechanisms. The hypothesis or reason for using EPR method in further elucidation of the effect of HCO_3^- in oxidation of GSH by PN is that $\text{HCO}_3^-/\text{CO}_2$ is likely to inhibit thiol oxidation via two electron mechanisms while stimulating thiol oxidation through a one electron oxidation. To test this hypothesis, the effects of $\text{HCO}_3^-/\text{CO}_2$ and probable formation of free radicals during the oxidation of GSH by PN was studied using EPR technique. **Figure 4.21** shows EPR spectra of DMPO radical adducts obtained during oxidation of glutathione (GSH) by peroxyntirite (PN) in the presence of sodium bicarbonate in sodium phosphate buffer at pH 7.4. This is physiological pH and it was the pH of choice for couple of reasons (i) mimic the effect of $\text{HCO}_3^-/\text{CO}_2$ in the physiological environment and (ii) relatively easily furnish the release of H^+ for easy conversion of HCO_3^- to CO_2 (reaction R4.9). Trace (a) in **Figure 4.21** shows the effect of reacting HCO_3^- with excess DMPO at pH 7.4. At this pH no signal was observed. Addition of HCO_3^- in the presence of PN and DMPO gave a weak signal which is observed in trace (b). EPR signal generated in trace (b) is due to adduct formed in the reaction of PN with $\text{HCO}_3^-/\text{CO}_2$:



This adduct is unstable and decomposes into $\text{CO}_3^{\cdot -}$ and NO_2/CO_2 and NO_3^- :



The formation of $\text{CO}_3^{\cdot -}$ radicals generates EPR spectra as observed in trace (b) of

Figure 4.21. EPR spectra of DMPO radical adduct of oxidation product (s) of GSH with PN was observed in trace (c), this shows the characteristic glutathioyl radical adduct, in trace (d) effect of added HCO_3^- was observed. It was seen that trace (d) had a stronger characteristic glutathioyl radical adduct compared to trace (c) although both had the same initial concentrations of PN, GSH and DMPO. This observation can be explained by reactions R4.14-15. If the decomposition of PN in the presence of sodium bicarbonate at pH 7.4 goes via the formation of bicarbonate radicals as shown in reaction (R4.11-13), and the rate of formation of ONOOCO_2^- adduct is faster than the rate of oxidation of GSH by PN, then the oxidation of GSH in the presence of HCO_3^- will be diverted to a one electron oxidation by $\text{CO}_3^{\cdot -}$ or by NO_2 . The proposed mechanism for the oxidation of GSH by $\text{CO}_3^{\cdot -}$ is given as follows:

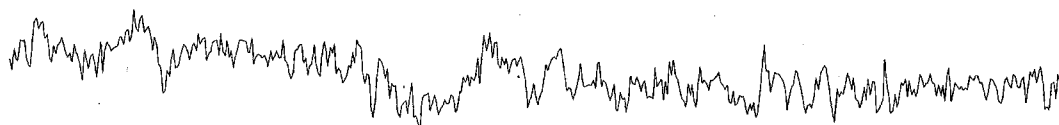




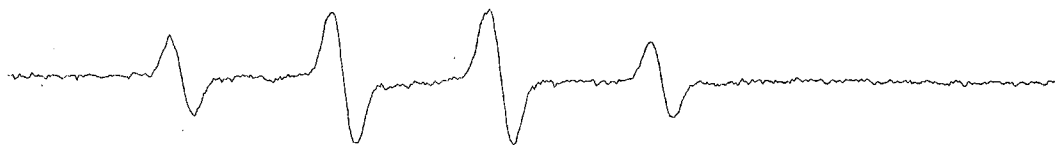
a) Fenton's reaction, after 5 min incubation: $[H_2O_2] = 0.2 \text{ mM}$, $[FeSO_4] = 0.05 \text{ mM}$, $[DMPO] = 80 \text{ mM}$



b) Peroxynitrite decomposition, after 5 min incubation: $[PN] = 20 \text{ }\mu\text{M}$, $[GSH] = 0 \text{ mM}$, $[DMPO] = 80 \text{ mM}$, pH 7.4



c) Peroxynitrite decomposition, after 5 min incubation: $[PN] = 60 \text{ }\mu\text{M}$, $[GSH] = 0 \text{ mM}$, $[DMPO] = 80 \text{ mM}$, pH 7.4



d) GSH oxidation by PN, after 5 min incubation: $[PN] = 0.8 \text{ mM}$, $[GSH] = 4.5 \text{ mM}$, $[DMPO] = 80 \text{ mM}$, pH 7.4



e) GSH oxidation by PN, after 5 min incubation: $[PN] = 0.8 \text{ mM}$, $[GSH] = 3.0 \text{ mM}$, $[DMPO] = 80 \text{ mM}$, pH 7.4



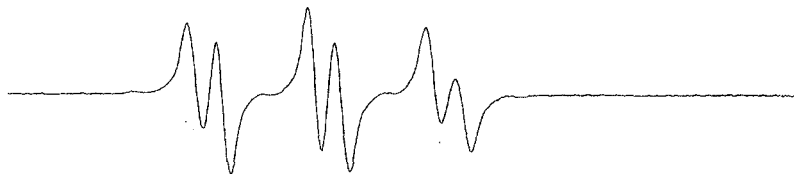
f) PN decomposition, after 5 min incubation: $[PN] = 20 \text{ }\mu\text{M}$, $[GSH] = 0 \text{ mM}$, $[DMPO] = 80 \text{ mM}$, $[Mannitol] = 0.125 \text{ mM}$, pH 7.4

3436-3536 G \rightarrow

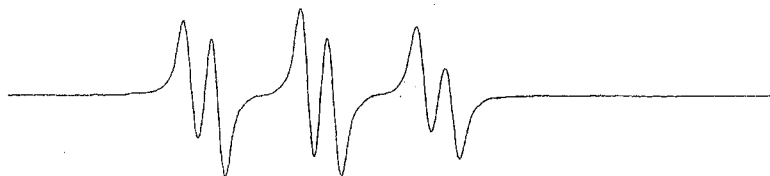
Figure 4.19: EPR radical adducts of DMPO with the oxidation products of GSH obtained at room temperature.



a) Fenton's reaction, after 5 min incubation: $[\text{H}_2\text{O}_2] = 0.2 \text{ mM}$, $[\text{FeSO}_4] = 0.05 \text{ mM}$, $[\text{PBN}] = 50 \text{ mM}$



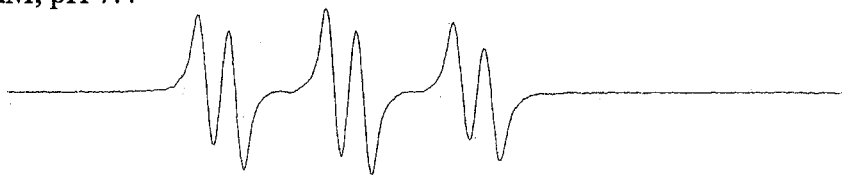
b) PN decomposition, after 15 min incubation: $[\text{PN}] = 1.5 \text{ mM}$, $[\text{GSH}] = 0 \text{ mM}$, $[\text{PBN}] = 50 \text{ mM}$, pH 7.4



c) PN decomposition, after 30 min incubation: $[\text{PN}] = 1.5 \text{ mM}$, $[\text{GSH}] = 0 \text{ mM}$, $[\text{PBN}] = 50 \text{ mM}$, pH 7.4



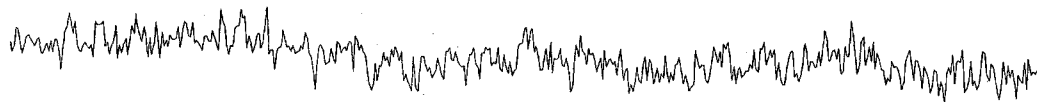
d) GSH oxidation by PN, after 15 min incubation: $[\text{PN}] = 1.5 \text{ mM}$, $[\text{GSH}] = 15 \text{ mM}$, $[\text{PBN}] = 50 \text{ mM}$, pH 7.4



e) GSH oxidation by PN, after 15 min incubation: $[\text{PN}] = 1.5 \text{ mM}$, $[\text{GSH}] = 7.5 \text{ mM}$, $[\text{PBN}] = 50 \text{ mM}$, pH 7.4

→
3436-3536 G

Figure 4.20: EPR radical adducts of PBN with oxidation products GSH, spectra obtained at room temperature.



a) Bicarbonate radical adduct, after 5 minute incubation: $[\text{HCO}_3^-] = 5 \text{ mM}$, $[\text{PN}] = 0 \text{ }\mu\text{M}$, $[\text{GSH}] = 0 \text{ mM}$, $[\text{DMPO}] = 80 \text{ mM}$, pH 7.4



b) Peroxynitrite carbon dioxide radical adduct, after 5 minute incubation: $[\text{HCO}_3^-] = 5 \text{ mM}$, $[\text{PN}] = 0.8 \text{ mM}$, $[\text{GSH}] = 0 \text{ mM}$, $[\text{DMPO}] = 80 \text{ mM}$, pH 7.4



c) Oxidation product GSH, after 5 minute incubation: $[\text{HCO}_3^-] = 0 \text{ mM}$, $[\text{PN}] = 0.8 \text{ mM}$, $[\text{GSH}] = 3 \text{ mM}$, $[\text{DMPO}] = 80 \text{ mM}$, pH 7.4



d) Effect bicarbonate on oxidation GSH, after 5 minute incubation: $[\text{HCO}_3^-] = 5 \text{ mM}$, $[\text{PN}] = 0.8 \text{ mM}$, $[\text{GSH}] = 3 \text{ mM}$, $[\text{DMPO}] = 80 \text{ mM}$, pH 7.4

—————→
3436-3536 G

Figure 4.21: EPR radical adducts of DMPO with HCO_3^- , PN and GSH, spectra obtained at room temperature.

4.5 Conclusion

PN mediates the oxidation of the thiol functional group of GSH. This process is highly pH-dependent. This was confirmed from the multiple stoichiometries exhibited in the reaction of PN with GSH yielding different products at different pH. Oxidation process occurred through a one or two electrons transfer depending on the pH conditions. Oxidation products are GSNO, GSSG, GSOH, NO_2^- , and HNO_2 . In the reaction dynamics at high acidic conditions ($\geq 0.3 \text{ M}$) GSNO was formed. The order of reaction with respect to acid, GSH and PN was first order. The relevant reactions in the production of GSNO were deduced based on the reaction dynamics as shown in section 4.3. They are listed as follows:



Reaction R 4.1 involves the rapid oxidation of thiol to the disulfide, with the release of nitrite ion. Nitrite ion produced in reaction R 4.1 is converted to nitrous acid in reaction R 4.2. Reaction R 4.2 is a rapid protolytic reaction whose equilibrium direction is dependent on the K_a value of nitrous acid. Once nitrous

acid is formed, reaction of nitrous acid with excess acid (that was used in reaction kinetics study) generates nitrosyl ion (reaction R4.16). Nitrosyl ion, being an electrophile, is able to nitrosate GSH, forming GSNO (reaction 4.18). Low acid concentrations will however, furnish nitrous acid, which reacts with GSH to form GSNO and water, see reaction 4.17. In the direct GSSG formation at the wavelength of absorption of PN (302 nm), two reaction dynamics were examined, the GSH dependence on the oxidation of GSH, and PN dependence on the oxidation of GSH. Both of these dependence exhibited simple first order kinetics. The pathway of oxidation was proposed to be a two-electron transfer from PN to the sulfur center of GSH. Two-electron transfers will form GSOH which is known to be highly unstable and will quickly react with another mole of GSH to form GSSG (reaction R4.6-7) and water. The inability to form GSNO is due to the fact that at high pH conditions, nitrite ($pK_a 3.1$)²²³ formed in reaction (R4.6), will not be sufficiently protonated to generate nitrous acid, which is needed to generate GSNO. The bimolecular rate constant for the overall second order formation of GSSG was pH-dependent. The rate constants, as a function of pH, are shown in **Figure 4.16**. The product of oxidation was confirmed to be GSSG (**Figure 4.2**).

At physiological pH of 7.4 EPR results shows the formation of a secondary reagent derived from PN decomposition. It is very likely that this secondary reagent is responsible for thiol oxidation in a one electron transfer mechanism, which may go via formation of nitrogen dioxide and thiyl radical, thiyl radical formed eventually forms stable disulfide of initial thiol (reaction 4.19-20):



EPR results of the effect of HCO_3^- on GSH oxidation by PN shows that oxidation of GSH by PN goes via a one electron pathway at pH 7.4. The produced radicals from GSH oxidation by PN is $\text{GSSG}^{\cdot-}$; $\text{GSSG}^{\cdot-}$ in aerobic conditions forms GSSG.

The formation of glutathionyl radicals from the oxidation of GSH by PN is an important deactivation process for reducing PN toxicity in physiological systems.

The plausible pathway(s) for the oxidation of GSH is shown in **Figure 4.22**.

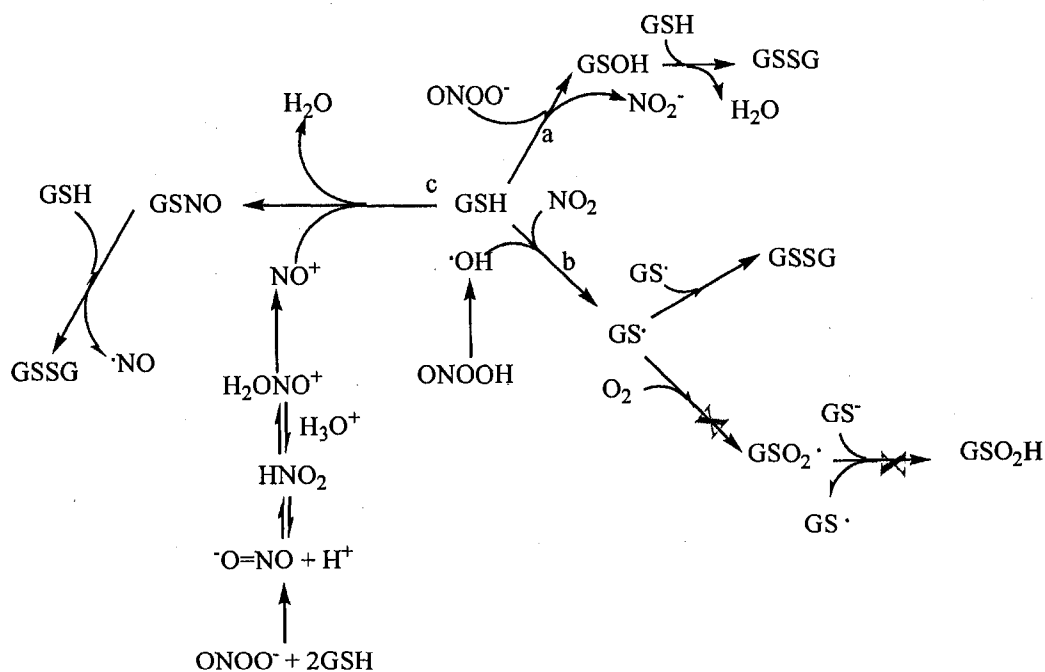


Figure 4.22: Pathways of GSH oxidation by peroxynitrite (a) two electron pathway (b) one electron pathway and (c) pathway leading to formation of nitrosothiols.

CHAPTER 5

KINETICS AND MECHANISMS OF THE OXIDATION OF CYSTEINE BY PEROXYNITRITE

5.1 INTRODUCTION

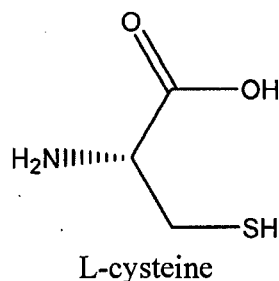
Cysteine (CYSH) is a non essential sulfur-containing amino acid with chemical formula $\text{HO}_2\text{CCH}(\text{NH}_2)\text{CH}_2\text{SH}$. It is non essential because the body can synthesize it from methionine²²⁴. CYSH is one of the few amino acids that contain sulfur.

Other sulfur-containing amino acids are glutathione and homocysteine. The presence of sulfur in cysteine allows it to participate in the forming and breaking of S-S bonds, especially in the endoplasmic reticulum (ER)²²⁵. Metabolites of CYSH serve as precursors to amino acids taurine and glutathione. It is known that CYSH strengthens the protective lining of the stomach and intestines, which may help prevent damage caused by aspirin and other similar drugs²²⁶. Modulation of lymphocyte functions and immune responses in humans is even said to be one of CYSH's functions²²⁷. Other thiols, including CYSH, have being implicated as antioxidants in human health^{228,229}.

Antioxidants are species needed to counteract damaging effects of reactive agents, such as oxygen species, which are generated *in vivo* and cause damage to DNA, lipids, and proteins^{230,231}. It is known that PN is formed by the reaction of damaging species like superoxide radical and nitric oxide in a near diffusion reaction rate²³². PN, being a very potent oxidizing species, oxidizes targets such as DNA, lipids, proteins and thiols²³³. Possible ways of intercepting PN's toxicity in the

physiological system could be to prevent its formation, either by inhibiting NO production or by dismutating all superoxide radicals formed. This is not plausible; because the rate constant for reaction of NO with superoxide is about 3-10 fold higher than for reaction of superoxide with any of the three (super oxide dismutase) SOD isoforms^{234,235}. Not all reactions of NO in the physiological systems however are deleterious. Efficient methods of intercepting PN's oxidative injury could be the use of scavengers, which can effectively mop up excess PN and totally absorb PN's oxidative power.

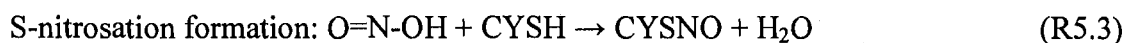
This is where CYSH, a thiol compound, comes in as an antioxidant. It is also the major reason why we are studying the oxidative reactions of CYSH with PN.



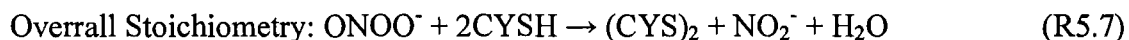
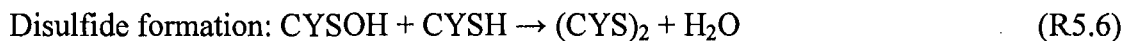
The aim of this chapter is to elucidate CYSH's deactivation capacity of PN radicals. These radicals are known to mediate toxicity in physiological systems. The above aim is hoped to be achieved through the study of oxidation mechanisms of CYSH by PN. While the oxidation of glutathione by PN has been studied in chapter 4, it is also important to study the oxidation of CYSH by PN. Questions such as, how their oxidation mechanisms might differ, what metabolites are formed in the oxidation pathway, how comparable are their rates of oxidation and whether we can relate these findings to thiols in general.

5.2 Stoichiometry and product determination

The stoichiometry of the formation of cysteine nitrosothiol by PN in high acid conditions was determined as:



In high pH conditions the stoichiometry of oxidation reaction of PN with CYSH was determined as:



Cysteine nitrosothiol (CYSNO) and disulfide ((CYS)₂) formed in reactions (R 5.3 and 5.7) were characterized using mass spectra and HPLC methods (**Figure 5.1**). HNO₂ and NO₂⁻ formed in reactions (R5.2 and 5.7) were characterized using their wavelength of absorption of 355 nm on the UV-vis spectrophotometer

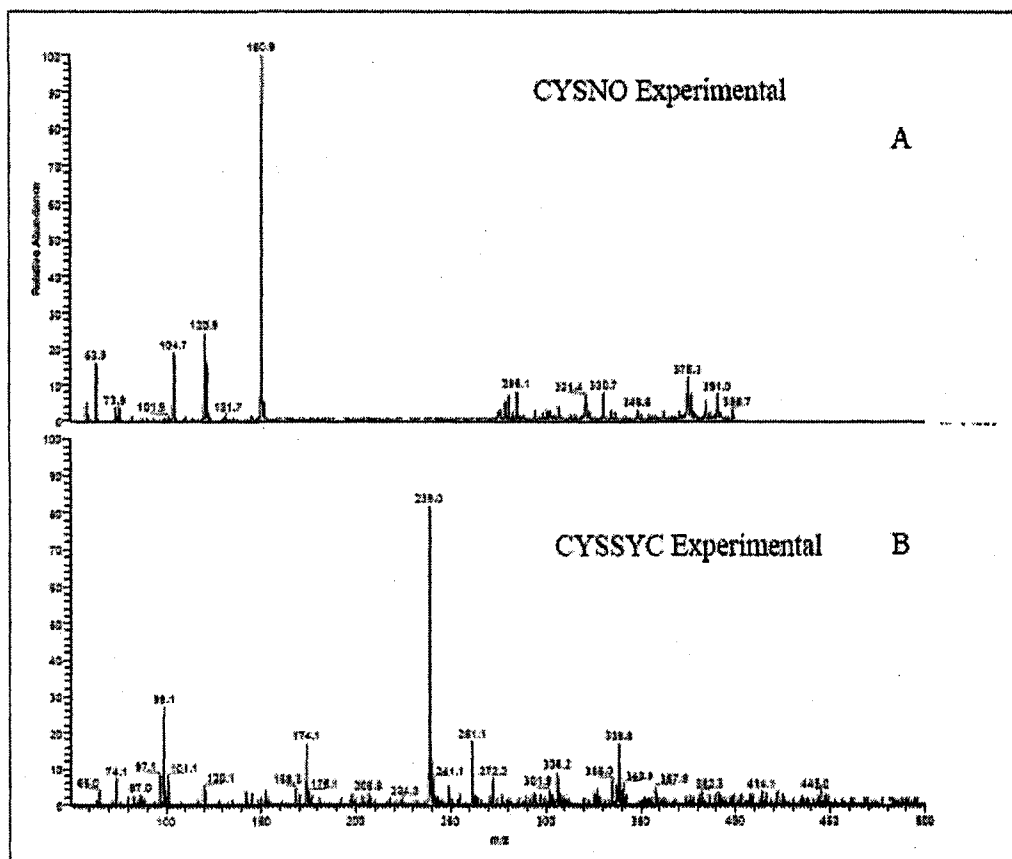


Figure 5.1: Product determination of the nitrosation reaction of CYSH by PN, a) 300 mM CYSH + 100 mM PN + 12.5 mM H⁺, b) 8.0 mM CYSH + 0.8 mM PN in buffer pH 7.4.

5.3 Reaction dynamics

The kinetics of the oxidation of cysteine (CYSH) by PN has been studied.

In acidic solutions S-nitrosothiol was found to be the major intermediate which eventually formed a disulfide as the final stable oxidation product. Further oxidation reactions were undertaken at alkaline pH using sodium phosphate buffer and the stable product was the disulfide of initial thiol compound, without the formation of a nitrosothiol. To ascertain pathway of reaction dynamics, EPR studies were also performed.

5.3.1 S-nitrosation reaction: The progress of the S-nitrosation reaction of CYSH with PN was followed at 544 nm. This is the best wavelength to follow the progress of this reaction without interference from absorption of PN, residual nitrite and CYSH itself. The relevant spectra are shown in **Figure 5.2**.

5.3.1.1 Acid dependence

The amount of CYSNO formed is seen in **Figure 5.3** and is directly dependent on the concentration of acid, until all PN is completely consumed. Once all PN is consumed, further increase in the acid concentration catalyzes the decomposition of CYSNO, which is unstable in high acid concentrations. This effect is shown in **Figure 5.3, trace (f)**. The initial rate plot seen in **Figure 5.4** seems to support the fact that the rate of formation of CYSNO is directly dependent on acid concentrations with a first order dependence.

Spectra of cysteine, nitrite, peroxy nitrite and reaction of peroxy nitrite with cysteine

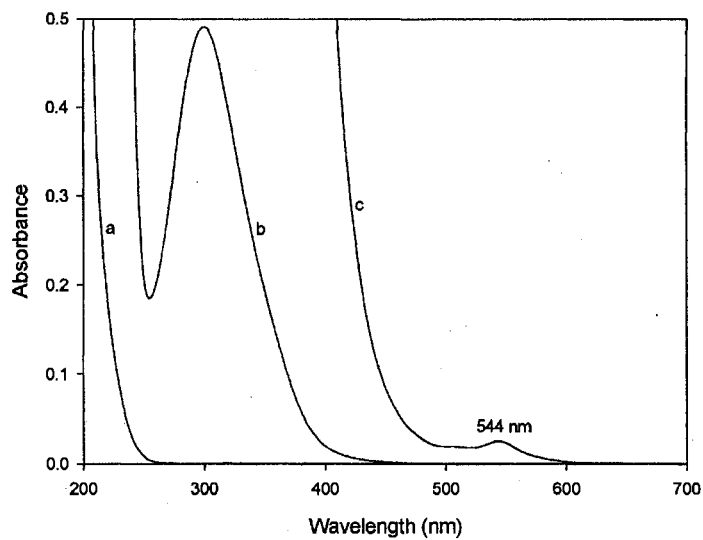


Figure 5.2: a) [CYSH] = 5.0×10^{-3} M, b) [PN] = 2.9×10^{-4} M, c) CYSH + HClO₄ + PN at 544 nm
For c) [CYSH] = 1.5×10^{-2} M, [HClO₄] = 0.175 M, [PN] = 1.7×10^{-3} M.

Acid variation in the formation of cysteine nitrosothiol

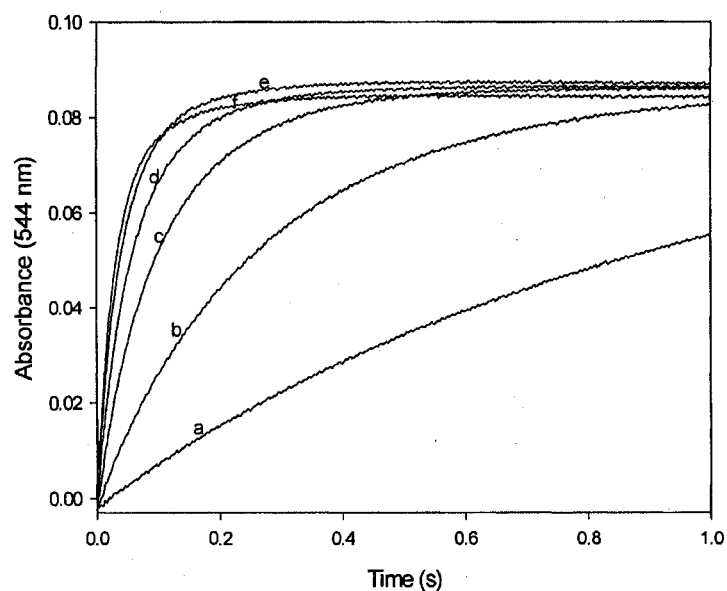


Figure 5.3: Fixed: [PN] = 5.8×10^{-3} M, [CYSH] = 1.0×10^{-1} M, [EDTA] = 1.0×10^{-4} M, NaClO₄ = 0.5 M.
[HClO₄] = a) 1.0×10^{-1} M, b) 2.0×10^{-1} M, c) 3.0×10^{-1} M, d) 4.0×10^{-1} M, e) 5.0×10^{-1} M, f) 6.0×10^{-1} M.

Initial rate plot for acid variation in the formation of cysteine nitrosothiol

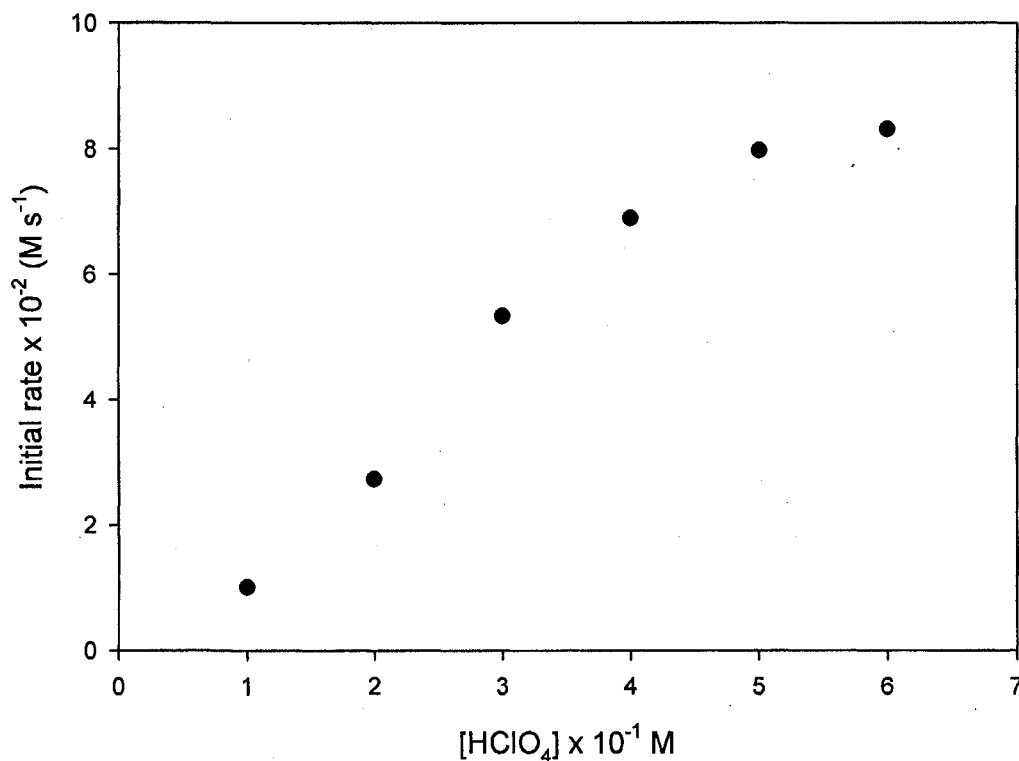


Figure 5.4: Fixed: [PN] = 5.8×10^{-3} M, [CYSH] = 1.0×10^{-1} M, [EDTA] = 1.0×10^{-4} M, I_{NaClO_4} = 0.5 M.
[HClO₄] = a) 1.0×10^{-1} M, b) 2.0×10^{-1} M, c) 3.0×10^{-1} M, d) 4.0×10^{-1} M, e) 5.0×10^{-1} M, f) 6.0×10^{-1} M

5.3.1.2 CYSH dependence

Absorbance traces for variation of CYSH in its oxidation by PN are shown in

Figure 5.5. The dependence of formation of CYSNO on CYSH concentration is

simple. Rate of formation of CYSNO is faster at higher concentrations of CYSH

compared to rate at lower concentrations. Initial rate plot for the formation of

CYSNO in Figure 5.6 shows that the reaction is first order with respect to CYSH

concentrations.

Cysteine variation in the formation of cysteine nitrosothiol

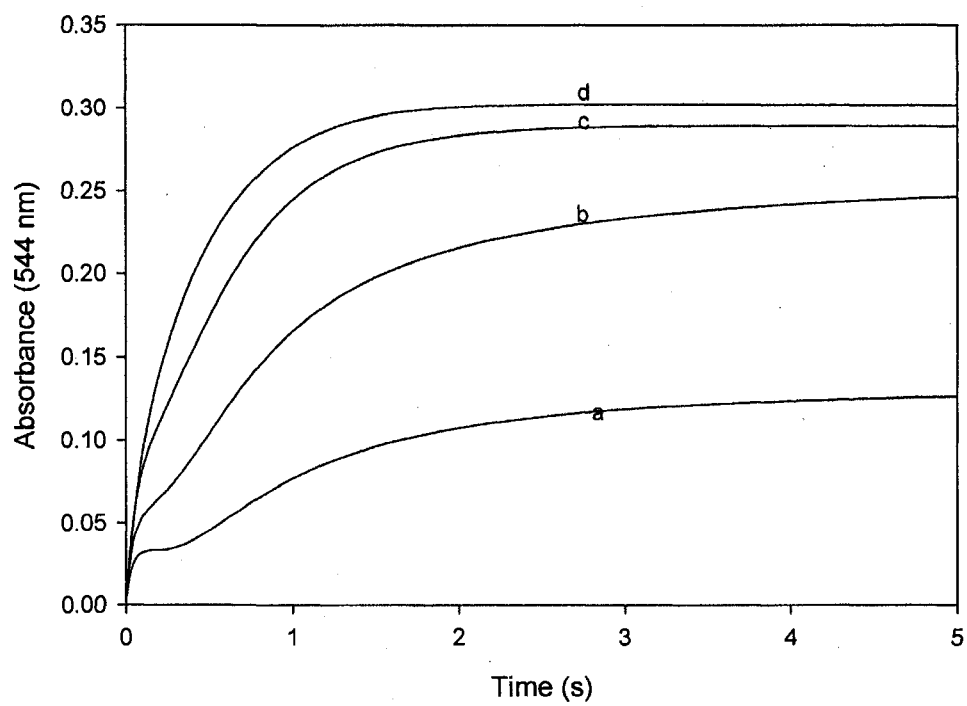


figure 5.5: Fixed [PN] = 1.9×10^{-2} M, $[\text{HClO}_4]$ = 4.0×10^{-1} M, [EDTA] = 1.0×10^{-4} M, I_{NaClO_4} = 0.5 M.
[CySH] = a) 2.5×10^{-2} M, b) 5.0×10^{-2} M, c) 7.5×10^{-2} M, d) 1.0×10^{-1} M.

Initial rate plot for cysteine variation in the formation of cysteine nitrosothiol

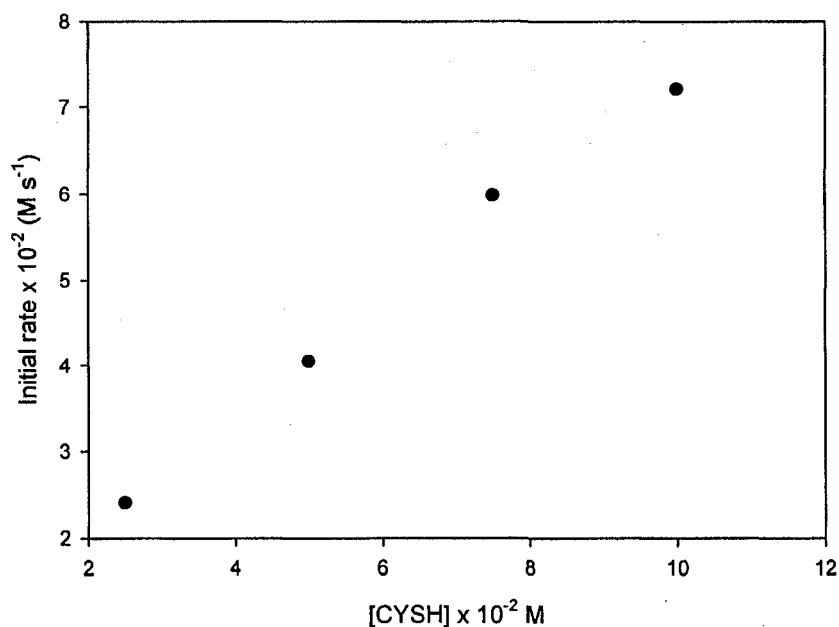


Figure 5.6: Fixed $[\text{PN}] = 1.9 \times 10^{-2} \text{ M}$, $[\text{HClO}_4] = 4.0 \times 10^{-1} \text{ M}$, $[\text{EDTA}] = 1.0 \times 10^{-4} \text{ M}$, $I_{\text{NaClO}_4} = 0.5 \text{ M}$.
 $[\text{CySH}] = \text{a) } 2.5 \times 10^{-2} \text{ M}$, $\text{b) } 5.0 \times 10^{-2} \text{ M}$, $\text{c) } 7.5 \times 10^{-2} \text{ M}$, $\text{d) } 1.25 \times 10^{-1} \text{ M}$.

5.3.1.3 PN dependence

Figure 5.7 shows the effect of varying PN at constant concentrations of acid and CYSH. Rate of formation of CYSNO is directly proportional to initial PN concentration. Initial rate plot with respect to PN concentrations (**Figure 5.8**) shows a linear plot. The reaction showed a first order dependence in PN over a wide range of PN concentrations for as long as $[\text{CYSH}]_0, [\text{H}^+]_0 > [\text{PN}]_0$.

Peroxynitrite variation in the formation of cysteine nitrosothiol

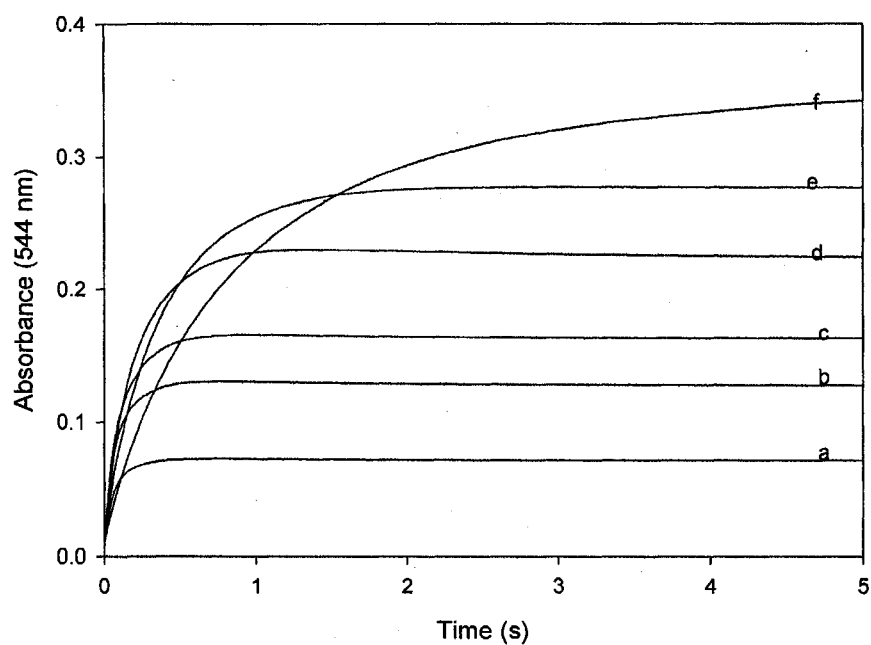


Figure 5.7: Fixed [CYSH] = 1.52×10^{-1} M, [HClO₄] = 4.0×10^{-1} M, [EDTA] = 1.0×10^{-4} M, I_{NaClO₄} = 0.5 M. [PN] = a) 4.7×10^{-3} M, b) 8.5×10^{-3} M, c) 1.0×10^{-2} M, d) 1.5×10^{-2} M, e) 1.8×10^{-2} M, f) 2.1×10^{-2} M.

Initial rate plot for peroxynitrite variation in the formation of cysteine nitrosothiol

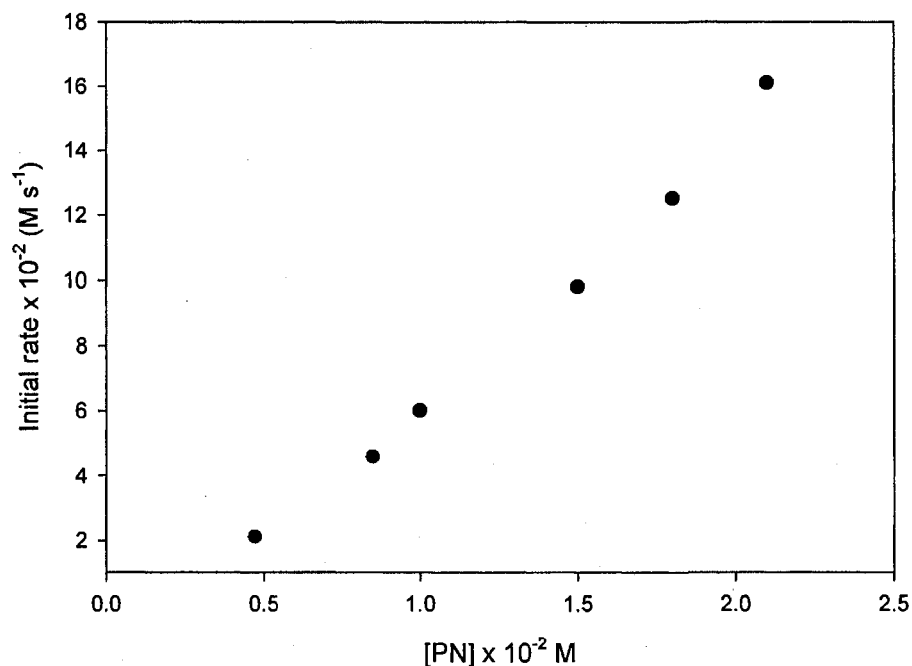


Figure 5.8: Fixed [CYSH] = 1.52×10^{-1} M, [HClO₄] = 4.0×10^{-1} M, [EDTA] = 1.0×10^{-4} M, I_{NaClO₄} = 0.5 M. [PN] = a) 4.7×10^{-3} M, b) 8.5×10^{-3} M, c) 1.0×10^{-2} M, d) 1.5×10^{-2} M, e) 1.8×10^{-2} M, f) 2.1×10^{-2} M.

5.3.2 Cystine (CYS)₂ formation at 302 nm

Oxidation of CYSH by PN in sodium phosphate buffer generated (CYS)₂ and nitrite without the formation of nitrosothiol. The progress of this reaction was monitored at PN's absorption wavelength of 302 nm. At this wavelength the rate of depletion of PN by CYSH was determined by following the reaction kinetics of CYSH consumption and PN's depletion. From the traces generated, the order of the reaction was then determined.

5.3.2.1 CYSH dependence

The rate of consumption of PN by CYSH is very rapid as seen in **Figure 5.9** with reaction over in approximately 1 second. The rate of consumption increases with increase in CYSH concentration until all $[PN]_0$ is consumed and absorbance of PN levels off. The initial rate plot (**Figure 5.10**) signifies the order of reaction with respect CYSH to be first order.

Oxidation of cysteine by peroxynitrite: Varying cysteine

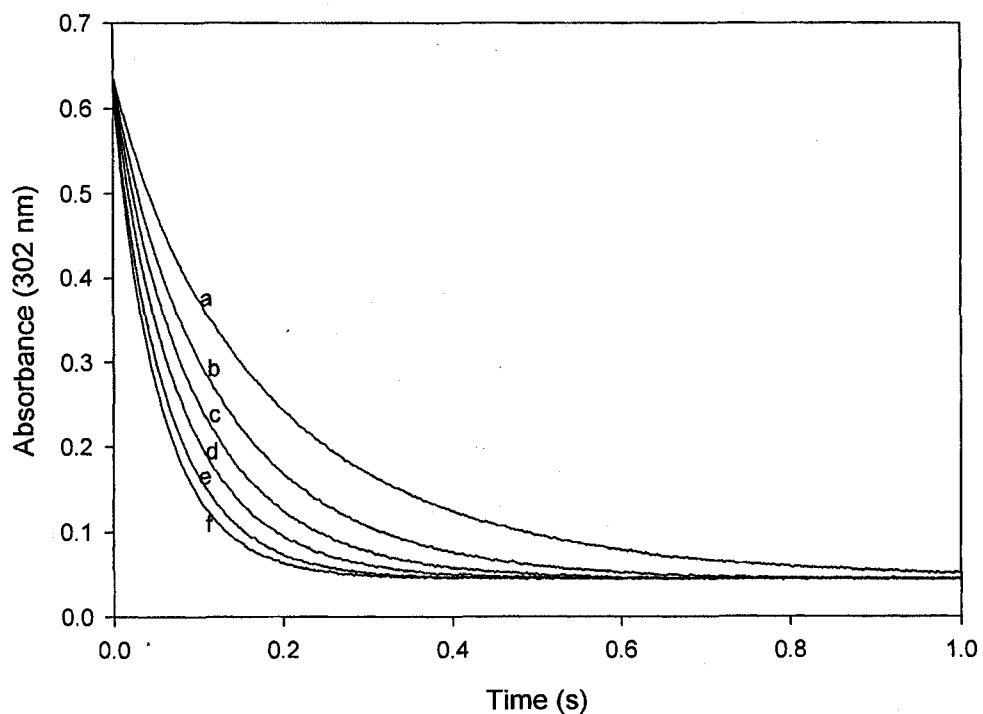


Figure 5.9: Fixed: $[PN] = 4.2 \times 10^{-4} \text{ M}$, $[EDTA] = 1.0 \times 10^{-4} \text{ M}$, $[\text{Phosphate buffer pH 7.4}] = 1.5 \times 10^{-1} \text{ M}$, $[\text{CYSH}] = \text{a) } 3.0 \times 10^{-3} \text{ M}$, $\text{b) } 4.0 \times 10^{-3} \text{ M}$, $\text{c) } 5.0 \times 10^{-3} \text{ M}$, $\text{d) } 6.0 \times 10^{-3} \text{ M}$, $\text{e) } 7.0 \times 10^{-3} \text{ M}$, $\text{f) } 8.0 \times 10^{-3} \text{ M}$.

Initial rate plot for oxidation of cysteine by peroxyxynitrite: Varying cysteine

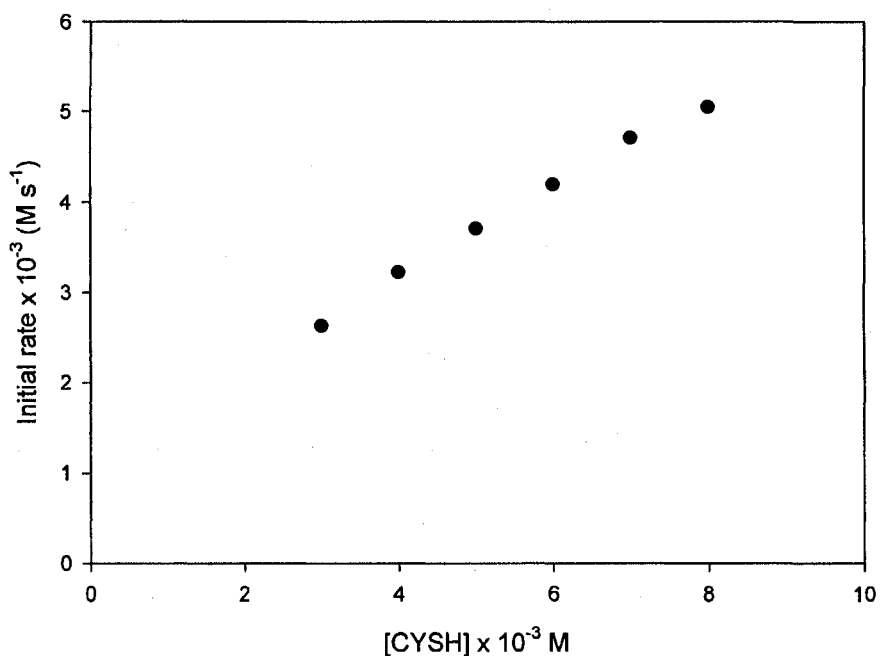


Figure 5.10: Fixed: [PN] = 4.2×10^{-4} M, [EDTA] = 1.0×10^{-4} M, [Phosphate buffer pH 7.4] = 1.5×10^{-1} M, [CYSH] = a) 3.0×10^{-3} M, b) 4.0×10^{-3} M, c) 5.0×10^{-3} M, d) 6.0×10^{-3} M, e) 7.0×10^{-3} M, f) 8.0×10^{-3} M.

5.3.2.2 PN dependence

Figure 5.11 show that the rate of consumption of PN has a direct dependence on its concentration. At excess concentrations of CYSH over PN concentrations, the reaction is complete in about 0.2 seconds in phosphate buffer pH 5.0. A plot of initial rate of consumption versus initial PN concentrations (Figure 5.12) shows simple first order dependence.

Variation of PN in oxidation of cysteine using phosphate buffer pH 5

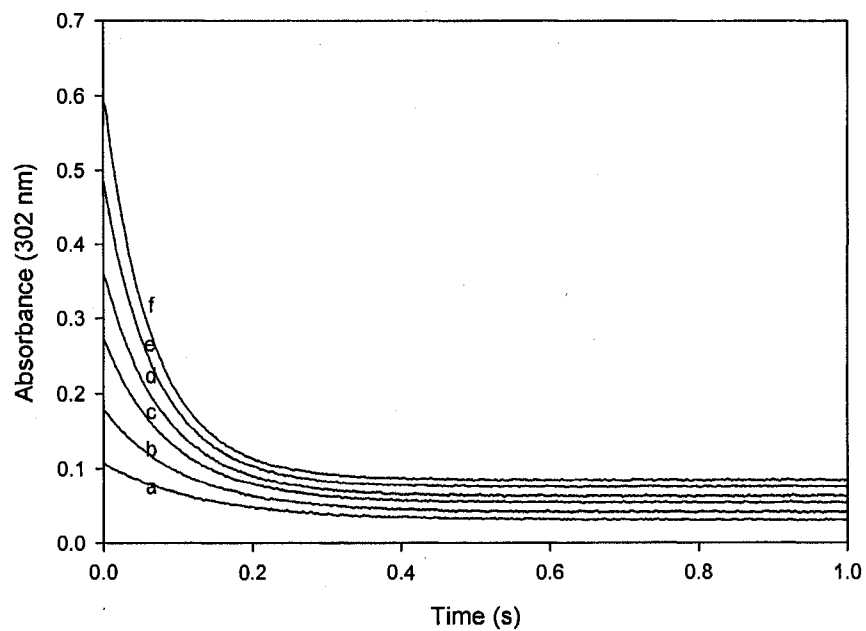


Figure 5.11: Fixed: [CYSH] = 1.0×10^{-2} M, [phosphate buffer pH 5] = 0.15 M, [EDTA] = 1.0×10^{-4} M, [PN] = a) 2.9×10^{-4} M, b) 4.3×10^{-4} M, c) 5.7×10^{-4} M, d) 7.2×10^{-4} M, e) 8.6×10^{-4} M, f) 1.0×10^{-3} M.

Initial rate plot for oxidation of cysteine done by variation of PN

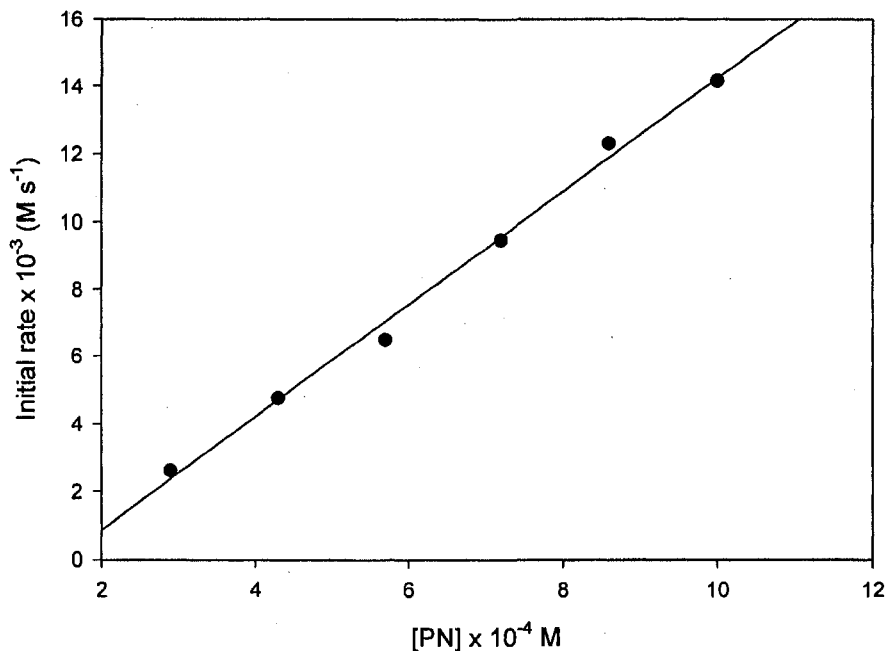


Figure 5.12: Fixed: [CYSH] = 1.0×10^{-2} M, [phosphate buffer pH 5] = 0.15 M, [EDTA] = 1.0×10^{-4} M, [PN] = a) 2.9×10^{-4} M, b) 4.3×10^{-4} M, c) 5.7×10^{-4} M, d) 7.2×10^{-4} M, e) 8.6×10^{-4} M, f) 1.0×10^{-3} M.

5.3.2.3 Effect of pH on oxidation of CYSH by PN

Cysteine oxidation is highly pH dependent. The effect of varying pH at constant concentrations of CYSH and PN is shown in **Figure 5.13**. The rate of consumption of PN by CYSH is inversely proportional to pH, with low pH having the highest rate.

The initial rate plot shows a nonlinear curve with respect to pH **Figure 5.14**.

Figure 5.15 shows the values of bimolecular rate constants of the oxidation of CYSH by PN at different pH.

Effect pH on cysteine oxidation by PN

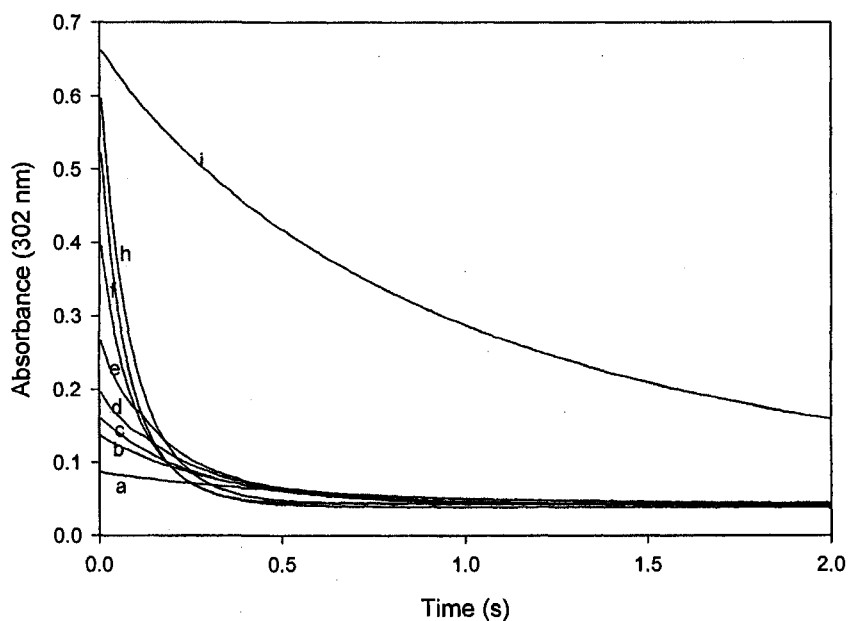


Figure 5.13: Fixed [CYSH] = 4.0×10^{-3} M, [PN] = 4.0×10^{-4} M, [EDTA] = 1.0×10^{-4} M, [Phosphate buffer] = 1.5×10^{-1} M
 [Phosphate buffer pH = a) 3.0, b) 4.0, c) 5.0, d) 5.5, e) 6.0, f) 6.5, g) 7.0, h) 7.4, i) 8.0

Initial rate plot for the effect pH on cysteine oxidation by PN

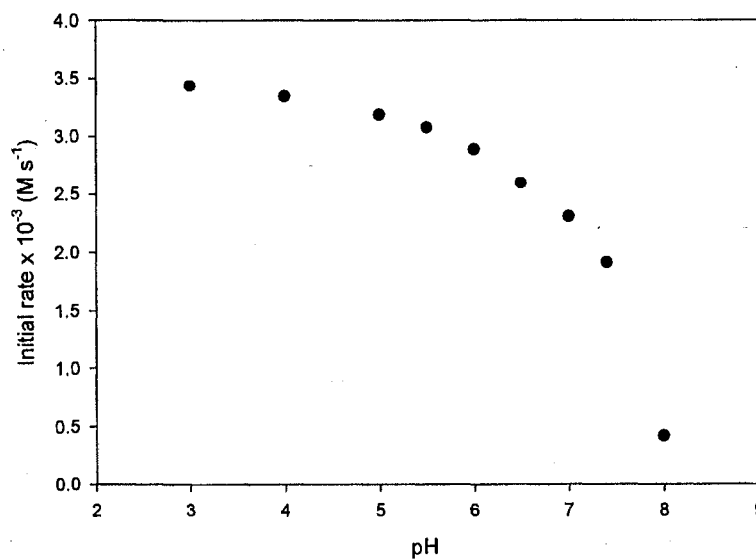


Figure 5.14: Fixed [CYSH] = 4.0×10^{-3} M, [PN] = 4.0×10^{-4} M, [EDTA] = 1.0×10^{-4} M, [Phosphate buffer] = 1.5×10^{-1} M
 [Phosphate buffer pH = a) 3.0, b) 4.0, c) 5.0, d) 5.5, e) 6.0, f) 6.5, g) 7.0, h) 7.4, i) 8.0

Rate constants plot against pH for effect pH on cysteine oxidation by PN

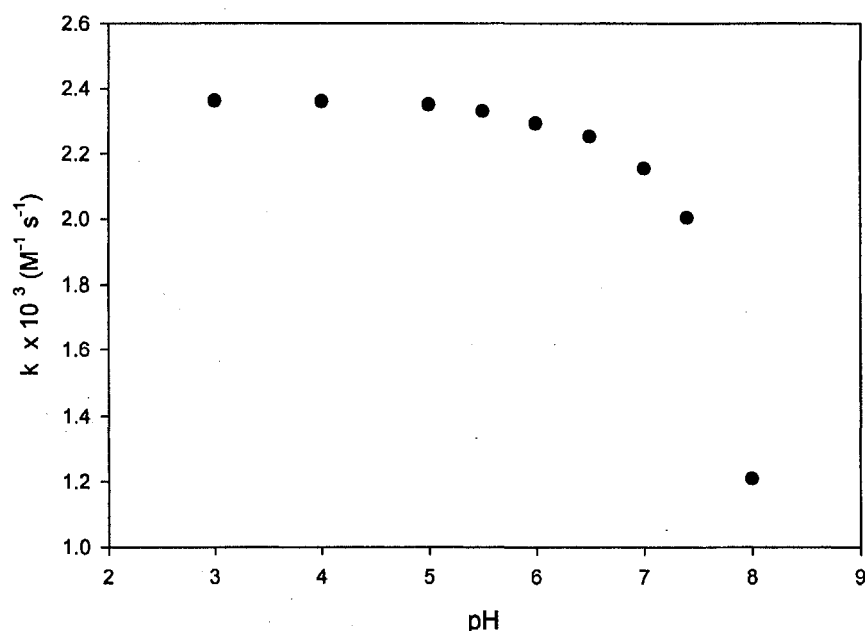


Figure 5.15: Fixed: [CYSH] = 4.0×10^{-3} M, [PN] = 4.0×10^{-4} M, [EDTA] = 1.0×10^{-4} M, [Phosphate buffer] = 1.5×10^{-1} M, Phosphate buffer pH = a) 3.0, b) 4.0, c) 5.0, d) 5.5, e) 6.0, f) 6.5, g) 7.0, h) 7.4, i) 8.0

5.3.2.4 Effect HCO_3^- on CYSH oxidation by PN

In the oxidation of CYSH by PN, the effect of HCO_3^- was examined. Bicarbonate in the presence of acidic protons is known to generate carbon dioxide. The aim of this section is to ascertain the effect of $\text{HCO}_3^-/\text{CO}_2$ on the oxidation of CYSH by PN.

Figure 5.16 shows the data generated from the reaction of HCO_3^- with CYSH in the presence of a constant concentration of PN. In the presence and absence of HCO_3^- , there seems to be little or no effect of HCO_3^- on CYSH's oxidation by PN.

Subsequent variations with varying concentrations of CYSH and excess constant concentration of HCO_3^- over PN shows rapid depletion of PN at 302 nm. The reaction is practically over in 0.5 seconds. **Figure 5.17** shows the initial rate plot of

data in **Figure 5.16**. This plot shows that there is very little effect of reacting HCO_3^- with CYSH on the initial rate of oxidation of CYSH and that the initial rate of oxidation of CYSH by PN in the presence of HCO_3^- is first order.

Effect of HCO_3^- on cysteine oxidation by PN: Varying cysteine

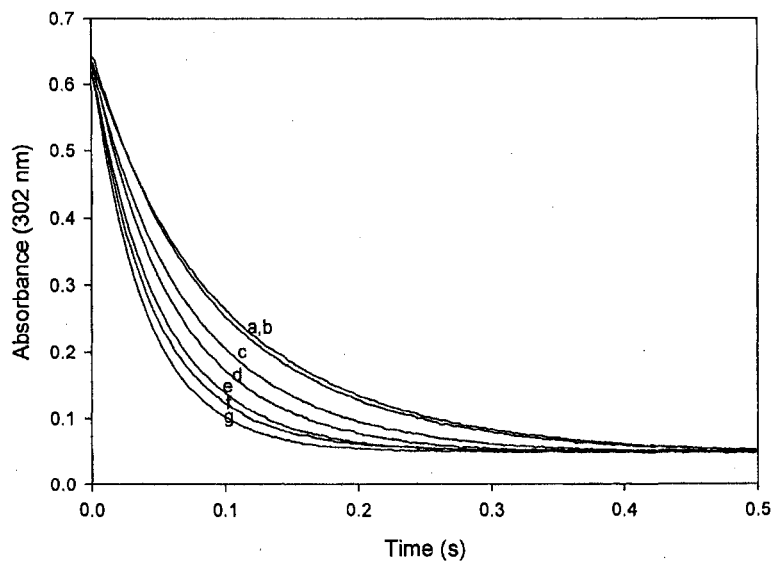


Figure 5.16: Fixed: $[\text{PN}] = 4.2 \times 10^{-4} \text{ M}$, $[\text{EDTA}] = 1.0 \times 10^{-4} \text{ M}$, Phosphate buffer pH 7.4] = $1.5 \times 10^{-1} \text{ M}$, $[\text{HCO}_3^-] = 1.5 \times 10^{-3} \text{ M}$, $[\text{CYSH}] = \text{a) } 4.0 \times 10^{-3} \text{ M} + 0 \text{ M HCO}_3^- \text{ b) } 4.0 \times 10^{-3} \text{ M}$, c) $5.0 \times 10^{-3} \text{ M}$, d) $6.0 \times 10^{-3} \text{ M}$, e) $7.0 \times 10^{-3} \text{ M}$, f) $8.0 \times 10^{-3} \text{ M}$, g) $9.0 \times 10^{-3} \text{ M}$

Initial rate plot for effect of HCO_3^- on CYSH oxidation by PN: Varying CYSH

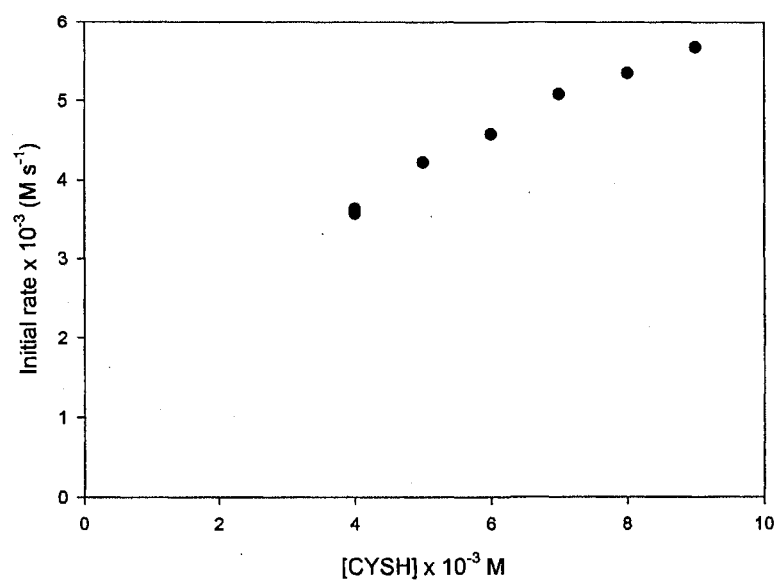
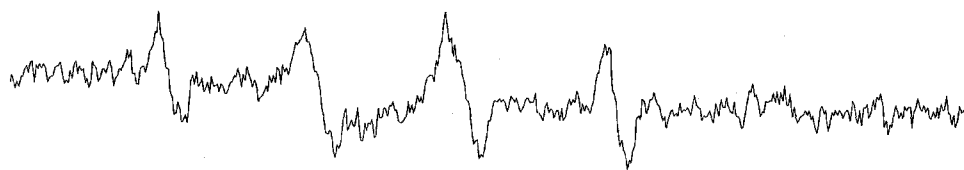


Figure 5.17: Fixed: [PN] = 4.2×10^{-4} M, [EDTA] = 1.0×10^{-4} M, [Phosphate buffer pH 7.4] = 1.5×10^{-1} M, $[\text{HCO}_3^-]$ = 1.5×10^{-3} M, [CYSH] = a) 4.0×10^{-3} M + 0 M HCO_3^- , b) 4.0×10^{-3} M, c) 5.0×10^{-3} M, d) 6.0×10^{-3} M, e) 7.0×10^{-3} M, f) 8.0×10^{-3} M, g) 9.0×10^{-3} M

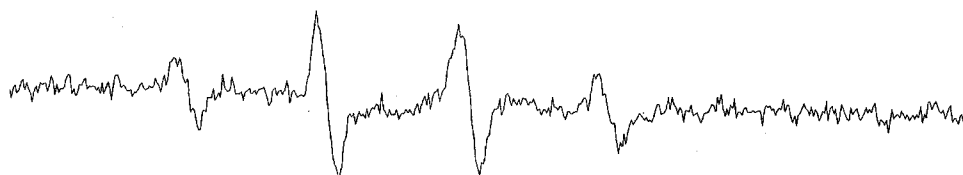
5.4 EPR study

EPR traces obtained from the oxidation of CYSH by PN are shown in **Figure 5.18**.

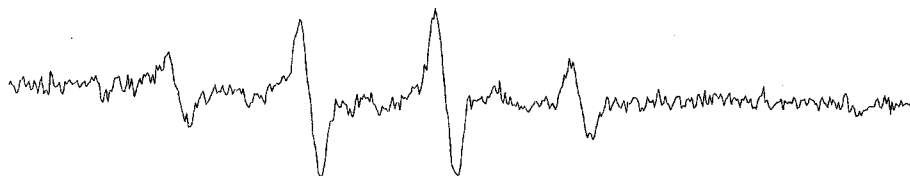
Traces were generated in a concentration dependent manner. Trace (a) has the lowest CYSH concentration, while trace (c) has the highest concentration CYSH. Trace (c) shows most clearly the 1:2:2:1 quartet with splitting of $a_N = 15.4 \text{ G}$; $a_H = 17.4 \text{ G}$ ²¹⁶ characteristic of cysteine radical adduct of DMPO. PN concentration was the limiting concentration, just like done in the kinetics experiments at pH 7.4, to mimick pH of the physiological system.



a) CYSH oxidation by PN, after 5 minutes incubation: [PN] = 0.8 mM, [CYSH] = 1.0 mM, [DMPO] = 80 mM, pH 7.4.



b) CYSH oxidation by PN, after 5 minutes incubation: [PN] = 0.8 mM, [CYSH] = 3.0 mM, [DMPO] = 80 mM, pH 7.4.



c) CYSH oxidation by PN, after 5 minutes incubation: [PN] = 0.8 mM, [CYSH] = 4.5 mM, [DMPO] = 80 mM, pH 7.4.

→
3436-3536 G

Figure 5.18: EPR spectra of DMPO radical adducts obtained during oxidation of cysteine (CYSH) by peroxynitrite (PN). Spectra were obtained after about 5 minute incubation period at room temperature with 80 mM DMPO dissolved in 0.15 M phosphate buffer at pH 7.4, with 0.1 mM EDTA a) 1.0 mM CYSH + 0.8 mM PN, b) 9.0 mM CYSH + 0.8 mM PN, c) 10 mM CYSH + 0.8 mM PN.

5.5 Conclusion

In similarity to dynamics observed in the oxidation of GSH by PN, oxidation of CYSH by PN is highly pH dependent. Cystine (CYS)₂, the disulfide of cysteine is the final product of oxidation of CYSH by PN. Cysteine nitrosothiol (CYSNO) was formed in strong acid conditions, as an intermediate before the formation of the cystine. At higher pH conditions, disulfides are formed directly without the formation of CYSNO. The reaction dynamics exhibit a first order dependence with respect to acid, CYSH and PN. The bimolecular rate constants obtained at 25 °C in pH 3.0-8.0 are shown in **Figure 5.15**. EPR results shows the formation of cysteine radical adduct at pH 7.4, this suggest that the pathway of CYSH oxidation at this pH might proceed via a one electron mechanism. In general, the oxidation mechanism of CYSH by PN is similar, with some little differences. The rate of oxidation is faster in CYSH compared to GSH. Bicarbonate does not seem to have much effect on the rate of oxidation of CYSH at pH 7.4 as compared to GSH. The proposed pathway of oxidation is shown in **Figure 5.19**:

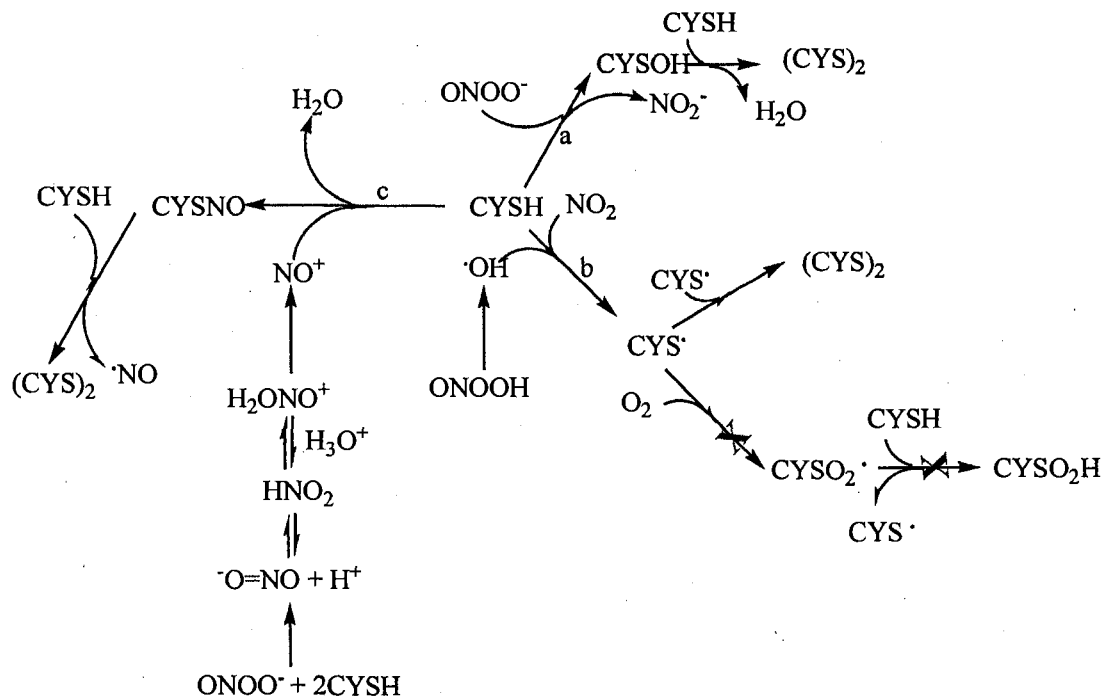


Figure 5.19: Pathways of CYSH oxidation by peroxynitrite (a) two electron pathway (b) one electron pathway and (c) pathway leading to formation of nitrosothiols.

Reference List

1. Santillan, M. B.; Ciuffo, G. M.; Jauregui, E. A.; Csizmadia, T. G. A model mechanism of nitric oxide (NO) formation by NO synthase. *Journal of Molecular Structure-Theochem* **1999**, *468*, 223-239.
2. Goldenbaum, G. C.; Dickerson, R. R. Nitric-Oxide Production by Lightning Discharges. *Journal of Geophysical Research-Atmospheres* **1993**, *98*, 18333-18338.
3. Bond, D. W.; Zhang, R. Y.; Tie, X. X.; Brasseur, G.; Huffines, G.; Orville, R. E.; Boccippio, D. J. NO_x production by lightning over the continental United States. *Journal of Geophysical Research-Atmospheres* **2001**, *106*, 27701-27710.
4. Stuhler, H.; Frohn, A. The production of NO by hypersonic flight. *Atmospheric Environment* **1998**, *32*, 3153-3155.
5. Niemeier, U.; Granier, C.; Kornbluh, L.; Walters, S.; Brasseur, G. P. Global impact of road traffic on atmospheric chemical composition and on ozone climate forcing. *Journal of Geophysical Research-Atmospheres* **2006**, *111*.
6. Lopez-Puertas, M.; Funke, B.; Gil-Lopez, S.; von Clarmann, T.; Stiller, G. P.; Hopfner, M.; Kellmann, S.; Fischer, H.; and Jackman, C. H. Observation of NO_x enhancement and ozone depletion in the Northern and Southern Hemispheres after the October-November 2003 solar proton events. *Journal of Geophysical Research-Space Physics* **2005**, *110*, A09S43-1-A09S43/12.
7. Ebbing G ammon General Chemistry. Houghton Mifflin: Boston, MA, 1999.
8. Jones, K. Comprehensive Inorganic Chemistry. Pergamon: Oxford, 1973.
9. Furchgott, R. F.; Zawadzki, J. V. The obligatory role of endothelial cells in the relaxation of arterial smooth muscle by acetylcholine. *Nature* **1980**, *288*, 373-376.
10. Cocks, T. M.; Angus, J. A.; Campbell, J. H.; Campbell, G. R. Release and properties of endothelium-derived relaxing factor (EDRF) from endothelial cells in culture. *Journal of Cellular Physiology* **1984**, *123*, 310-320.
11. Griffith, T. M.; Edwards, D. H.; Lewis, M. J.; Newby, A. C.; Henderson, A. H. The nature of endothelium-derived vascular relaxant factor. *Nature* **1984**, *308*, 645-647.

12. Ignarro, L. J.; Lippton, H.; Edwards, J. C.; Baricos, W. H.; Hyman, A. L.; Kadowitz, P. J.; Gruetter, C. A. Mechanism of vascular smooth muscle relaxation by organic nitrates, nitrites, nitroprusside and nitric oxide: evidence for the involvement of S-nitrosothiols as active intermediates. *J. Pharmacol. Exp. Ther.* **1981**, *218*, 739-749.
 13. Arnold, W. P.; Mit tal, C. K.; Katsuki, S.; Murad, F. Nitric Oxide Activates Guanylate Cyclase and Increases Guanosine 3':5' -cyclic Monophosphate Levels in Various Tissue Preparations. *Proceedings of the National Academy of Sciences of the United States of America (PNAS)* **1977**, *74*, 3203-3207.
 14. Louis J. Ignarro; Georgette M. Buga; Keith S. Wood; Russell E. Byrns; Gautam Chaudhuri Endothelium-Derived Relaxing Factor Produced and Released from Artery and Vein is Nitric Oxide. *PNAS* **1987**, *84*, 9265-9269.
 15. Moncada, S.; Herm an, A. G.; Vanhoutte, P. Endothelium-Derived Relaxing Factor Is Identified As Nitric-Oxide. *Trends in Pharmacological Sciences* **1987**, *8*, 365-&.
 16. Palmer, R. M. J.; Rees, D. D.; Ashton, D. S.; Moncada, S. L-Arginine Is the Physiological Precursor for the Formation of Nitric-Oxide in Endothelium-Dependent Relaxation. *Biochemical and Biophysical Research Communications* **1988**, *153*, 1251-1256.
 17. Palmer, R. M. J.; Ashton, D. S.; Moncada, S. Vascular Endothelial-Cells Synthesize Nitric-Oxide from L-Arginine. *Nature* **1988**, *333*, 664-666.
 18. Moncada, S.; Palmer, R. M. J.; Higgs, E. A. The Discovery of Nitric-Oxide As the Endogenous Nitrovasodilator. *Hypertension* **1988**, *12*, 365-372.
 19. Moncada, S.; Radomski, M. W.; Palmer, R. M. J. Endothelium-Derived Relaxing Factor - Identification As Nitric-Oxide and Role in the Control of Vascular Tone and Platelet-Function. *Biochemical Pharmacology* **1988**, *37*, 2495-2501.
 20. Vanin, A. F. 1998 N obel Prize winners for physiology or medicine - Robert Furchgott - Louis Ignarro - Farid Murad. *Biochemistry-Moscow* **1999**, *64*, 98-100.
 21. Thompson Sc ientific. Citation Superstars of the U.K., 1990 - 1999. *Science Watch*® 10[6], 1. 1999.
- Ref Type: Magazine Article
22. Stuehr, D. J.; Kwon, N. S .; Nathan, C. F.; Griffith, O. W.; Feldman, P. L.; Wiseman, J. N-Omega-Hydroxy-L-Arginine Is An Intermediate in the

Biosynthesis of Nitric-Oxide from L-Arginine. *Journal of Biological Chemistry* **1991**, *266*, 6259-6263.

23. Stuehr, D. J.; Griffith, O. W.; Kwon, N. S.; Nathan, C. F.; Feldman, P. L. N-Omega-Hydroxy-L-Arginine Is An Intermediate in the Biosynthesis of Nitric-Oxide from L-Arginine. *Faseb Journal* **1991**, *5*, A1151.
24. White, K. A.; Marletta, M. A. Nitric -Oxide Synthase Is A Cytochrome-P-450 Type Hemoprotein. *Biochemistry* **1992**, *31*, 6627-6631.
25. Klatt, P.; Schmidt, K.; Ur ay, G.; Mayer, B. Multiple Catalytic Functions of Brain Nitric-Oxide Synthase - Biochemical-Characterization, Cofactor-Requirement, and the Role of N(G.W)-Hydroxy-L-Arginine As An Intermediate. *Journal of Biological Chemistry* **1993**, *268*, 14781-14787.
26. Marietta, M. A.; Yoon, P. S.; Iyengar, R.; Leaf, C. D.; Wishnokll, J. S. Macrophage Oxidation of L-Arginine to Nitrite and Nitrate: Nitric Oxide Is an Intermediate. *Biochemistry* **1988**, *27*, 8706-8711.
27. Hibbs, J. B.; Taintor, R. R.; Vavrin, Z.; Rachlin, E. M. Nitric oxide: A cytotoxic activated macrophage effector molecule. *Biochemical and Biophysical Research Communications* **1988**, *157*, 87-94.
28. Kiechle, F. L.; Malinski, T. Nitric-Oxide - Biochemistry, Pathophysiology, and Detection. *American Journal of Clinical Pathology* **1993**, *100*, 567-575.
29. Nakane, M.; Schmidt, H. H. W.; Pollock, J. S.; Forstermann, U.; Murad, F. Cloned Human Brain Nitric-Oxide Synthase Is Highly Expressed in Skeletal-Muscle. *Febs Letters* **1993**, *316*, 175-180.
30. Geller, D. A.; Lowenstein, C. J.; Shapiro, R. A.; Nussler, A. K.; Disilvio, M.; Wang, S. C.; Nakayama, D. K.; Simmons, R. L.; Snyder, S. H.; Billiar, T. R. Molecular-Cloning and Expression of Inducible Nitric-Oxide Synthase from Human Hepatocytes. *Proceedings of the National Academy of Sciences of the United States of America* **1993**, *90*, 3491-3495.
31. Forstermann, U. Constitutive Isoforms of Nitric-Oxide Synthase. *Abstracts of Papers of the American Chemical Society* **1992**, *204*, 176-MEDI.
32. Nathan, C.; Xie, Q. W. Nitric -Oxide Synthases - Roles, Tolls, and Controls. *Cell* **1994**, *78*, 915-918.
33. Sessa, W. C.; Harrison, J. K.; Luthin, D. R.; Pollock, J. S.; Lynch, K. R. Genomic Analysis and Expression Patterns Reveal Distinct Genes for Endothelial and Brain Nitric-Oxide Synthase. *Hypertension* **1993**, *21*, 934-938.

34. Forstermann, U.; Boissel, J. P.; Kleinert, H. Expressional control of the 'constitutive' isoforms of nitric oxide synthase (NOS I and NOS III). *FASEB Journal* **1998**, *12*, 773-790.
35. Knowles, R. G.; Moncada, S. Nitric-Oxide Synthases in Mammals. *Biochemical Journal* **1994**, *298*, 249-258.
36. Forstermann, U.; Boissel, J. P.; Kleinert, H. Expressional control of the 'constitutive' isoforms of nitric oxide synthase (NOS I and NOS III). *FASEB Journal* **1998**, *12*, 773-790.
37. Richter-Addo, G. B.; Legzdins, P. Metal Nitrosyls. Oxford University press: New York, 1992.
38. Wayland, B. B.; Olson, L. W. Spectroscopic studies and bonding model for nitric oxide complexes of iron porphyrins. *J. Am. Chem. Soc* **1974**, *96*, 6037-6041.
39. Tran, D.; Skelton, B. W.; White, A. H.; Laverman, L. E.; Ford, P. C. Investigation of the nitric oxide reduction of the bis(2,9-dimethyl-1,10-phenanthroline) complex of copper(II) and the structure of [Cu(dmp)(2)(H₂O)](CF₃SO₃)(2). *Inorganic Chemistry* **1998**, *37*, 2505-2511.
40. Antonini, E.; Brunori, M. Hemoglobin and Myoglobin and Their Reaction With Ligands. North-Holland Publishers: Amsterdam, 1971.
41. Traylor, T. G.; Sharma, V. S. Why No. *Biochemistry* **1992**, *31*, 2847-2849.
42. Olson, J. S.; Phillips, G. N. Myoglobin discriminates between O₂, NO, and CO by electrostatic interactions with the bound ligand. *Journal of Biological Inorganic Chemistry* **1997**, *2*, 544-552.
43. Doherty, M. P.; Hoekstra, J. W. Oxidation of nitrogen oxides by bound dioxygen in hemoproteins. *J. Inorganic Biochemistry* **1981**, *14*, 351-358.
44. Addison, A. W.; Stephanos, J. J. Nitrosyliron (III) hemoglobin: Autoreduction and spectroscopy. *Biochemistry* **1986**, *25*, 4104.
45. Vandegriff, K. D.; Letellier, Y. C.; Hess, J. R.; Shrager, R. I. Evaluation of Methemoglobin Formation and Quaternary Transition During Measurements of Oxygen Equilibrium Binding to Human Hemoglobin by Rapid-Scanning Spectrophotometry. *FASEB Journal* **1992**, *6*, A55.
46. Murad, F. The Nitric-Oxide Cyclic-Gmp Signal-Transduction System for Intracellular and Intercellular Communication. *Recent Progress in Hormone Research, Vol 49* **1994**, *49*, 239-248.

47. Marletta, M. A. Mammalian Synthesis of Nitrite, Nitrate, Nitric-Oxide, and N-Nitrosating Agents. *Chemical Research in Toxicology* **1988**, *1*, 249-257.
48. Yu, A. E.; Hu, S. Z.; Spir o, T. G.; Burstyn, J. N. Resonance Raman-Spectroscopy of Soluble Guanylyl Cyclase Reveals Displacement of Distal and Proximal Heme Ligands by No. *Journal of the American Chemical Society* **1994**, *116*, 4117-4118.
49. Feelisch, M.; Stamler, J. *Methods in Nitric Oxide Research*. Wiley: New York, 1996.
50. Estevez, A. G.; Spear, N. ; Thompson, J. A.; Cornwell, R. L.; Radi, R.; Barbeito, L.; Beckman, J. S. Nitric oxide-dependent production of cGMP supports the survival of rat embryonic motor neurons cultured with brain-derived neurotrophic factor. *Journal of Neuroscience* **1998**, *18*, 3708-3714.
51. Adams, M. L.; Nock, B.; Truong, R.; Cicero, T. J. Nitric-Oxide Control of Steroidogenesis - Endocrine Effects of Ng-Nitro-L-Arginine and Comparisons to Alcohol. *Life Sciences* **1992**, *50*, L35-L40.
52. Khatsenko, O. G.; Gross, S. S.; Rifkind, A. B.; Vane, J. R. Nitric-Oxide Is A Mediator of the Decrease in Cytochrome-P450-Dependent Metabolism Caused by Immunostimulants. *Proceedings of the National Academy of Sciences of the United States of America* **1993**, *90*, 11147-11151.
53. Griffith, O. W.; Stuehr, D. J. Nitric Ox ides Synthases - Properties and Catalytic Mechanism. *Annual Review of Physiology* **1995**, *57*, 707-736.
54. Griscava ge, J. M.; Fukuto, J. M.; Komori, Y.; Ignarro, L. J. Nitric-Oxide Inhibits Neuronal Nitric-Oxide Synthase by Interacting with the Heme Prosthetic Group - Role of Tetrahydrobiopterin in Modulating the Inhibitory-Action of Nitric-Oxide. *Journal of Biological Chemistry* **1994**, *269*, 21644-21649.
55. Hurshman, A. R.; Marlet ta, M. A. Nitric-Oxide Complexes of Inducible Nitric-Oxide Synthase - Spectral Characterization and Effect on Catalytic Activity. *Biochemistry* **1995**, *34*, 5627-5634.
56. Hurshman, A. R.; Marlet ta, M. A. Spectral Characterization of Nitrosyl Complexes of Nitric-Oxide Synthase. *Faseb Journal* **1995**, *9*, A1495.
57. Abusoud, H. M.; Stuehr, D. J. Nitric -Oxide Synthases Reveal A Role for Calmodulin in Controlling Electron-Transfer. *Proceedings of the National Academy of Sciences of the United States of America* **1993**, *90*, 10769-10772.

58. Schwartz, S. E.; White, W. H. Trace Atmospheric Constituents. John Wiley & Sons, New York, 1983.
59. I rany, E. P. A Theory of Liquid Structure. *Journal of the american chemical society* **1939**, *61*, 1436-1443.
60. Guillor y, W. A.; Johnston, H. S. Infrared Absorption by Peroxy-Nitrogen Trioxide Free Radical in the Gas Phase. *J. Chem. Phys.* **1965**, *42*, 2457.
61. Arnelle, D. R.; Stamle r, J. S. No⁺, No(Center-Dot), and No⁻ Donation by S-Nitrosothiols - Implications for Regulation of Physiological Functions by S-Nitrosylation and Acceleration of Disulfide Formation. *Archives of Biochemistry and Biophysics* **1995**, *318*, 279-285.
62. Awad, H. H.; Stanbury, D. M. Autoxidation of No in Aqueous-Solution. *International Journal of Chemical Kinetics* **1993**, *25*, 375-381.
63. Beckm an, J. S.; Beckman, T. W.; Chen, J.; Marshall, P. A.; Freeman, B. A. Apparent Hydroxyl Radical Production by Peroxynitrite - Implications for Endothelial Injury from Nitric-Oxide and Superoxide. *Proceedings of the National Academy of Sciences of the United States of America* **1990**, *87*, 1620-1624.
64. I schiropoulos, H.; Zhu, L.; Beckman, J. S. Peroxynitrite Formation from Macrophage-Derived Nitric-Oxide. *Archives of Biochemistry and Biophysics* **1992**, *298*, 446-451.
65. Wink, D. A.; Darb yshire, J. F.; Nims, R. W.; Saavedra, J. E.; Ford, P. C. Reactions of the Bioregulatory Agent Nitric-Oxide in Oxygenated Aqueous-Media - Determination of the Kinetics for Oxidation and Nitrosation by Intermediates Generated in the No/O₂ Reaction. *Chemical Research in Toxicology* **1993**, *6*, 23-27.
66. Hurst, J. K.; L ymar, S. V. Toxicity of peroxynitrite and related reactive nitrogen species toward Escherichia coli. *Chemical Research in Toxicology* **1997**, *10*, 802-810.
67. Stanbur y, D. M. Reduction potentials involving inorganic free radicals in aqueous solution. In *Advanced Inorganic Chemistry*; 1989; pp. 69-138.
68. Akhtar, M. J.; Bonner, F. T.; Hughes, M. N. Reaction of nitric oxide with hyponitrous acid: a hydrogen atom abstraction reaction. *Inorganic Chemistry* **1985**, *24*, 1934.
69. Cooper, J. N.; Chil ton, J. E.; Powell, R. E. Jr. Reaction of nitric oxide with alkaline hydroxylamine. *Inorg. Chem.* **1970**, *9*, 2303-2304.

70. Rubbo, H.; Radi, R.; Trujillo, M.; Telleri, R.; Kalyanaraman, B.; Barnes, S.; Kirk, M.; Freeman, B. A. Nitric-Oxide Regulation of Superoxide and Peroxynitrite-Dependent Lipid-Peroxidation - Formation of Novel Nitrogen-Containing Oxidized Lipid Derivatives. *Journal of Biological Chemistry* **1994**, *269*, 26066-26075.
71. Hogg, N.; Kalyanaraman, B.; Joseph, J.; Struck, A.; Parthasarathy, S. Inhibition of Low-Density-Lipoprotein Oxidation by Nitric-Oxide - Potential Role in Atherogenesis. *Febs Letters* **1993**, *334*, 170-174.
72. Koppenol, W. H.; Moreno, J. J.; Pryor, W. A.; Ischiropoulos, H.; Beckman, J. S. Peroxynitrite, A Cloaked Oxidant Formed by Nitric-Oxide and Superoxide. *Chemical Research in Toxicology* **1992**, *5*, 834-842.
73. Radi, R.; Beckman, J. S.; Bush, K. M.; Freeman, B. A. Peroxynitrite-Induced Membrane Lipid-Peroxidation - the Cytotoxic Potential of Superoxide and Nitric-Oxide. *Archives of Biochemistry and Biophysics* **1991**, *288*, 481-487.
74. Radi, R.; Beckman, J. S.; Bush, K. M.; Freeman, B. A. Peroxynitrite Oxidation of Sulfhydryls - the Cytotoxic Potential of Superoxide and Nitric-Oxide. *Journal of Biological Chemistry* **1991**, *266*, 4244-4250.
75. Pfeiffer, S.; Gorren, A. C. F.; Schmidt, K.; Werner, E. R.; Hansert, B.; Bohle, D. S.; Mayer, B. Metabolic fate of peroxynitrite in aqueous solution - Reaction with nitric oxide and pH-dependent decomposition to nitrite and oxygen in a 2:1 stoichiometry. *Journal of Biological Chemistry* **1997**, *272*, 3465-3470.
76. Merenyi, G.; Lind, J. Free radical formation in the peroxynitrous acid (ONOOH) peroxynitrite (ONOO-) system. *Chemical Research in Toxicology* **1998**, *11*, 243-246.
77. Merenyi, G.; Lind, J. Thermodynamics of peroxynitrite and its CO₂ adduct. *Chemical Research in Toxicology* **1997**, *10*, 1216-1220.
78. Pryor, W. A.; Church, D. F.; Govindan, K. Oxidation of thiols by nitric oxide and nitrogen dioxide: synthetic utility and toxicological implications. *J. Org. Chem.* ; **1982**, *47*, 156-159.
79. Demaster, E. G.; Quast, B. J.; Redfern, B.; Nagasawa, H. T. Reaction of Nitric-Oxide with the Free Sulfhydryl-Group of Human Serum-Albumin Yields A Sulfenic Acid and Nitrous-Oxide. *Biochemistry* **1995**, *34*, 11494-11499.
80. Liu, Z.; Rudd, M. A.; Freedman, J. E.; Loscalzo, J. S-Transnitrosation reactions are involved in the metabolic fate and biological actions of nitric oxide. *Journal Pharmacol. Exp. Ther.* **1998**, *284*, 526-534.

81. Ignarro, L. J.; Edwards, J. C.; Gruetter, D. Y.; Barry, B. K.; Gruetter, C. A. Possible involvement of S-nitrosothiols in the activation of guanylate cyclase by nitroso compounds. *FEBS Letters* **1980**, *110*, 275-278.
82. Stamler, J. S. ; Jaraki, O.; Osborne, J.; Simon, D. I.; Keaney, J.; Vita, J.; Singel, D.; Valeri, C. R.; Loscalzo, J. Nitric-Oxide Circulates in Mammalian Plasma Primarily As An S-Nitroso Adduct of Serum-Albumin. *Proceedings of the National Academy of Sciences of the United States of America* **1992**, *89*, 7674-7677.
83. Gaston, B.; Sears, S.; Woods, J.; Hunt, J.; Ponaman, M.; McMahon, T.; Stamler, J. S. Bronchodilator S-nitrosothiol deficiency in asthmatic respiratory failure. *Lancet* **1998**, *351*, 1317-1319.
84. Clancy, R. M.; Levartovsky, D.; Leszczynskapiziak, J.; Yegudin, J.; Abramson, S. B. Nitric-Oxide Reacts with Intracellular Glutathione and Activates the Hexose-Monophosphate Shunt in Human Neutrophils - Evidence for S-Nitrosoglutathione As A Bioactive Intermediary. *Proceedings of the National Academy of Sciences of the United States of America* **1994**, *91*, 3680-3684.
85. Stamler, J. S. ; Jaraki, O.; Osborne, J.; Simon, D. I.; Keaney, J.; Vita, J.; Singel, D.; Valeri, C. R.; Loscalzo, J. Nitric-Oxide Circulates in Mammalian Plasma Primarily As An S-Nitroso Adduct of Serum-Albumin. *Proceedings of the National Academy of Sciences of the United States of America* **1992**, *89*, 7674-7677.
86. Gaston, B.; Reilly, J.; Drazen, J. M.; Fackler, J.; Ramdev, P.; Arnette, D.; Mullins, M. E.; Sugarbaker, D. J.; Chee, C.; Singel, D. J.; Loscalzo, J.; Stamler, J. S. Endogenous Nitrogen-Oxides and Bronchodilator S-Nitrosothiols in Human Airways. *Proceedings of the National Academy of Sciences of the United States of America* **1993**, *90*, 10957-10961.
87. Stamler, J. S. ; Loh, E.; Roddy, M. A.; Currie, K. E.; Creager, M. A. Nitric-Oxide Regulates Basal Systemic and Pulmonary Vascular-Resistance in Healthy Humans. *Circulation* **1994**, *89*, 2035-2040.
88. Keane y, J. F.; Puyana, J. C.; Francis, S.; Loscalzo, J. F.; Stamler, J. S.; Loscalzo, J. Methylene-Blue Reverses Endotoxin-Induced Hypotension. *Circulation Research* **1994**, *74*, 1121-1125.
89. Williams, D. L. H. Nitrosation Reactions and the Chemistry of Nitric Oxide. Elsevier: New York, 2004.

90. Arulsamy, N.; Bohle, D. S.; Butt, J. A.; Irvine, G. J.; Jordan, P. A.; Sagan, E. Interrelationships between Conformational Dynamics and the Redox Chemistry of S-Nitrosothiols. *J. Am. Chem. Soc.* **1999**, *121*, 7115-7123.
91. Kharitonov, V. G.; Sundquist, A. R.; Sharma, V. S. Kinetics of Nitrosation of Thiols by Nitric-Oxide in the Presence of Oxygen. *Journal of Biological Chemistry* **1995**, *270*, 28158-28164.
92. Goldstein, S.; Czapski, G. Mechanism of the nitrosation of thiols and amines by oxygenated (center dot) NO solutions: The nature of the nitrosating intermediates (vol 118, pg 3419, 1996). *Journal of the American Chemical Society* **1996**, *118*, 6806.
93. Goldstein, S.; Czapski, G. Kinetics of Nitric-Oxide Autoxidation in Aqueous-Solution in the Absence and Presence of Various Reductants - the Nature of the Oxidizing Intermediates. *Journal of the American Chemical Society* **1995**, *117*, 12078-12084.
94. Patel, H. M. S.; Williams, D. L. H. Nitrosation by alkyl nitrites. Part 3. Reactions with cysteine in water in the pH range 6-13. *Chem. Soc., Perkin Trans. 2*, **1989**, 339-341.
95. Patel, H. M. S.; Williams, D. L. H. Nitrosation by alkyl nitrites. Part 6. Thiolate nitrosation. *J. Chem. Soc., Perkin Trans. 2* **1990**, 37-42.
96. Aldred, S. E.; Williams, D. L. H.; Garley, M. Kinetics and mechanism of the nitrosation of alcohols, carbohydrates, and a thiol. *J. Chem. Soc., Perkin Trans. 2* **1982**, 777-782.
97. Dix, L. R.; Williams, D. L. H. Kinetics and mechanism of thionitrite formation. Mercapto-carboxylic acid: a new range of efficient nitrous acid scavengers. *J. Chem. Soc., Perkin Trans. 2* **1984**, 109-112.
98. Morris, P. A.; Williams, D. L. H. Kinetics and mechanism of S-nitrosation of some thiol-containing amino acids and other thiols. *J. Chem. Soc., Perkin Trans. 2* **1988**, 513-516.
99. Williams, D. L. H. The Chemistry of S-Nitrosothiols. *Acc. Chem. Res.* **1999**, *32*, 869-876.
100. Dicks, A. P.; Swift, H. R.; Williams, D. L. H.; Butler, A. R.; AlSadoni, H. H.; Cox, B. G. Identification of Cu⁺ as the effective reagent in nitric oxide formation from S-nitrosothiols (RSNO). *Journal of the Chemical Society-Perkin Transactions 2* **1996**, 481-487.

101. Dicks, A. P.; Beloso, P. H.; Williams, D. L. H. Decomposition of S-nitrosothiols: The effects of added thiols. *Journal of the Chemical Society-Perkin Transactions 2* **1997**, 1429-1434.
102. Holmes, A. J. Reaction of S-nitrosothiols with ascorbate: clear evidence of two reactions. *Chem. Commun.* **1998**, 1711-1712.
103. Singh, R. J.; Hogg, N.; Joseph, J.; Kalyanaraman, B. Mechanism of nitric oxide release from S-nitrosothiols. *Journal of Biological Chemistry* **1996**, *271*, 18596-18603.
104. Joseph, P. D.; Rehorek, D.; Janzen, E. G. Electron spin resonance spin trapping of thiyl radicals from the decomposition of thionitrites. *Tetrahedron Letters* **1984**, *25*, 1685-1688.
105. Bainbridge, N.; Butler, A. R.; Görbitz, C. The thermal stability of S-nitrosothiols: experimental studies and ab initio calculations on model compounds. *Chem. Soc., Perkin Trans. 2* **1997**, 351-354.
106. Barnett, D. J.; McAninly, J.; Williams, D. L. H. Transnitrosation Between Nitrosothiols and Thiols. *Journal of the Chemical Society-Perkin Transactions 2* **1994**, 1131-1133.
107. Hogg, N. The kinetics of S-transnitrosation - A reversible second-order reaction. *Analytical Biochemistry* **1999**, *272*, 257-262.
108. Meyer, D. J.; Kramer, H.; Özer, N.; Coles, B.; Ketterer, B. Kinetics and equilibria of S-nitrosothiol—thiol exchange between glutathione, cysteine, penicillamines and serum albumin. *Febs Letters* **1994**, *345*, 177-180.
109. Wang, K.; Wen, Z.; Zhang, W.; Xian, M.; Cheng, J.; Wang, P. Equilibrium and kinetics studies of transnitrosation between S-nitrosothiols and thiols. *Bioorganic & Medicinal Chemistry Letters* **2001**, *11*, 433-436.
110. Mohr, S.; Stamler, J. S.; Brune, B. Mechanism of Covalent Modification of Glyceraldehyde-3-Phosphate Dehydrogenase at Its Active-Site Thiol by Nitric-Oxide, Peroxynitrite and Related Nitrosating Agents. *Febs Letters* **1994**, *348*, 223-227.
111. Singh, R. J.; Hogg, N.; Neese, F.; Joseph, J.; Kalyanaraman, B. Trapping of Nitric-Oxide Formed During Photolysis of Sodium-Nitroprusside in Aqueous and Lipid Phases - An Electron-Spin-Resonance Study. *Photochemistry and Photobiology* **1995**, *61*, 325-330.

112. Singh, R. J.; Hogg, N.; Joseph, J.; Kal yanaraman, B. Photosensitized Decomposition of S-Nitrosothiols and 2-Methyl-2-Nitrosopropane Possible Use for Site-Directed Nitric-Oxide Production. *Febs Letters* **1995**, *360*, 47-51.
113. Zhel yaskov, V. R.; Gee, K. R.; Godwin, D. W. Control of no concentration in solutions of nitrosothiol compounds by light. *Photochemistry and Photobiology* **1998**, *67*, 282-288.
114. Wood, P. D.; Mutus, B.; Redmond, R. W. The mechanism of photochemical release of nitric oxide from S-nitrosoglutathione. *Photochemistry and Photobiology* **1996**, *64*, 518-524.
115. Mutus, B.; Redmond, R. W.; Akhter, S. Evidence for peroxyxynitrite formation during S-nitrosoglutathione photolysis in air saturated solutions. *Febs Letters* **1999**, *449*, 79-82.
116. Sexton, D. J.; Muruganandam, A.; Mckenney, D. J.; Mutus, B. Visible-Light Photochemical Release of Nitric-Oxide from S-Nitrosoglutathione - Potential Photochemotherapeutic Applications. *Photochemistry and Photobiology* **1994**, *59*, 463-467.
117. Murad, F. Dis covery of some of the biological effects of nitric oxide and its role in cell signaling (Nobel lecture). *Angewandte Chemie-International Edition* **1999**, *38*, 1857-1868.
118. Whitfield, J. B. Gamma glutamyl transferase. *Critical Reviews in Clinical Laboratory Sciences* **2001**, *38*, 263-355.
119. Askew, S. C.; Butler, A. R.; Flitney, F. W.; Kemp, G. D.; Megson, I. L. Chemical mechanisms underlying the vasodilator and platelet anti-aggregating properties of S-nitroso-N-acetyl--penicillamine and S-nitrosoglutathione. *Bioorganic & Medicinal Chemistry* **1995**, *3*, 1-9.
120. Megson, L.; Greig, I. R.; Gray, G. A.; Webb, D. J.; Butler, A. R. Prolonged effect of a novel S-nitrosated glyco-amino acid in endothelium-denuded rat femoral arteries: potential as a slow release nitric oxide donor drug. *Br J Pharmacol.* **1997**, *122*, 1617-1624.
121. Maalej, N.; Albre cht, R.; Loscalzo, J.; Folts, J. D. The potent platelet inhibitory effects of S-nitrosated albumin coating of artificial surfaces. *Journal of the American College of Cardiology* **1999**, *33*, 1408-1414.
122. Sogo, N.; Campanella, C .; Webb, D. J.; Megson, I. L. S-nitrosothiols cause prolonged, nitric oxide-mediated relaxation in human saphenous vein and internal mammary artery: therapeutic potential in bypass surgery. *British Journal of Pharmacology* **2000**, *131*, 1236-1244.

123. Kiris, T.; Karasu, A.; Yavuz, C.; Erdem, T.; Ünal, F.; Hepgül, K.; Baloglu, H. Reversal of Cerebral Vasospasm by the Nitric Oxide Donor SNAP in an Experimental Model of Subarachnoid Haemorrhage. *Acta Neurochirurgica* **1999**, *141*, 1323-1329.
124. Sehajpal, P. K.; Basu, A.; Ogiste, J. S.; Lander, H. M. Reversible S-nitrosation and inhibition of HIV-1 protease. *Biochemistry* **1999**, *38*, 13407-13413.
125. Mannick, J. B.; Stamler, J. S.; Teng, E.; Simpson, N.; Lawrence, J.; Jordan, J.; Finberg, R. W. Nitric oxide modulates HIV-1 replication. *Journal of Acquired Immune Deficiency Syndromes* **1999**, *22*, 1-9.
126. Merriman, P. F.; Clancy, R. M.; He, X. Y.; Abramson, S. B. Modulation of Human T-Cell Responses by Nitric-Oxide and Its Derivative, S-Nitrosoglutathione. *Arthritis and Rheumatism* **1993**, *36*, 1414-1422.
127. Beckman, J. S.; Conger, K. A. Direct measurement of dilute nitric oxide in solutions with an ozone chemiluminescence detector. *Methods* **1995**, *7*, 35-39.
128. Brunelli, L.; Crow, J. P.; Beckman, J. S. The Comparative Toxicity of Nitric-Oxide and Peroxynitrite to Escherichia-Coli. *Archives of Biochemistry and Biophysics* **1995**, *316*, 327-334.
129. I schiropoulos, H.; Zhu, L.; Beckman, J. S. Peroxynitrite Formation from Macrophage-Derived Nitric-Oxide. *Archives of Biochemistry and Biophysics* **1992**, *298*, 446-451.
130. Carreras, M. C.; Catz, S. D.; Pargament, G. A.; Del Bosco, G.; Oderoso, J. J. Decreased production of nitric oxide by human neutrophils during septic multiple organ dysfunction syndrome. *Inflammation* **1994**, *18*, 151-161.
131. Maria Cecilia Carreras; Griselda A. Pargament; Sergio D. Catz; Juan J. Poderoso; Alberto Boveris Kinetics of nitric oxide and hydrogen peroxide production and formation of peroxynitrite during the respiratory burst of human neutrophils. *FEBS Letters* **1994**, *341*, 65-68.
132. Koo Y. N. W.; Royall J. A. Agonist-Induced Peroxynitrite Production from Endothelial Cells. *Arch. Biochem. Biophys.* **1994**, *310*, 352-359.
133. Koppenol, W. H. The chemistry of peroxynitrite, a biological toxin. *Quimica Nova* **1998**, *21*, 326-331.
134. Kelm, M.; Dahmann, R.; Wink, D.; Feelisch, M. The nitric oxide superoxide assay - Insights into the biological chemistry of the NO/O₂⁻ interaction. *Journal of Biological Chemistry* **1997**, *272*, 9922-9932.

135. Goldstein, S.; Czapski, G. The Reaction of NO[•] with O₂^{•-} and HO₂[•]: A Pulse-Radiolysis Study. *Free Radical Biology and Medicine* **1995**, *19*, 505-510.
136. Kissner, R.; Nauser, T.; Bugnon, P.; Lye, P. G.; Koppenol, W. H. Formation and properties of peroxynitrite as studied by laser flash photolysis, high-pressure stopped-flow technique, and pulse radiolysis. *Chemical Research in Toxicology* **1997**, *10*, 1285-1292.
137. Nauser, T.; Koppenol, W. H. The rate constant of the reaction of superoxide with nitrogen monoxide: Approaching the diffusion limit. *Journal of Physical Chemistry A* **2002**, *106*, 4084-4086.
138. Kobayashi, K.; Miki, M.; Tagawa, S. Pulse-Radiolysis Study of the Reaction of Nitric-Oxide with Superoxide. *Journal of the Chemical Society-Dalton Transactions* **1995**, 2885-2889.
139. Huie, R. E.; Padmaja, S. The Reaction of NO with Superoxide. *Free Radical Research Communications* **1993**, *18*, 195-199.
140. Marla, S. S.; Lee, J.; Groves, J. T. Peroxynitrite rapidly permeates phospholipid membranes. *Proc. Natl. Acad. Sci. USA* **1997**, *94*, 14243-14248.
141. Denicola, A.; Souza, J. M.; Radi, R. Diffusion of peroxynitrite across erythrocyte membranes. *Proceedings of the National Academy of Sciences of the United States of America* **1998**, *95*, 3566-3571.
142. Radi, R.; Beckman, J. S.; Bush, K. M.; Freeman, B. A. Peroxynitrite-induced membrane lipid peroxidation: The cytotoxic potential of superoxide and nitric oxide. *Arch. Biochem. Biophys.* **1991**, *288*, 481-487.
143. Radi, R.; Beckman, J. S.; Bush, K. M.; Freeman, B. A. Peroxynitrite oxidation of sulfhydryls. The cytotoxic potential of superoxide and nitric oxide. *J. Biol. Chem.* **1991**, *266*, 4244-4250.
144. Koppenol, W. H.; Perrin, D. Is HOONO[•] involved in the reaction of peroxynitrite with methionine? *Free Radical Biology and Medicine* **1999**, *27*, S79.
145. Alvarez, B.; Radi, R. Peroxynitrite reactivity with amino acids and proteins. *Amino Acids* **2003**, *25*, 295-311.
146. Liu, P.; Xu, B. H.; Quilley, J.; Wong, P. Y. K. Peroxynitrite attenuates hepatic ischemia-reperfusion injury. *American Journal of Physiology-Cell Physiology* **2000**, *279*, C1970-C1977.

147. Pacher, P.; Beckman, J. S.; Liaudet, L. Nitric oxide and peroxynitrite in health and disease. *Physiological Reviews* **2007**, *87*, 315-424.
148. Levrard, S.; Vannay-Bouchiche, C.; Pesse, B.; Pacher, P.; Feihl, F.; Waeber, B.; Liaudet, L. Peroxynitrite is a major trigger of cardiomyocyte apoptosis in vitro and in vivo. *Free Radical Biology and Medicine* **2006**, *41*, 886-895.
149. Nicklin, H. G.; Hughes, M. N. The chemistry of pernitrites. Part I. Kinetics of decomposition of pernitrous acid. *J. Chem. Soc. A*, **1968**, 450-452.
150. Crow, J. P.; Spruell, C.; Chen, J.; Gunn, C.; Ischiropoulos, H.; Tsai, M.; Smith, C. D.; Radi, R.; Koppenol, W. H.; Beckman, J. S. On the Ph-Dependent Yield of Hydroxyl Radical Products from Peroxynitrite. *Free Radical Biology and Medicine* **1994**, *16*, 331-338.
151. Worle, M.; Latal, P.; Kissner, R.; Nesper, R.; Koppenol, W. H. Conformation of peroxynitrite: Determination by crystallographic analysis. *Chemical Research in Toxicology* **1999**, *12*, 305-307.
152. Xu, M.; Lesar, A.; Prebil, S.; Muhlhauser, M.; Hodoscek, M. Induction of microglial reaction and expression of nitric oxide synthase I in the nucleus dorsalis and red nucleus following lower thoracic spinal cord hemisection
Conformational potential energy surface of BrOONO. *Brain Research* **2003**, *368*, 23-30.
153. Tsai, J. -H. M.; Harrison, J. G.; Martin, J. C.; Hamilton, T. P.; Mark van der Woerd; Jablonsky, M. J.; Beckman, J. S. Role of Conformation of Peroxynitrite Anion (ONOO⁻) with Its Stability and Toxicity. *J. Am. Chem. Soc.* **1994**, *116*, 4115-4116.
154. Manuszak, M.; Koppenol, W. H. The enthalpy of isomerization of peroxynitrite to nitrate. *Thermochimica Acta* **1996**, *273*, 11-15.
155. Koppenol, W. H.; Kissner, R. Can O = NOOH undergo homolysis? *Chemical Research in Toxicology* **1998**, *11*, 87-90.
156. Reed, J. W.; Ho, H. H.; Jolly, W. L. Chemical synthesis with a quenched flow reactor. Hydroxytrihydroborate and peroxynitrite. *J. Am. Chem. Soc.* **1974**, *96*, 1248-1249.
157. Uppu, R. M.; Squadrito, G. L.; Cueto, R.; Pryor, W. A. Synthesis of peroxynitrite by azide-ozone reaction. *Methods in Enzymology*. **1996**, *269*, 311-321.
158. Hughes, M. N.; Nicklin, H. G. Autoxidation of hydroxylamine in alkaline solutions. *J. Chem. Soc. A*, **1971**, 164-168.

159. Robinson, K. M.; Beckman, J. S. Synthesis of peroxynitrite from nitrite and hydrogen peroxide. *Nitric Oxide, Pt e* **2005**, *396*, 207-214.
160. Koppenol, W. H.; Kissner, R.; Beckman, J. S. Syntheses of peroxynitrite: To go with the flow or on solid grounds? *Methods in Enzymology*. **1996**, *269*, 296-302.
161. Uppu, R. M. Synthesis of peroxynitrite using isoamyl nitrite and hydrogen peroxide in a homogeneous solvent system. *Analytical Biochemistry* **2006**, *354*, 165-168.
162. Petriconi, G. L.; Papee, H. M. Aqueous solutions of "Sodium pernitrite" from alkaline hydrogen peroxide and nitric oxide. *Can. J. Chem. /Rev. can. chim.* **1966**, *44*, 977-980.
163. Bohle, D. C.; Glassbrunner, P. A.; Hansert, B. Synthesis of pure tetramethylammonium peroxynitrite. *Methods in Enzymology*. **1996**, *269*, 302-311.
164. Arulsamy, N.; Bohle, D. S.; Imonigie, J. A.; Sagan, E. S. Synthesis and characterization of alkylammonium hyponitrites and base-stabilized hyponitrous acid salts. *Inorganic Chemistry* **1999**, *38*, 2716-2725.
165. Bohle, D. S.; Hansert, B.; Paulson, C. S.; Smith, B. D. Biomimetic Synthesis of the Putative Cytotoxin Peroxynitrite, ONOO-, and Its Characterization as a Tetramethylammonium Salt. *J. Am. Chem. Soc.* **1994**, *116*, 7423-7424.
166. Plumb, R. C.; Edwards, J. O. Color centers in UV-irradiated nitrates. *J. Phys. Chem.* **1992**, *96*, 3245-3247.
167. Joseph A.Hrabie; John R.Klose; David A.Wink; Larry K.Keefer New nitric oxide-releasing zwitterions derived from polyamines. *J. Org. Chem.* ; **1993**; *58*, 1472-1476.
168. Hogg, N.; Darleyusmar, V. M.; Wilson, M. T.; Moncada, S. Production of Hydroxyl Radicals from the Simultaneous Generation of Superoxide and Nitric-Oxide. *Biochemical Journal* **1992**, *281*, 419-424.
169. Beckman, J. S.; Robinson, K. M. Synthesis of peroxynitrite from nitrite and hydrogen peroxide. *Methods in Enzymology*. **2005**, *369*, 207-213.
170. Richeson, C. E.; Mulder, P.; Bowry, V. W.; Ingold, K. U. The complex chemistry of peroxynitrite decomposition: New insights. *Journal of the american chemical society* **1998**, *120*, 7211-7219.

171. Beckman, J. S.; Beckman, T. W.; Chen, J.; Marshall, P. A.; Freeman, B. A. Apparent Hydroxyl Radical Production by Peroxynitrite: Implications for Endothelial Injury from Nitric Oxide and Superoxide. *Proceedings of the National Academy of Sciences* **1990**, *87*, 1620-1624.
172. van der Vliet, A.; O'Neill, C. A.; Halliwell, B.; Cross, C. E.; Kaur, H. Aromatic hydroxylation and nitration of phenylalanine and tyrosine by peroxynitrite: Evidence for hydroxyl radical production from peroxynitrite. *FEBS Letters* **1994**, *339*, 89-92.
173. Koppenol, W. H.; Moreno, J. J.; Pryor, W. A.; Ischiropoulos, H.; Beckman, J. S. Peroxynitrite, A Cloaked Oxidant Formed by Nitric-Oxide and Superoxide. *Chemical Research in Toxicology* **1992**, *5*, 834-842.
174. Koppenol, W. H.; Moreno, J. J.; Pryor, W. A.; Ischiropoulos, H.; Beckman, J. S. Peroxynitrite, A Cloaked Oxidant Formed by Nitric-Oxide and Superoxide. *Chemical Research in Toxicology* **1992**, *5*, 834-842.
175. Pryor, W. A.; Jin, X.; Squadrito, G. L. One- and Two-Electron Oxidations of Methionine by Peroxynitrite. *PNAS* **1994**, *91*, 11173-11177.
176. Pfeiffer, S.; Gorren, A. C. F.; Schmidt, K.; Werner, E. R.; Hansert, B.; Bohle, D. S.; Mayer, B. Metabolic Fate of Peroxynitrite in Aqueous Solution. Reaction with Nitric oxide and pH dependent decomposition to nitrite and oxygen in 2:1 stoichiometry. *J. Biol. Chem.* **1997**, *272*, 3465-3470.
177. Uppu, R. M.; Lemercier, J. N.; Squadrito, G. L.; Zhang, H. W.; Bolzan, R. M.; Pryor, W. A. Nitrosation by peroxynitrite: Use of phenol as a probe. *Archives of Biochemistry and Biophysics* **1998**, *358*, 1-16.
178. Kirsch, M.; Lomonosova, E. E.; Korth, H. G.; Sustmann, R.; de Groot, H. Hydrogen peroxide formation by reaction of peroxynitrite with HEPES and related tertiary amines - Implications for a general mechanism. *Journal of Biological Chemistry* **1998**, *273*, 12716-12724.
179. Nauser, T.; Koppenol, W. H. The rate constant of the reaction of superoxide with nitrogen monoxide: Approaching the diffusion limit. *Journal of Physical Chemistry A* **2002**, *106*, 4084-4086.
180. Goldstein, S.; Czapski, G. Viscosity effects on the reaction of peroxynitrite with CO₂: Evidence for radical formation in a solvent cage. *Journal of the American Chemical Society* **1999**, *121*, 2444-2447.
181. Hodges, G. R.; Ingold, K. U. Cage-escape of geminate radical pairs can produce peroxynitrate from peroxynitrite under a wide variety of experimental

- conditions. *Journal of the American Chemical Society* **1999**, *121*, 10695-10701.
182. Bonini, M. G.; Radi, R.; Ferrer-Sueta, G.; Ferreira, A. M. D.; Augusto, O. Direct EPR detection of the carbonate radical anion produced from peroxyxynitrite and carbon dioxide (vol 274, pg 10802, 1999). *Journal of Biological Chemistry* **1999**, *274*, 19508.
183. Ramezani, M. S.; Padmaja, S.; Koppenol, W. H. Nitration and hydroxylation of phenolic compounds by peroxyxynitrite. *Chemical Research in Toxicology* **1996**, *9*, 232-240.
184. Ischiropoulos, H.; Zhu, L.; Chen, J.; Tsai, M.; Martin, J. C.; Smith, C. D.; Beckman, J. S. Peroxyxynitrite-Mediated Tyrosine Nitration Catalyzed by Superoxide-Dismutase. *Archives of Biochemistry and Biophysics* **1992**, *298*, 431-437.
185. Goldstein, S.; Czapski, G.; Lind, J.; Merenyi, G. Tyrosine nitration by simultaneous generation of (NO)-N-center dot and O-2(center dot) under physiological conditions - How the radicals do the job. *Journal of Biological Chemistry* **2000**, *275*, 3031-3036.
186. Pfeiffer, S.; Schmidt, K.; Mayer, B. Dityrosine formation outcompetes tyrosine nitration at low steady-state concentrations of peroxyxynitrite - Implications for tyrosine modification by nitric oxide/superoxide in vivo. *Journal of Biological Chemistry* **2000**, *275*, 6346-6352.
187. Quijano, C.; Alvarez, B.; Gatti, R. M.; Augusto, O.; Radi, R. Pathways of peroxyxynitrite oxidation of thiol groups. *Biochemical Journal* **1997**, *322*, 167-173.
188. Rosen, G. M.; Freeman, B. A. Detection of superoxide generated by endothelial cells. *Proc. Natl. Acad. Sci. USA* **1984**, *81*, 7269-7273.
189. Pietraforte, D.; Minetti, M. Direct ESR detection of peroxyxynitrite-induced tyrosine-centred protein radicals in human blood plasma. *Biochemical Journal* **1997**, *325*, 675-684.
190. Pietraforte, D.; Minetti, M. One-electron oxidation pathway of peroxyxynitrite decomposition in human blood plasma: Evidence for the formation of protein tryptophan-centred radicals. *Biochemical Journal* **1997**, *321*, 743-750.
191. Grossi, L.; Montecchi, P. C.; Strazzari, S. S-nitrosothiol and disulfide formation through peroxyxynitrite-promoted oxidation of thiols. *European Journal of Organic Chemistry* **2001**, 131-135.

192. Grossi, L.; Montevecchi, P. C.; Strazzari, S. S-nitrosothiol and disulfide formation through peroxyxynitrite-promoted oxidation of thiols. *European Journal of Organic Chemistry* **2001**, 131-135.
193. Grossi, L.; Montevecchi, P. C.; Strazzari, S. S-nitrosothiol and disulfide formation through peroxyxynitrite-promoted oxidation of thiols. *European Journal of Organic Chemistry* **2001**, 131-135.
194. Groves, J. T.; Wang, C. C. Y. Nitric oxide synthase: models and mechanisms. *Current Opinion in Chemical Biology* **2000**, *4*, 687-695.
195. Iwanaga, T.; Yamazaki, T.; Kominami, S. Kinetic studies on the successive reaction of neuronal nitric oxide synthase from L-arginine to nitric oxide and L-citrulline. *Biochemistry* **1999**, *38*, 16629-16635.
196. Hughes, M. N.; Nicklin, H. G. The chemistry of peroxyxynitrites. Part II. Copper(II)-catalysed reaction between hydroxylamine and peroxyxynitrite in alkali. *J. Chem. Soc. A*, **1970**, 925.
197. Miranda, K. M.; Espey, M. G.; Yamada, K.; Krishna, M.; Ludwick, N.; Kim, S.; Jour'dheuil, D.; Grisham, M. B.; Feelisch, M.; Fukuto, J. M.; Wink, D. A. Unique oxidative mechanisms for the reactive nitrogen oxide species, nitroxyl anion. *Journal of Biological Chemistry* **2001**, *276*, 1720-1727.
198. Hi-Tech Scientific. Operator's Manual for the SF-61 DX2 Double-Mixing Stopped-Flow Spectrofluorimeter. 1996. Salisbury, UK, Hi-Tech Limited.
Ref Type: Catalog
199. Documentation Manual for Bruker EMX EPR Spectrometer. Bruker Instruments, Inc: 1998.
200. Frejaville, C.; Karoui, H.; Tuccio, B.; Le Moigne, F.; Culcasi, M.; Pietri, S.; Lauricella, R.; Tordo, P. 5-(Diethoxyphosphoryl)-5-methyl-1-pyrroline N-oxide: A New Efficient Phosphorylated Nitron for the in Vitro and in Vivo Spin Trapping of Oxygen-Centered Radicals. *J. Med. Chem.* ; **1995**, *38*, 258-265.
201. Karoui, H.; Hogg, N.; Frejaville, C.; Tordo, P.; Kalyanaraman, B. Characterization of sulfur-centered radical intermediates formed during the oxidation of thiols and sulfite by peroxyxynitrite - ESR-SPIN trapping and oxygen uptake studies. *Journal of Biological Chemistry* **1996**, *271*, 6000-6009.
202. Whitehouse, C. M.; Dreyer, R. N.; Yamashita, M.; Fenn, J. B. Electrospray interface for liquid chromatographs and mass spectrometers. *Anal. Chem.* **1985**, *57*, 675-679.

203. Fenn, J. B.; Mann, M.; Meng, C. K.; Wong, S. F.; Whitehouse, C. M. Electrospray ionization for mass spectrometry of large biomolecules. *Science* **1989**, *246*, 64-71.
204. Fenn, J. B.; Mann, M.; Meng, C. K.; Wong, S. F.; Whitehouse, C. M. Electrospray ionization for mass spectrometry of large biomolecules. *Science* **1989**, *246*, 64-71.
205. Costello, C. E. Time, life ... and mass spectrometry. New techniques to address biological questions. *Biophys. Chem.* **1997**, *68*, 173-188.
206. Ernest J. Corrado Computer Simulation Methods to Aid National Growth Policy. US Government printing office, Washington: 1975.
207. Trochim, W.; Davis, J. Computer simulation for program evaluation. *Evaluation review.* **1986**, *5*, 609-634.
208. Ianni, C. J. Kintecus: The Kinetics Program Modules for the Ultimate Lazy Scientist. <http://www.theochem.kth.se/html/pemac/links/KINTECUS.en.html>. **1996**, Accessed August 26th 2004.
209. Darkwa, J.; Olojo, R.; Olagunju, O.; Otoikhian, A.; Simoyi, R. Oxyhalogen-sulfur chemistry: Oxidation of N-acetylcysteine by chlorite and acidic bromate. *Journal of Physical Chemistry A* **2003**, *107*, 9834-9845.
210. Goldstein, S.; Czapski, G. The Reaction of NO-Center-Dot with O₂(Center-Dot) and HO₂-Center-Dot - A Pulse-Radiolysis Study. *Free Radical Biology and Medicine* **1995**, *19*, 505-510.
211. Kissner, R.; Nauser, T.; Bugnon, P.; Lye, P. G.; Koppenol, W. H. Formation and properties of peroxyxynitrite as studied by laser flash photolysis, high-pressure stopped-flow technique, and pulse radiolysis. *Chemical Research in Toxicology* **1997**, *10*, 1285-1292.
212. Kalinga, S. Interaction of peroxyxynitrite with myoglobin and hemoglobin. *Canadian Journal of Chemistry-Revue Canadienne de Chimie* **2006**, *84*, 788-793.
213. Ducrocq, C.; Blanchard, B.; Pignatelli, B.; Ohshima, H. Peroxyxynitrite: an endogenous oxidizing and nitrating agent. *Cellular and Molecular Life Sciences* **1999**, *55*, 1068-1077.
214. Shi, X.; Lenhart, A.; Mao, Y. ESR spin trapping investigation on peroxyxynitrite decomposition: No evidence for hydroxyl radical production. *Biochemical and Biophysical Research Communication.* **1994**, *203*, 1515-1521.

215. Hirofumi Arai; Barbara S. Berlett; P. Boon Chock Effect of bicarbonate on iron-mediated oxidation of low-density lipoprotein. *Proc Natl Acad Sci U S A.* **2005**, *102*, 10472-10477.
216. Buettner, G. R. Spin Trapping - Electron-Spin-Resonance Parameters of Spin Adducts. *Free Radical Biology and Medicine* **1987**, *3*, 259-303.
217. Beak e, B. D.; Moodie, R. B. Nitrous and nitric acid ionisation equilibria and nitrous acid-catalysed nitration of 4-fluorophenol, in aqueous trifluoroacetic acid. *Journal of the Chemical Society-Perkin Transactions 2* **1998**, 1-5.
218. Scorza, G.; Minetti, M. One-electron oxidation pathway of thiols by peroxynitrite in biological fluids: bicarbonate and ascorbate promote the formation of albumin disulphide dimers in human blood plasma. *Biochemical Journal* **1998**, *329*, 405-413.
219. Moro, M. A.; Darley-Usmar, V. M.; Goodwin, D. A.; Read, N. G.; Zamorapino, R.; Feelisch, M.; Radomski, M. W.; Moncada, S. Paradoxical Fate and Biological Action of Peroxynitrite on Human Platelets. *Proceedings of the National Academy of Sciences of the United States of America* **1994**, *91*, 6702-6706.
220. Rees, W. D. W.; Botham, D.; Turnberg, A. A demonstration of bicarbonate production by the normal human stomach in vivo. *Digestive Diseases and Sciences* **1982**, *27*, 961-966.
221. Feldman, M. Gastric Bicarbonate Secretion in Humans - Effect of Pentagastrin, Bethanechol, and 11,16,16-Trimethyl Prostaglandin-E2. *Journal of Clinical Investigation* **1983**, *72*, 295-303.
222. Odes, H. S.; Hogan, D. L.; Steinbach, J. H.; Ballesteros, M. A.; Koss, M. A.; Isenberg, J. I. Measurement of Gastric Bicarbonate Secretion in the Human Stomach - Different Methods Produce Discordant Results. *Scandinavian Journal of Gastroenterology* **1992**, *27*, 829-836.
223. Coupe, P. J.; Williams, D. L. H. Formation of peroxynitrite at high pH and the generation of S-nitrosothiols from thiols and peroxynitrous acid in acid solution. *Journal of the Chemical Society-Perkin Transactions 2* **2001**, 1595-1599.
224. Bianchi, G.; Brizi, M.; Rossi, B.; Ronchi, M.; Grossi, G.; Marchesini, G. Synthesis of glutathione in response to methionine load in control subjects and in patients with cirrhosis. *Metabolism-Clinical and Experimental* **2000**, *49*, 1434-1439.

225. Mirazimi, A.; Svensson, L. Carbohydrates facilitate correct disulfide bond formation and folding of rotavirus VP7. *Journal of Virology* **1998**, *72*, 3887-3892.
226. Salim, A. S. Sulfhydryl-Containing Agents in the Treatment of Gastric Bleeding Induced by Nonsteroidal Antiinflammatory Drugs. *Canadian Journal of Surgery* **1993**, *36*, 53-58.
227. Droge, W.; Eck, H. P.; Gmunder, H.; Mihm, S. Modulation of Lymphocyte Functions and Immune-Responses by Cysteine and Cysteine Derivatives. *American Journal of Medicine* **1991**, *91*, S140-S144.
228. Droge, W.; Eck, H. P.; Mihm, S. HIV-Induced Cysteine Deficiency and T-Cell Dysfunction - A Rationale for Treatment with N-Acetylcysteine. *Immunology Today* **1992**, *13*, 211-214.
229. Droge, W. Cysteine and Glutathione Deficiency in AIDS Patients - A Rationale for the Treatment with N-Acetyl-Cysteine. *Pharmacology* **1993**, *46*, 61-65.
230. Halliwell, B.; Gutteridge, J. M. C. Free-Radicals, Lipid-Peroxidation, and Cell-Damage. *Lancet* **1984**, *2*, 1095.
231. Halliwell, B.; Gutteridge, J. M. C. Lipid-Peroxidation, Oxygen Radicals, Cell-Damage, and Antioxidant Therapy. *Lancet* **1984**, *1*, 1396-1397.
232. Blough, N. V.; Zafiriou, O. C. Reaction of superoxide with nitric oxide to form peroxynitrite in alkaline aqueous solution. *Inorganic Chemistry* **1985**, *24*, 3502-3504.
233. Konorev, E. A.; Hogg, N.; Kalyanaraman, B. Rapid and irreversible inhibition of creatine kinase by peroxynitrite. *FEBS Letters*. **1998**, *427*, 171-174.
234. Forman, H. J.; Fridovich, I. Superoxide dismutase: a comparison of rate constants. *Arch. Biochem. Biophys.* **1973**, *158*, 396-400.
235. McCord, J. M.; Fridovich, I. Superoxide dismutase: The first twenty years (1968-1988). *Free Radical Biology and Medicine* **1988**, *5*, 363-369.